AN ABSTRACT OF THE DISSERTATION OF

Martin Roy for the degree of Doctor of Philosophy in Geology presented on October 2, 2003.

Title: Constraints on the Origin of the Middle Pleistocene Transition from the Glacial Sedimentary Record of the North-Central United States.

Abstract approved: _____

Peter U. Clark

This dissertation focuses on the role of ice sheets in the transition during the middle Pleistocene (~1.2 Ma) from 41-kyr glacial cycles to 100-kyr glacial cycles. This research evaluates the hypothesis that the middle Pleistocene transition (MPT) was related to the glacial erosion of a regolith mantle and the subsequent exposure of fresh crystalline bedrock. This issue is addressed through the study of glacial sedimentary sequences in Iowa, Nebraska, Kansas, and Missouri.

Testing the hypothesis first required the establishment of a stratigraphic framework for pre-Illinoian glacial sequences. A chronology developed around till compositional data and chronological constraints provided by paleomagnetic measurements on glacigenic sediments, and three volcanic ashes, indicate that the midcontinent tills can be grouped under three categories representing at least seven ice advances: two older groups of reverse-polarity tills containing a low and intermediate proportion of clasts and minerals derived from crystalline bedrock, respectively, and one younger group of normal-polarity tills enriched in crystalline materials.

The bulk geochemistry of the silicate fraction of the midcontinent tills was then used to evaluate the character of the rock source eroded by ice sheets. The results show a general trend in which geochemical indices, from oldest to youngest tills, fall parallel

to a mixing line defined by the composition of a weathered and fresh crystalline rock sources, respectively. The content in meteoric ^{10}Be of tills also supports the existence of a regolith and its glacial erosion by ~1.3 Ma, thus concordant with the onset of the MPT. Marine records of strontium, hafnium, and osmium isotopes provide additional support for the hypothesis.

The nature of the till compositional changes was further addressed through a provenance study based on 504 $^{40}Ar/^{39}Ar$ ages measured on individual K-feldspar grains retrieved from tills that span the last 2 Myr. Most samples yielded ages identical to those of numerical ages of the Churchill Province, thereby constraining deposition by ice from the western (Keewatin) sector of the Laurentide ice sheet. These results rule out a change in provenance, and thus show support for a change in the composition of the Churchill bedrock source during the late Cenozoic.

Constraints on the Origin of the Middle Pleistocene Transition from the Glacial Sedimentary Record of the North-Central United States

by
Martin Roy

A DISSERTATION

submitted to

Oregon State University

in partial fulfillment of
the requirements for the
degree of

Doctor of Philosophy

Presented October 2, 2003
Commencement June 2004

Doctor of Philosophy dissertation of Martin Roy presented on October 2, 2003.

APPROVED:

Major Professor representing Geology

Chair of Department of Geosciences

Dean of Graduate School

I understand that my dissertation will become part of the permanent collection of Oregon State University libraries. My Signature below authorizes release of my dissertation to any reader upon request.

Martin Roy, Author

ACKNOWLEDGEMENTS

I would like to express my sincere thanks and appreciation to the people t possible – directly or indirectly – the realization of this project.

Peter Clark played a major role in this project as a research advisor. This stemmed from an innovative hypothesis proposed by Peter a few years earlier, grateful to have had the opportunity to explore this concept. Peter also provid guidance, insightful ideas, and the financial support necessary to complete thi: I benefited from his broad knowledge in the fields of glacial geology and paleoclimatology. Peter also made numerous thoughtful reviews of the manu: But more importantly, Peter let me play on 'his' various soccer teams.

Andrew Meigs, Alan Mix, and Reed Glasmann agreed to serve on my the committee. Their time and efforts in the different stages related to this degree highly acknowledged. R. Glasmann also spent time in enlightening the task o quantitatively documenting the clay mineralogy of samples.

Many others contributed to various aspects of this project. René Barendr organized the technical aspects of the paleomagnetic study and agreed to com field at numerous occasions. René also generously provided accommodation three AGU Fall Meetings. Randy Enkin kindly accepted to let hundreds of sa through his lab for paleomagnetic analysis. Grant Raisbeck and Francoise Yi to venture in the meteoric ^{10}Be study, and provided good hospitality while doi sample preparations in their laboratory facilities in Paris. Bob Duncan was cu enough to explore the idea of a provenance study using glacial sediments. Jol provided training in the ^{40}Ar/^{39}Ar lab. Art Bettis, Joe Mason, and Carrie Patte time showing diverse features of the midcontinent Quaternary geology. Vince Rinterknetch kindly offered assistance in the preparation of ^{10}Be targets. Disc with other OSU graduate students were also appreciated.

Beyond the OSU environment, discussions with Michel Lamothe and Jean Veillette were always a good source of advice and encouragement. Other people met throughout my stay in Oregon made my life much more enjoyable. While citing names inevitably leads to the unforgiving omissions of others, some people fully deserve to be mentioned. In this regard, many roller and ice hockey teammates, both in Corvallis and Eugene, contributed to make me feel 'at home'. In particular, Tom Alexander, Jonathan Brooks, and Brian Dixon made our weekly drive to Eugene an enjoyable and 'safe' trip. In the same vein, many soccer teammates like Chris Heinemann and 'notorious' Justin Azhocar became over the years more than reliable friends. Sharing a house with Drew Eriksson was an unforgettable 'experience' and probably the best introduction I could get to 'life in the U.S.'. Friends at home are also deeply thanked for their loyalty and remembering my name during my random and too rare visits. Alain Labrecque provided technical assistance in figure drafting while I was writing in Montréal. Above all, Christelle Duffours deserves a lot of recognition for her patience and understanding of the often unexplainable. Finally, I would like to express my deepest thanks to my family. Jacques, Diane, Mathieu, and Sophie provided continuous encouragement and gave me the support I needed to get there and complete this work. I consider myself extremely lucky to be surrounded by great people like them. Merci encore.

CONTRIBUTION OF AUTHORS

The three manuscripts in this dissertation result from the collaboration with different co-authors. Peter U. Clark is co-author of Chapters 2, 3, and 4. Peter provided direction in the completion of the different research projects from which these manuscripts evolved, and contributed significantly to the organization and editing of these three papers. Peter also deserves credit for formulating the hypothesis addressed in this thesis. The following co-authors read the manuscripts and offered many helpful suggestions. As a co-author of Chapter 2, J. Reed Glasmann provided direction in the analysis of the mineral content of glacial sediments, and assisted in the interpretation of results. As a co-author of Chapter 2, René W. Barendregt assisted in the collection of paleomagnetic samples in the field, interpretation of paleomagnetic data, and editing of the manuscript. Randy J. Enkin was also involved in the paleomagnetic study described in Chapter 2, in which he oversaw the analytical procedures and contributed significantly to the final interpretation of paleomagnetic results. Grant R. Raisbeck and Françoise Yiou are co-authors of Chapter 3. They provided advice in the development of a laboratory protocol for extracting meteoric beryllium 10 of the glacial sediments, oversaw the final analysis of the ^{10}Be measurements, and provided assistance in the interpretation of the ^{10}Be data. Robert A. Duncan helped in the development of the provenance study described in Chapter 4. Robert also oversaw the $^{40}Ar/^{39}Ar$ analytical procedures and assisted in the data acquisition. As a co-author of Chapter 4, John Huard contributed to sample preparation and provided assistance in the acquisition of the $^{40}Ar/^{39}Ar$ data.

TABLE OF CONTENTS

TABLE OF CONTENTS (continued)

TABLE OF CONTENTS (continued)

LIST OF FIGURES

LIST OF FIGURES (continued)

LIST OF TABLES

LIST OF APPENDIX TABLES

Constraints on the origin of the middle Pleistocene transition from the glacial sedimentary record of the north-central United States

CHAPTER 1

Introduction

The late Cenozoic climate is characterized by the development of large ice sheets that repeatedly advanced and retreated across significant areas of the Northern Hemisphere. Because of their size, continental ice sheets can alter climate directly and indirectly, through changes in sea-surface temperatures, ocean circulation, land- and sea-surface albedo, and vegetation. Consequently, ice sheets are an important component of the climate system and their evolution and behavior have the capability to amplify and pace global climate changes. Studies have also proposed that the composition of the geological substrate underlying ice sheets may have a strong influence on their dynamics, and this effect may in turn be reflected in ice sheet-climate interactions (e.g. Clark et al., 1999). Indeed, substrate-modulated ice sheets may have been at the origin of several climate variations operating at different time scales. For example, during the last glacial cycle, the Laurentide and Scandinavian ice sheets expanded outward from harder igneous and metamorphic rocks onto softer sedimentary rocks and sediments, resulting in an outer ice sheet margin with a reduced profile. The thin ice margin may have been involved in minor ice advances and retreats through rapid response to insolation changes (Clark, 1994; Lowell, 1999), or in millennial-scale variability through re-routing of meltwaters along the southern margin of the LIS (Broecker et al., 1989; Licciardi et al, 1996). Furthermore, the presence of a soft substrate underlying the center of these ice sheets may have led to ice sheet instability, and possibly collapse, which may have resulted in episodic release of icebergs in the

North Atlantic ocean (MacAyeal, 1993a, 1993b). Changing ice sheet behavior in response to contrasting substrate may also be reflected on longer time scales. For instance, during the late Cenozoic, the transition from dominant 41-kyr glacial cycles to dominant 100-kyr glacial cycles in the middle Pleistocene (~1.2 Ma) may have been a consequence of a change from soft to hard substrates under the late Cenozoic ice sheets (Clark and Pollard, 1998). This thesis further addresses the role of subglacial substrate in the dynamics of ice sheets with respect to the origin of the middle Pleistocene transition.

1.1 Background

Oxygen isotopes ($\delta^{18}O$) and Mg/Ca measurements on benthic forams from deep-sea sediments indicate that the long global cooling-trend of the Cenozoic culminated with the development of large continental ice sheets in the Northern Hemisphere ~2.5 Ma (Raymo, 1994). Statistical analyses of paleoclimate data indicate that continental ice volumes fluctuated at periodicities of 23, 41, and 100 ka, similar to the cyclic variations of the Earth's orbital precession, tilt, and eccentricity, respectively (Hays et al., 1976; Imbrie et al., 1984). These results provide support for the Milankovich hypothesis in which fluctuations of continental ice volume are attributed to orbitally-induced changes in the amount of solar radiation received at the high Northern Hemisphere latitudes.

Despite the success of the Milankovitch theory in explaining ice ages, many issues remain regarding ice volume variability at orbital time scale. For instance, the transition in the middle Pleistocene (~1.2 Ma) that caused ice volume to increase and to vary from dominant 41-kyr cycles to dominant 100-kyr cycles is a long lasting issue in paleoclimatology, mainly because orbital forcing remained largely the same across that interval (Pisias and Moore, 1981; Ruddiman et al., 1989; Imbrie et al., 1993; Mix et al., 1995) (Figure 1.1). Similarly, the dominance of the 100-kyr ice sheet cycle after the

transition represents another problem since changes in insolation at the eccentricity level are too small to generate such a strong climate response (Imbrie et al., 1992).

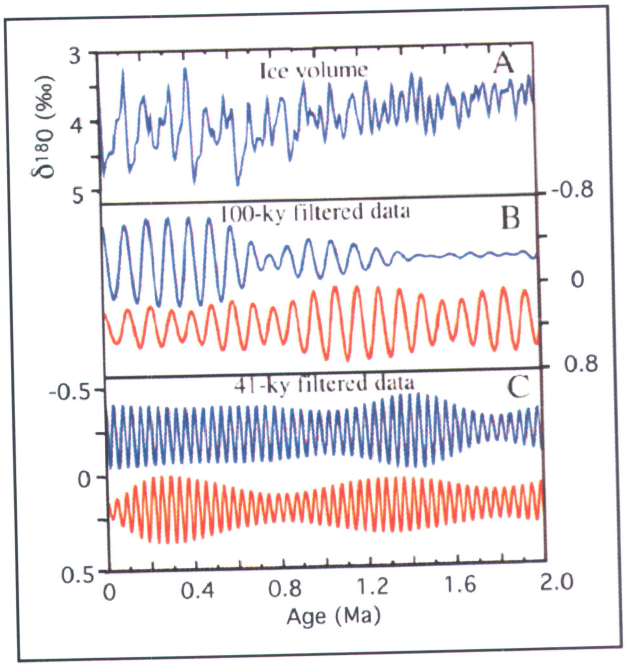

Figure 1.1: **[A]** Deep-sea $\delta^{18}O$ record of global ice volume variations over the past 2 My from ODP site 849 (Mix et al., 1995). **[B]** Blue (upper) curve is the filtered $\delta^{18}O$ record shown in [A] using a 100-ky filter (in ‰ and offset from scale in [A]). Red (lower) curve is the filtered eccentricity index from Berger (1978) obtained by using the same filter as used for the $\delta^{18}O$ data (arbitrary scale). **[C]** Blue (upper) curve is the filtered $\delta^{18}O$ record shown in [A] using a 41-ky filter (in ‰ and offset from scale in [A]). Red (lower) curve is the filtered obliquity index from Berger (1978) obtained by using the same filter as used for the $\delta^{18}O$ data (arbitrary scale). The middle Pleistocene transition consists in the onset of large amplitude 100-ky ice volume cycles, which took place during an interval when the amplitude of the 100-ky eccentricity cycles decreases and the amplitude of the 41-ky obliquity cycles does not change (from Clark et al., 1999).

The middle Pleistocene transition (MPT) is even more perplexing when the areal extent of the late Cenozoic ice sheets is taken into account. While the global $\delta^{18}O$ record suggest that the pre-transition ice sheets were about half as large as the post-transition ice sheets, geological records of glaciation indicate that the maximum extent of the pre-transition ice sheets was the same, and at times greater, than the post-

transition ice sheets. Therefore, if ice sheets were as extensive before and after the transition, the marked increase in ice volume following the MPT thus translates into a change from thin to thick ice sheets. Consequently, the MPT not only represents a change in the frequency and amplitude of ice volumes, but it also reflects a change in ice sheet thickness. Studies of modern and former ice sheets indicate that ice-sheet size and dynamics are strongly dictated by the geology of the subglacial substrate (Boulton and Jones, 1979; Alley et al., 1986, Paterson, 1994, Clark et al., 1999). These observations thus suggest that glaciological processes may be involved in the mechanisms that produced the MPT.

A number of hypotheses have been proposed to explain this peculiar feature of the late Cenozoic climate but no satisfying consensus on its origin has yet emerged (Imbrie et al., 1993; Elkibbi and Rial, 2001). This dissertation explores the hypothesis that the MPT is a consequence of a change in the character of the underlying geological substrate of the Laurentide ice sheets and possibly other Northern Hemisphere ice sheets.

1.2 The hypothesis

Clark and Pollard (1998) proposed that a change in the basal boundary conditions of former ice sheets occurred in the middle Pleistocene, resulting in a transition from ice sheets underlain entirely by soft beds to ice sheets underlain by a mixture of hard-and-soft beds. In this hypothesis, the initial soft beds are represented by thick clayey soils (regolith) that developed through prolonged chemical weathering on areas of crystalline bedrock during the tens of millions of years that preceded the inception of Northern Hemisphere glaciations. Specifically, the transition occurred through the gradual erosion of the regolith by ice sheets that subsequently uncovered fresh crystalline bedrock. Before the transition, the regolith mantle maintained thin and areally extensive ice sheets that responded linearly to the 23- and 41-kyr orbital forcing

whereas the exhumation of crystalline rocks provided hard bed conditions that caused a fundamental change in ice sheet dynamics and response to orbital forcing, and thereby initiated the 100-kyr climate cycle.

The rationale behind this hypothesis is centered on glaciological processes that govern ice sheet motion and that relates to their thickness. Glaciers and ice sheets are primarily driven by gravity, and three processes may combine and contribute to ice movement. Ice sheets resting on deformable sediments (or soft beds) move by some combination of (1) internal ice deformation, (2) sliding at the ice/substrate interface, and (3) deformation of the water-saturated sediments beneath the ice. A soft-bedded ice sheet generally flows faster than an ice sheet resting on hard beds such as crystalline bedrock, where subglacial sediment deformation is absent, and most of ice movement is achieved through internal ice deformation, and sliding to lesser extent (Paterson, 1994). As a result a soft-bedded ice sheet will tend to be thinner (reduced surface slope) than its hard-bedded counter part (steeper surface slope). Thin ice sheets will thus be particularly sensitive to external (orbital) forcing since small positive changes in insolation will result in an increase in the surface area of the ablation zone, thus exposing a large fraction of the ice sheet to a net ablation regime, and potentially causing their disappearance (Figure 1.2a). On the other hand, a thick ice sheet is more likely to resist equivalent changes in insolation, since the steeper ice profile will allow a larger portion of the ice sheet to remain in the accumulation zone (Figure 1.2b). Consequently, the occurrence of large areas of hard beds in the central part of glaciated area following the MPT may have favored the development of volumetrically bigger ice sheets, which are more susceptible to survive warming episodes associated with precessional and obliquity insolation maxima, thereby allowing a substantial amount of ice to be preserved for the next glacial episode. The presence of larger areas of hard beds since the middle Pleistocene may thus be at the origin of the transition from 41-kyr to 100-kyr glacial cycles.

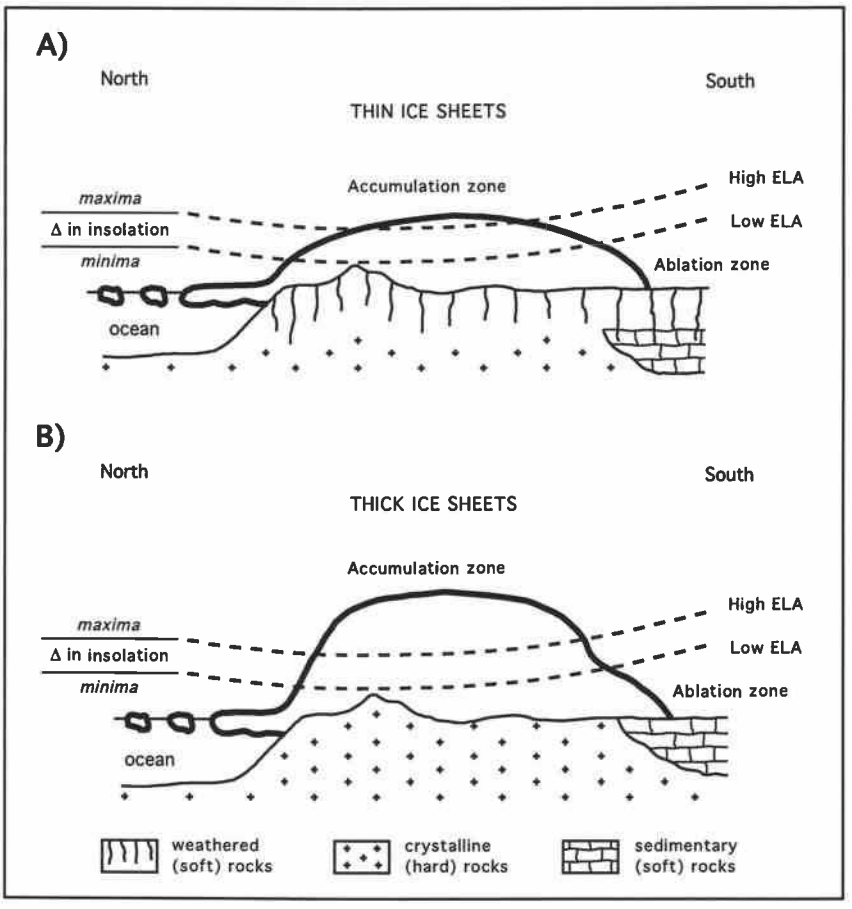

Figure 1.2: Sketch of an idealized cross-section through an ice sheet showing the effect of changes in solar radiation to the regime (mass balance) of a thin [A] and a thick [B] ice sheets. Most glaciers and ice sheets can be divided in two zones: the inner (upper) accumulation zone where annual accumulation exceeds losses by ablation; and the outer (lower) ablation zone where ablation exceeds accumulation. The boundary between the two zones, where net annual accumulation and ablation are equals, is the equilibrium line. The position of the equilibrium line (also called the equilibrium line of altitude or ELA) is primarily dictated by changes in insolation, but is also influenced by local and regional climate, as well as topography. Insolation changes will have the main consequence of displacing the ELA. During summer insolation minima, the ELA is driven downwards (toward southern regions) and most of the thin and thick ice sheets lie in a regime of net accumulation - ice sheets can grow. During summer insolation maxima, the ELA is driven upwards (towards northern regions) and a large fraction of the thin ice sheet lies in a regime of net ablation whereas a significant portion of the thick ice sheet remains above the ELA. Consequently, a thin ice sheet would be easier to destroy during insolation maxima, and in contrast, a thick ice sheet would be likely to survive into the next interval of ice growth.

1.3 Research objective and strategy

The main objective of this research is to evaluate whether evidence for a change in basal-ice boundary conditions exists in continental records of glaciations spanning the MPT. For this purpose, the composition of glacial sedimentary sequences of this age were investigated in order to document geochemical, mineralogic and petrographic changes that could indicate a significant shift in till composition reflecting the glacial erosion of a regolith source to a fresh bedrock source. Sampling of glacial sediments was carried out on 25 stratigraphic sections in the region of Iowa, Nebraska, Kansas and Missouri where extensive late Pliocene to middle Pleistocene glacial deposits are preserved.

1.4 Summary of chapters

In addressing the regolith hypothesis for the MPT, this thesis evolved in three major research components that form the core chapters of this dissertation. First, Chapter 2 describes the lithostratigraphy and chronology of late Cenozoic glacial sedimentary sequences in Iowa, Nebraska, Kansas, and Missouri. Although previous studies had considerably improved of our understanding of the glacial geology of this region, uncertainties regarding the number and age of some pre-Illinoian lithostratigraphic units remained. This study presents an improved stratigraphic framework for the north-central U.S. based on till lithological and mineralogical data, and constrained by paleomagnetic measurements of glacial and nonglacial units as well as the presence in the sedimentary sequences of three volcanic ashes of different ages. The new stratigraphic framework significantly improved the history of late Pliocene to middle Pleistocene glaciations in the midcontinent, and thereby provide a template for future stratigraphic studies in this region.

Chapter 3 addresses the soft- to hard-bed hypothesis proposed by Clark and Pollard (1998). For this purpose, the bulk geochemistry of the silicate fraction of the midcontinent tills was used to derive indices that document the degree of weathering experienced by the bedrock source prior its erosion by ice sheets. The content in major-element oxides of pre-Illinoian and last glacial maximum (LGM) tills suggests that ice sheets initially eroded a rock source where most feldspars and ferromagnesians were weathered from the parent rock, leaving quartz, K-feldspars, other resistates, and iron oxides as the main constituents of the residuum, and that subsequently, ice sheets progressively excavated a much fresher rock source, with LGM tills showing major-oxides concentrations resembling the most that of crystalline shield rocks. The contribution of the regolith and crystalline source-rock was constrained through the analyses of the meteoric ^{10}Be present in strategic till samples. Previous studies on soil chronosequences have demonstrated that old saprolites can accumulate a large amount of ^{10}Be, and that conversely, fresh crystalline bedrock is virtually devoid of ^{10}Be. The ^{10}Be concentrations in tills of different age suggest the disappearance of the soft and ^{10}Be-enriched upper horizon of the regolith by ~1.3 Ma. The change from highly weathered substrate to a fresher bedrock source thus occurred in the vicinity of the transition from 41-kyr to 100-kyr ice sheet cycles, thereby reinforcing the hypothesis that a change in subglacial geology may have contributed to the mechanisms acting behind the MPT. The unroofing of fresh crystalline rocks documented in this study has also implications for the evolution of the marine Sr, Hf, and Os isotope systems in the ocean.

Finally, Chapter 4 evaluates the possibility that the compositional variations of the midcontinent glacial sediments could be related to changes in provenance of the rock source through time rather than a temporal change in the composition of a single bedrock source region. The provenance of the material eroded by ice sheets was thus constrained using ~500 ^{40}Ar/^{39}Ar ages measured on individual K-feldspar grains present in the matrix of 14 tills that span the last 2 Myr. This investigation evaluates two

probable ice flow trajectories linking the study area to the main centers of ice dispersal of the Laurentide ice sheet: a western source associated with the Keewatin ice divide, and an eastern source associated with the Labrador/Quebec ice divide. The path of each flow line involves the erosion of rocks of the Canadian Shield with significantly different ages: the Churchill Province (2.00-1.75 Ga) in the west, and the Superior Province (>2.60 Ga) in the east. The results do not support a provenance change but rather identify a long-lived pattern of till deposition during the late Cenozoic, in which midcontinent tills were consistently deposited by ice originating from the Keewatin ice center of the western sector of the Laurentide ice sheet.

Each of these three chapters forms a stand-alone paper that is either intended for publication or in the process of being published. The first paper (Chapter 2) entitled "Glacial stratigraphy and paleomagnetism of late Cenozoic deposits from the north-central U.S." is in press and will be published in a forthcoming issue of the Geological Society of America Bulletin. The second paper (Chapter 3), "Geochemical constraints on the regolith hypothesis for the middle Pleistocene transition" will be submitted to Earth and Planetary Science Letters. Finally, the third paper (Chapter 4), "Provenance of glacial deposits from the north-central U.S. using $^{40}Ar/^{39}Ar$ ages of individual feldspar grains of tills" will be submitted to Geology.

CHAPTER 2

Glacial stratigraphy and paleomagnetism of late Cenozoic deposits of the north-central United States

M. Roy [†], P.U. Clark [†], R.W. Barendregt [‡], J.R. Glasmann [†], R.J. Enkin [§]

[†]Department of Geosciences,
Oregon State University, Corvallis, OR 97331-5506, USA

[‡]Faculty of Art and Science,
University of Lethbridge, Lethbridge, AB, T1K 3M4, Canada

[§]Geological Survey of Canada-Pacific,
Sidney, BC, V8L 4B2, Canada

Roy, M., Clark, P.U., Barendregt, R.W., Glasmann, J.R., Enkin, R.J., (*in press*), Glacial stratigraphy and paleomagnetism of late Cenozoic deposits in the north-central U.S.: Geological Society of America Bulletin.

2.1 Abstract

The north-central U.S. preserves one of the best continental records of late Pliocene and early-middle Pleistocene glaciations in the Northern Hemisphere. The glaciogenic sequences of this region consist of multiple tills interbedded with paleosols and volcanic ashes. Here we present results on paleomagnetic measurements and till compositional data from glacial sedimentary sequences in Iowa, Nebraska, Kansas, and Missouri. Periods of normal polarity (Brunhes Chron) and reverse polarity (Matuyama Chron) were identified in the sedimentary sequences investigated. This chronology is further constrained by the presence of three volcanic ashes derived from dated eruptions of the Yellowstone caldera, which indicate that the oldest till was deposited >2.0 Ma. Based on these results we identify three groups of tills representing at least seven pre-Illinoian glaciations: two older groups of reverse-polarity tills containing a low and intermediate proportion of crystalline clasts, respectively, and one younger group of normal-polarity tills enriched in crystalline lithologies. The clay mineralogy of the reverse-polarity tills is enriched in kaolinite and depleted in expandable clays relative to the normal-polarity tills, which are also characterized by minor amount of chlorite. The silt fraction of tills also show mineralogical contrasts whereby the normal-polarity tills are characterized by increases in calcite, dolomite, and feldspar, whereas the older tills show depletion in these minerals, and a relative enrichment in quartz. These petrographic and mineralogic changes are indicative of an increase with time in the areal distribution of unweathered igneous and metamorphic source bedrock.

2.2 Introduction

The north-central U.S. (Figure 2.1) encompasses some of the type areas from which the former stratigraphic classification of the North American Pleistocene glacial stages was originally developed (Hallberg, 1986). Early workers placed the glacial and nonglacial deposits of this region into a conceptual framework composed of four

glaciations and interglaciations. This stratigraphic framework persisted until subsequent stratigraphic investigations revealed greater complexity of the older sedimentary sequences, ultimately requiring the abandonment of the Nebraskan-Aftonian-Kansan-Yarmouthian terminology, and its replacement by the broader term 'pre-Illinoian' (Hallberg, 1986; Richmond and Fullerton, 1986a, 1986b).

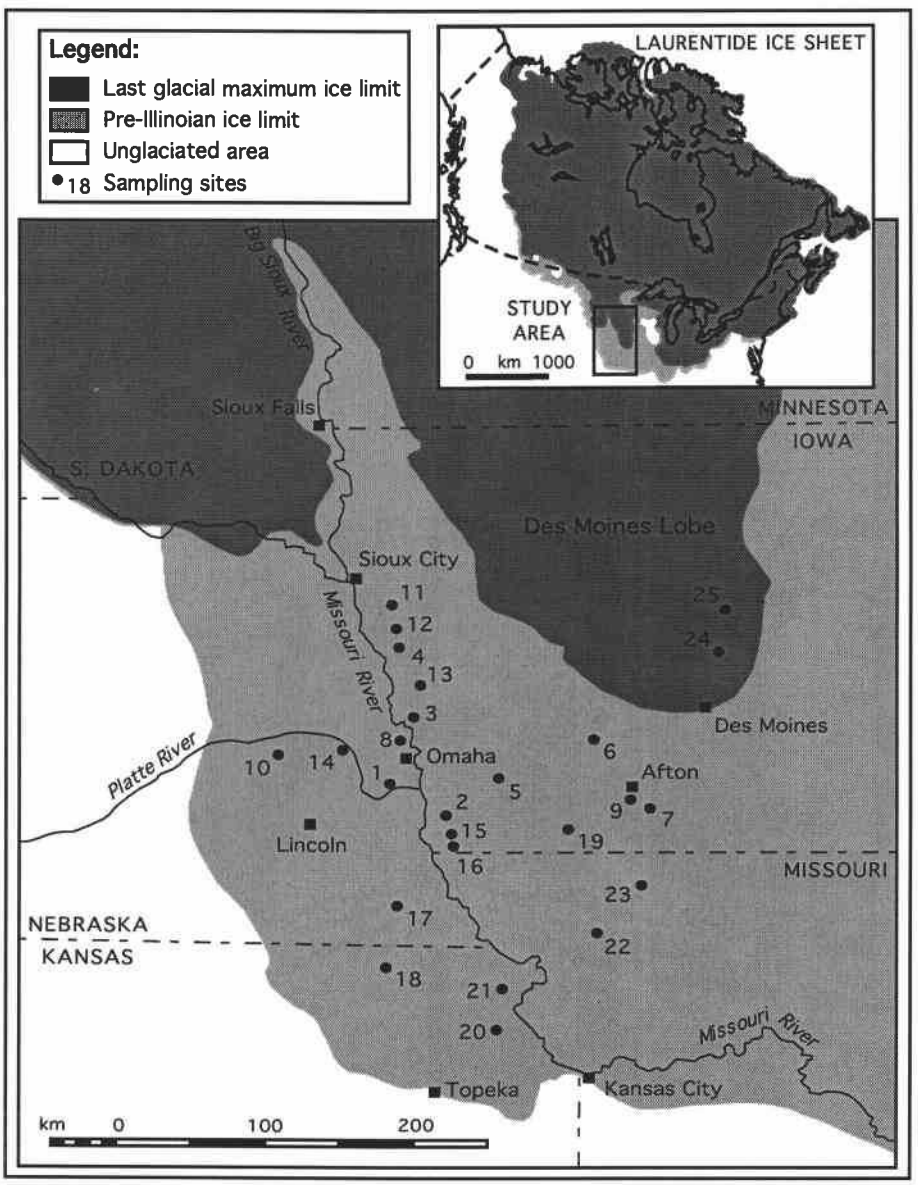

Figure 2.1: Location of the stratigraphic sections investigated and maximum extent of pre-Illinoian and late Pleistocene ice sheets.

Evidence for a more complex stratigraphy arose primarily from the work of Boellstorff (1973, 1978a, 1978b), who demonstrated that numerous tills and paleosols were present beneath type localities and key sections of the Nebraskan-Aftonian-Kansan sequence. Moreover, fission track dating of the Pearlette volcanic ash bed indicated that what was thought to be a single marker bed consisted of three distinct volcanic ashes of significantly different ages (Boellstorff, 1973, 1976, 1978c). These results led Boellstorff (1978a, 1978b, 1978c) to propose a stratigraphic framework based on till compositional data and stratigraphic relationships of till units with paleosols and fission-track dated volcanic ashes. In this framework, the tills were grouped into three categories labeled "A", "B" and "C" tills. The "A" and "C" tills were further divided into four and two subgroups, respectively (Figure 2.2). Easterbrook and Boellstorff (1984) later refined this chronology on the basis of paleomagnetic measurements. Examination of their data, however, reveals some inconsistencies, such as the occurrence of samples showing both normal and reversed polarity within single lithostratigraphic units. This was particularly common for the older till units (C tills), thereby raising the possibility of till sheets recording deposition during the latest part of the Gauss Normal Chron (Figure 2.2). Many of the paleomagnetic inclinations reported from these sites were ambiguous near-horizontal results, making polarity assignment difficult. Nonetheless, an important contribution of Boellstorff (1978a, 1978b, 1978c) was to reconcile the continental record of glaciations with the deep-sea oxygen isotope ($\delta^{18}O$) record available at that time (Hays et al., 1976) in showing evidence for many more glaciations than originally suggested from the classic four-fold stratigraphic framework.

Here we report the results of the investigation of stratigraphic sections from the midcontinent region (Figure 2.1). The purpose of this study is to develop an improved chronology for the midcontinent glacial deposits through paleomagnetic analyses and a refinement of the relation of volcanic ashes to the composition of till units. Based on chronological and lithological constraints, we define three till groups that represent at

least seven pre-Illinoian glaciations separated by major soil-forming intervals. This framework will facilitate correlations with the late Cenozoic record of glaciation elsewhere in the midcontinent (Hallberg, 1980; Aber, 1991; Kemmis et al., 1992; Rovey and Kean, 1996; Colgan, 1999).

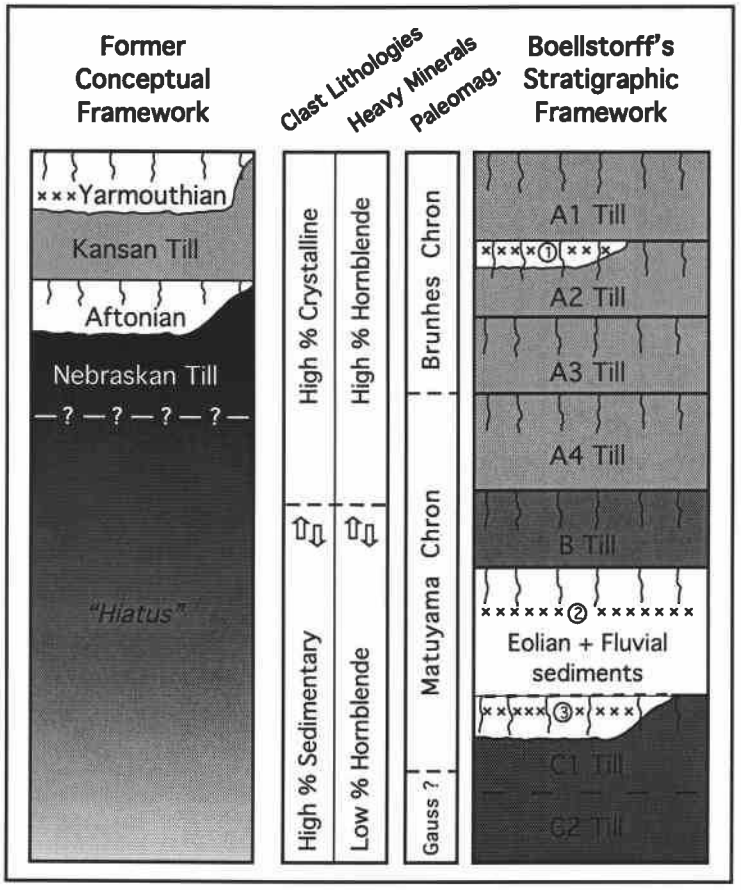

Figure 2.2: Simplified version of the former conceptual framework for the deposits of the study area, and in which the Pearlette ash bed (x's) was thought to be late Kansan or early Yarmouthian in age (modified from Reed and Dreezen, 1965). Stratigraphic framework of Boellstorff for the pre-Illinoian deposits of the study area (modified from Boellstorff, 1978b; Easterbrook and Boellstorff, 1984). Paleosols indicated by the wavy vertical lines. Tephras indicated by x's: (1) 0.602-Ma Lava Creek ash; (2) 1.293-Ma Mesa Falls ash; (3) 2.003-Ma Huckleberry Ridge ash. Petrographic and geochemial studies indicate that the tephras originated from calderas of the Yellowstone National Park in Wyoming (Izett, 1981). Ash ages after Gansecki et al. (1998).

2.3 Methods

2.3.1 Sampling sites and field methods

Field investigations and sampling were carried out at 25 localities (Figure 2.1). Stratigraphic sections usually showed evidence for multiple glaciations (Table 2.1). Sampling sites consist mostly of outcrops associated with rock quarries and road cuts, and a few natural sections exposed along rivers. We also drilled cores at three sites where Boellstorff (1973, 1976, 1978b) reported volcanic ashes. Volcanic ash beds or shards were also identified in the ash-bearing unit reported in Table 2.1. In addition to pre-Illinoian deposits, we sampled till deposited by the late Wisconsinan Des Moines Lobe in order to obtain a more complete range of compositional data over the spectrum of late Cenozoic glaciations. Prior to sampling, the stratigraphic sections were cleaned over a width of at least a meter and to a depth of 50 cm. Till sampling interval was based on unit thickness and the nature of the exposure, and varied from 0.5 to 1.5 m.

2.3.2 Paleomagnetic sampling and measurements

We collected 711 samples from 53 glacial and nonglacial units for paleomagnetic measurements. Prior to collection, we cleaned the sediment exposure to a vertical face and inserted 2.5 cm-diameter plastic cylinders horizontally into the sediment. We measured the azimuth of the samples using a magnetic compass corrected for local declination. Samples from fully oriented sediment cores were also obtained. Sampling and measurements of paleomagnetism in glacial sedimentary sequences may be complicated by the heterogeneous composition of till units. For example, the presence of a granitic pebble in a sample may obscure the detrital remnant magnetization signal. This problem was avoided, for the most part, by collecting multiple samples from each unit, and by sampling in fine-grained intratill beds (clay to fine-sand beds). The till bounding these intratill beds was also sampled.

The paleomagnetic remanence of samples was measured on an AGICO JR-5A spinner magnetometer at the Geological Survey of Canada-Pacific in Sidney, British Columbia. Stepwise alternating field demagnetization was carried out using a Schonstedt GSD-5 with tumbler in peak fields up to 100 mT. Samples were demagnetized using 5-10 step increments, and directions were determined by principal component analysis (Kirschvink, 1980).

Table 2.1: Summary of stratigraphy exposed at sampling sites

Site[†]	Latitude	Longitude	Site name (state)	Unit summary[‡] (from bottom to top)	Ref.[§]
1	41°04'27"	95°57'50"	City Wide Quarry (NE)	bedrock / till-*psl* / till-*psl* / silt / till / loess	[1]
2	41°06'09"	95°49'20"	Glenwood Quarry (IA)	bedrock / diamicton / till / sand+gravel / till-*psl* / loess	new
3	41°20'59"	95°53'46"	Crescent Quarry (IA)	bedrock / till-*psl* / silt+sand / loess	new
4	41°51'20"	95°59'13"	County Line Section (IA)	bedrock / sand / till / s.+ gr. / silts (0.6 Myr **ash**) / loess	[1]
5	41°09'40"	95°22'12"	Macedonia Quarry (IA)	bedrock / till-*psl* / loess	new
6	41°27'32"	94°25'51"	Greenfield Quarry (IA)	bedrock / till-*psl* / till / sand+gravel / loess	new
7	40°59'38"	94°02'25"	Thayer Quarry (IA)	bedrock / gravel+sand+silt-*psl* / till-*psl*	new
8	41°22'21"	95°56'51"	Florence Section (NE)	till / silt (0.6-Ma **ash**) / loess	[1]
9	40°59'46"	94°12'16"	Afton drill site (IA)	bedrock / till / silts (2.0-Ma **ash**) / till-*psl* / loess	[1]
10	41°14'59"	97°10'00"	David City drill site (NE)	bedrock / silt (1.3-Ma **ash**) / till-*psl* / s.+gr. / till-*psl* / loess	[1]
11	42°50'25"	96°08'56"	LeMars Landfill (IA)	till-*psl* / loess	new
12	42°03'46"	95°59'13"	Turin Section (IA)	till-*psl* / loess	new
13	41°28'51"	95°52'56"	Loveland Section (IA)	bedrock / till-*psl* / loess	new
14	41°23'59"	96°31'24"	Fremont Section (NE)	till-*psl* / till-*psl* / loess	[1]
15	40°51'24"	95°45'30"	Thurman Quarry (IA)	bedrock / diamicton / till / sand+gravel / till-*psl* / loess	new
16	40°45'05"	95°42'45"	Thurman Section (IA)	till-*psl* / loess	new
17	40°15'56"	96°09'37"	Elk Creek Section	till-*psl* / sand+gravel	[1]
18	39°49'37"	96°03'09"	Seneca Section (KS)	till-*psl* / diamicton	new
19	40°40'24"	94°15'02"	Bedford Quarry (IA)	bedrock / till-*psl* / silt / till-*psl* / loess	new
20	39°32'29"	95°10'09"	Atchisson Section (KS)	till / till-*psl* / loess	[2]
21	39°44'34"	94°56'38"	Wathena Quarry (KS)	bedrock /gravel+silt+sand / (slump) till / till-*psl* / loess	[3]
22	40°17'32"	94°00'13"	Bethany Quarry (MO)	bedrock / till-*psl* / loess	new
23	40°30'31"	93°28'55"	Mercer Quarry (MO)	bedrock / till-*psl* / loess	new
24	42°01'45"	93°35'48"	Whatoff Quarry (IA)	bedrock / Wisconsinan till-*psl*	new
25	42°31'33"	93°22'15"	Alden Quarry (IA)	bedrock / diamicton-*psl* / till / sands+loess / Wisconsinan till	new

Notes: [†]See Figure 1 for location; site coordinates given for latitude north and longitude west.

[‡]till-*psl* indicates till unit with well-developed paleosol (>1m in thickness); 's. + gr.' indicates sand and gravel unit.

[§]References for sites previously studied: [1] Boellstoff (1973, 1978b); [2] Aber (1991); [3] Dort (1985); and references therein.

2.3.3 Laboratory methods for sediment analyses

For each of the 95 till samples, ~4 kg of material was sieved and the lithology of ~200 clasts of the 4-12.5 mm fraction of till was identified. Clast lithologies were

divided into 14 classes that were later regrouped under 2 categories for the purpose of this study: sedimentary (e.g. limestone, dolomite, shale, and sandstone) and crystalline (igneous and metamorphic) lithologies. The mineralogy of the clay (<2 μm) and silt (<15 μm) fraction of till was analyzed using standard X-ray diffraction techniques. XRD analyses were performed using a Phillips XRG3100 equipped with a focussing monochromater (Cu Kα radiation, 0.02° 2 theta/step, 1 sec. count/step). The clay mineral content of the till samples was based upon the interpretation of weighted intensities of X-ray diffraction (XRD) pattern basal reflections, and the bulk sample mineralogy was determined using JADE+ software. The semi-quantitative analysis of the mineral phases present in till samples was based on comparisons (profile fitting) of peak area measurements of unknown samples to peak areas of internal standards with known mineral composition. These standards consist of five different XRD patterns that best represent the variety of XRD patterns obtained in this study. The composition and content of minerals present in the standards was determined through computer-assisted modeling using the program NEWMOD (Reynolds, 1985). The unknown XRD patterns were then compared to the modeled XRD patterns in order to identify which of the standards most closely resembled the mineral content of the unknown XRD patterns. The peak areas of the unknown patterns were measured. Knowing the content of each mineral phase present in the modeled patterns, comparisons of the peak areas of the unknown pattern with the modeled pattern allowed the determination of the amount of mineral phases present in each sample. The clay mineral abundances of the <2 μm fraction of tills were later normalized to 100% and expressed as weight % values.

2.4 General characteristics of the till units

The study area is part of a gently rolling till plain deeply incised by streams that have exposed surficial units of different ages (Hallberg, 1986). The bedrock geology of the study area consists of upper Pennsylvanian limestone, shale, and sandstone. Most pre-Illinoian sections investigated lie directly on carbonate bedrock. The thickness of till units ranges from 2-18 m, with stratigraphic sections exposing up to 30 m of pre-

Illinoian glacial sediments. The pre-Illinoian sections investigated typically expose one to three till units separated in places by nonglacial and glaciofluvial sorted sediments, and/or thick paleosols developed on the upper part of till units (Figure 2.3, Table 2.1). Most sections are capped by loess deposits of varying thickness, some containing soil-forming horizons of the last and previous interglacials.

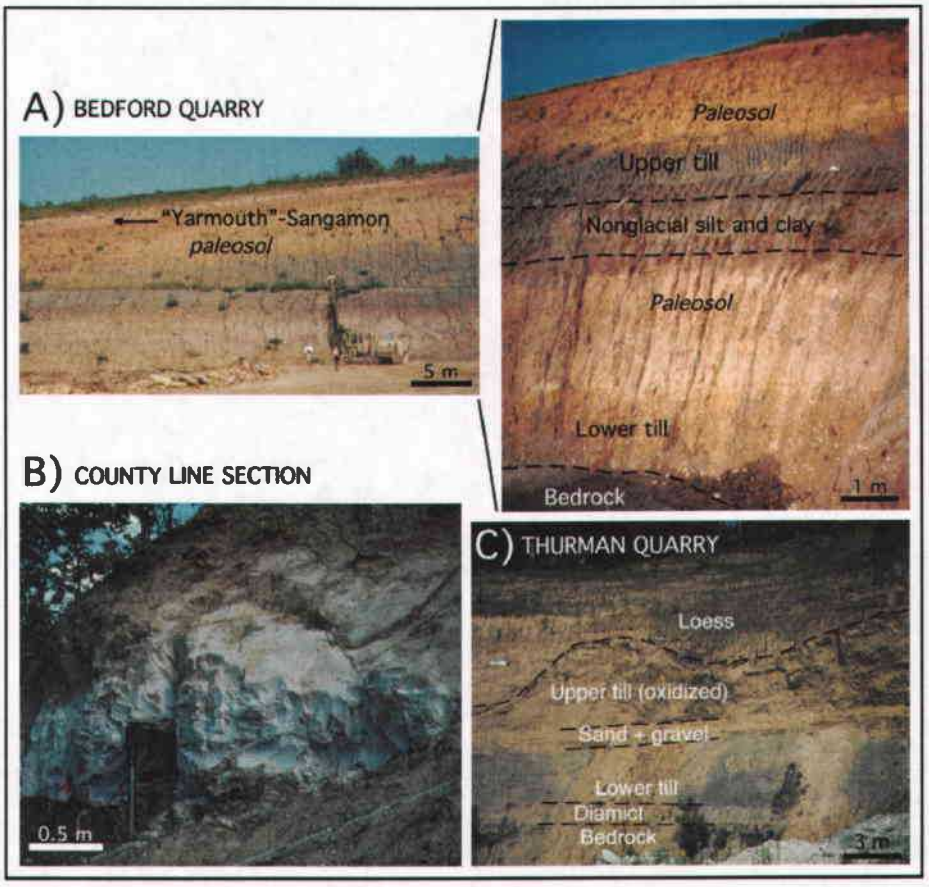

Figure 2.3: Examples of pre-Illinoian sections. (A) Two till units with paleosols separated by a nonglacial silt and clay unit at site 19 (blow-up of units to the right). (B) Lava Creek ash (0.602 Ma) cropping out near site 4. (C) Two-till unit sequence capped by loess deposits at site 15. Lower till is truncated by a sand and gravel unit whereas the upper till is affected by paleosol development. A sandy diamicton is present between the lower till and bedrock.

The glacial deposits consist of fine-grained, matrix-dominated tills. Tills are mostly homogeneous, both laterally and vertically. Minor variations are related to slight upward color changes associated with post-glacial development of paleosols. Unweathered tills typically have a very dark gray color (Munsell color 5Y 3/1), which may show slight variations related to the lithological content of units. This massive appearance is interrupted in places by the presence of intra-till beds composed of sorted material. Sorted sediments are not abundant and appear erratically within the sedimentary sequences. These beds consist of fine sand to coarse gravel, and range in thickness from a few centimeters to less than a meter. The beds are distributed horizontally in the till units, with flat to wavy lower and upper contacts, and some beds bearing primary sedimentary structures. Most till units show sharp and planar contacts with the underlying and overlying deposits. The clast (4-12 mm) content of the tills is low, consisting, on average, of <2 % of the deposits, and clasts are matrix supported. Large boulders (>1m) are rare, and when present, are found at the base of units. A few faceted bullet-shaped clasts, some bearing striations, are also present. Compressed wood fragments are common within the deposits. Structural indicators of deformation such as folds or boudinage structures were encountered at only one locality (site 20). At five sites, information on ice flow directions was determined from striated bedrock and/or striated bullet-shape clasts. In all cases, a general southward ice flow was documented, with azimuths ranging from 163°-192°, consistent with models of ice deposition for the study area (Aber, 1999).

2.5 Paleomagnetism results

Of the 711 samples analyzed for paleomagnetism, ~80% gave coherent results, the remainder having incoherent directions or unstable magnetization (Table 2.2). The natural remnant magnetization (NRM) intensities of the samples range from 0.5 to 43.1 mA/m (geometric average = 5.6 mA/m). Loess provided the highest NRM, followed

closely by intratill silt beds. Tills tend to show lower NRM as well as a larger magnitude variation

Table 2.2: Paleomagnetic results

Site	Lithostratigraphy at each site	N†	Polarity‡	Paleomagnetic properties of units§ NRM	X_0	k_n	Dec	Inc	k	α_{95}
1	Loess	8	N	36.1	11.0	0.82	4.2	57.9	134.4	4.8
	Upper till *(underlying silt)*	7	N	12.0	6.5	0.55	0.5	50.5	51.3	8.5
	Middle till	28	R	1.8	2.2	0.22	186.9	-48.2	3.0	20.8
	Lower till *(upper part)*	8	R	2.1	5.8	0.11	171.4	-53.4	16.0	32.1
	Lower till *(lower part)*	37	R	1.3	1.8	0.17	184.9	-58.3	7.5	16.0
2	Loess	8	N	1.8	8.3	0.55	18.1	61.6	282.1	5.5
	Upper till	16	R	1.3	1.3	0.25	215.8	-57.5	21.0	14.3
	Lower till	21	R	2.2	2.7	0.21	180.6	-51.6	6.0	17.1
3	Silt+sand	7	N	12.0	3.0	0.80	2.6	58.0	183.3	4.5
	Till	15	R	1.0	1.6	0.16	167.5	-48.0	14.9	16.5
4	Silts	6	N	11.2	1.1	2.65	358.1	52.4	84.4	7.3
	Till	18	R?	1.2	1.4	0.21	180.6	-61.7	4.2	24.0
5	Loess	7	N	18.0	7.5	0.41	342.6	56.7	33.0	16.2
	Till	22	i	1.3	2.5	0.15	~	~	~	~
6	Loess	12	N	12.0	2.5	0.80	358.9	58.6	39.7	8.9
	Cut and fill	20	N	1.8	1.3	0.33	8.6	42.0	22.9	9.7
	Paleosol (upper till)	9	N?	3.6	1.9	0.50	10.1	47.0	10.0	22.2
	Upper till	10	R	1.2	1.0	0.30	166.0	-50.3	7.0	27.3
	Intratill silt bed (upper till)	14	i	3.1	0.8	0.90	5.6	20.1	37.4	8.0
	Lower till	28	R	1.9	2.6	0.18	192.0	-57.6	4.2	23.1
7	Till	41	i	1.0	1.9	0.13	~	~	~	~
	Sand and silt unit	15	N	3.2	1.4	0.57	359.8	47.5	13.2	13.8
8	Till	8	i	2.2	0.7	0.77	~	~	~	~
	Intratill silt bed	7	N	5.2	0.6	2.11	275.9	36.6	27.6	11.7
9	Upper till	16	i	1.2	1.8	0.20	~	~	~	~
	Silt (2.0 Myr ash)	18	i	~	~	~	~	~	~	~
	Lower till	12	R	1.8	1.1	0.45	154.0	-34.8	4.4	24.6
10	Upper till	12	R??	5.8	2.7	0.55	180.7	-14.3	45.6	18.5
	Lower till	32	R	0.9	1.9	0.13	183.2	-60.6	13.0	10.6
	Silts (1.2 Myr ash)	12	R	4.0	3.5	0.29	137.0	-58.3	40.3	7.3
11	Till *(upper part)*	4	N	18.0	1.7	1.90	8.1	38.9	168.6	7.1
	Till *(lower part)*	3	R?	1.4	0.8	0.60	147.5	-46.1	136.2	59.3
12	Till	8	R?	1.6	0.9	0.47	19436	-49.7	7.8	41.7
13	Till	6	R	0.9	0.8	0.28	162.3	-55.7	13.4	31.3

(continued next page)

Table 2.2: Paleomagnetic results *(continued)*

Site	Lithostratigraphy at each site	N†	Polarity‡	Paleomagnetic properties of units§ NRM	X_0	k_n	Dec	Inc	k	α_{95}
14	Silt	6	N	11.7	2.8	1.07	346.8	67.9	438.6	4.4
	Upper till	20	N	8.4	2.3	0.90	357.2	60.9	31.7	7.5
	Lower till *(upper part)*	12	N	5.7	2.5	0.47	343.3	60.7	46.6	11.3
	Lower till *(lower part)*	9	i	1.4	1.8	0.19	~	~	~	~
15	Upper till	3	R	6.1	2.3	0.65	163.7	-35.8	472.2	30.8
	Silt	6	R?	1.4	0.7	0.49	112.5	-45.2	31.4	20.2
	Middle till	6	R	3.5	2.3	0.38	195.0	-64.7	35.2	30.2
	Lower till *(diamicton)*	5	R	6.9	4.8	0.36	182.7	-42.0	29.6	42.0
16	Till	4	N	4.8	2.5	0.47	349.1	60.4	16.4	23.4
17	Intratill silt bed	6	R	13.3	1.1	3.04	142.4	-32.0	63.4	8.5
	Till	6	i	1.1	1.1	0.26	~	~	~	~
18	Till	8	R	2.1	0.5	1.11	173.1	-13.8	7.3	27.0
19	Upper till	7	R?	0.5	7.3	0.19	127.2	-79.7	4.5	57.2
	Nonglacial silt	18	R	1.9	1.2	0.27	194.3	-33.3	15.9	9.0
	Lower till	9	R	0.8	1.2	0.17	245.6	-44.1	7.4	24.6
20	Upper till	6	R	1.9	0.5	0.89	203.5	-22.9	6.9	27.9
	Sand unit	3	R	1.2	1.3	0.25	166.8	-34.4	10	48.4
	Lower till	6	R	8.8	0.8	3.50	199.3	-19.8	10.5	21.7
21	Upper till	6	N	4.3	0.8	1.60	65.3	38.6	7.5	26.3
	Lower till	8	R	4.2	0.7	1.57	146.8	-24.0	7.8	23.1
22	Till	9	i	0.8	0.9	0.22	~	~	~	~
23	Till	6	N	5.1	1.0	1.20	6.4	54.7	13.1	21.9
	Intratill silt bed	13	N	5.5	8.9	1.20	350.3	34.9	19.8	11.9
24	Wisonsinan till	~	~	~	~	~	~	~	~	~
25	Wisonsinan till	6	N	12.0	2.5	1.20	345.8	61.2	38.0	11.0
	Nonglacial sand, silt, loess	8	N	43.1	5.0	2.18	352.8	61.1	99.9	5.6
	Middle till	6	N	5.2	3.1	0.40	154.1	83.0	8.3	24.7
	Lower till	14	N	3.3	0.6	0.40	2.8	61.6	17.3	10.2

Notes: †N = number of sample analyzed; ~ = no data.

‡N = unit with normal polarity (Brunhes Chron); R = unit with reverse polarity (Matuyama Chron); N?, R? = unit with weak remant magnetism suggesting a normal, reverse polarity, respectively; N??, R?? = unit with faint remant magnetism suggesting a possible normal and reverse polarity, respectively; i = unit with inderteminate polarity;

(N.B.: N?? or R?? units are considered as 'i units' in treatment of till compositional data).

§NRM = natural remnant magnetization (mA/m); X_0 = bulk magnetic susceptibility (10E-4 SI/vol); K_n = Koenigsberger ratio (unitless); Dec = declination (degree); Inc = inclination (degree); k = precision parameter; α_{95} = circle of confindence (P=0.05).

in NRM. The relatively intense magnetization and demagnetization features of the samples suggest that magnetite is the main mineral carrier for the remnant magnetization.

Samples with coherent directions and within-site homogeneity accurately record the earth's paleofield. Samples showing a larger degree of scatter within a single horizon less faithfully record the paleofield but are still useful in assigning polarity to such units. Our samples reveal both positive (downward) and negative (upward) inclinations, representing units with normal and reverse polarity, respectively (Figure 2.4). Incoherent directions in glacial samples are attributed to the presence of very weak or unstable magnetizations, and/or the presence of crystalline pebbles that mask the ambient magnetic field of the sediment matrix. The presence of such pebbles in a sample was verified after analysis. Samples with incoherent directions were therefore rejected from the data set. Our results allowed the identification of 12 till units with a normal polarity and 21 till units with a reversed polarity. Incoherent results precluded the assignment of a polarity to 4 till units. At a few sites containing multiple-till sequences, normal-polarity units consistently overlay reverse-polarity units. Intratill beds yielded directions in general agreement with the one of the bounding till unit, and all loess samples revealed normal polarity.

Here we interpret that the normal and reversed polarities recorded by the sediments can be assigned to the Brunhes Normal Chron and Matuyama Reverse Chron, respectively, and do not represent deposition during subchrons. This interpretation is required by the lack of other dating control on the sedimentary sequences, but is supported by several considerations. Subchrons exhibit relatively short time spans (~10 to 100 kyr) with respect to chrons (~1000 kyr), thus increasing the likelihood that we sampled sediment recording the polarity of a chron, rather than a subchron. Some subchrons also fall almost entirely, or for a large part, during interglacials. Where multiple-till sections exhibit units with different polarity, the stratigraphic succession

always consists of a reverse-polarity unit overlain by a normal-polarity unit. At no site was a normal-polarity unit found underlying a reverse-polarity unit. Nevertheless, the occurrence of normal and reverse polarity subchrons within the Brunhes and Matuyama Chrons has the potential to complicate our record, and the development of independent dating methods may eventually identify evidence of deposition during a subchron.

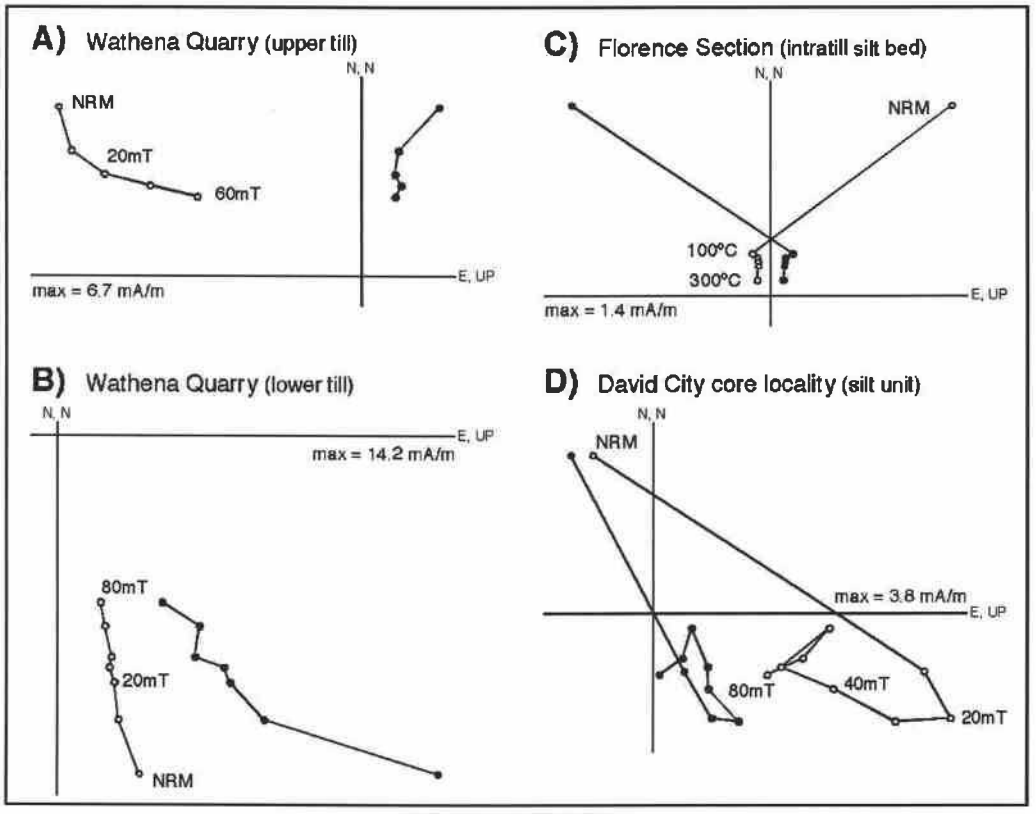

Figure 2.4: Demagnetization characteristics of pre-Illinoian units. Horizontal component of magnetization after stepwise alternating demagnetization is marked with solid dots; vertical component is marked with open dots. Alternating field steps are given in mT, thermal steps are given in °C. (A) and (B) are from normal- and reverse-polarity till units at site 21; (C) is from a normal-polarity intratill silt bed at site 8; and (D) is from a reverse-polarity silt unit containing a 1.3-Ma ash at site 10, and depicts the complex nature of some of the magnetization records. The initial demagnetization steps (0-20 mT) removed a soft (normal) viscous overprint possibly due in part to a Brunhes-age weathering phase. Steps 20 to 50 mT reveal the original (reversed) detrital remanant magnetization component. The hard overprint (over 50 mT) likely reflects a chemical remanence associated with authigenic formation of hematite and/or goethite.

2.6 Till compositional results

2.6.1 Clast Lithology of tills

The composition of the 4-12.5 mm clast fraction of tills shows wide variations. Within the context of the paleomagnetic polarity of the till units, however, there are significant lithological similarities (Figure 2.5). Till units with reverse polarity are primarily dominated by sedimentary lithologies whereas till units with normal polarity show an increase in crystalline lithologies. Further lithological distinction within the group of reverse-polarity tills suggests that two populations are present (Figure 2.5): one, named **R2 tills**, that is composed almost entirely of sedimentary lithologies (>77%; average of 85%) and one, **R1 tills**, that is intermediate between the latter cluster and the group of normal-polarity tills (R1-till average: 63% of sedimentary clasts). The average composition of normal polarity tills (53% of sedimentary clasts) is nearly identical to the composition of Wisconsinan tills (55%). Wisconsinan tills are also characterized by a clast content that is on average nearly three times greater than the one of pre-Illinoian tills.

The stratigraphic relation of some of our till samples to volcanic ashes suggests that the R2 tills are older than the R1 tills. Till units associated with volcanic ashes are present at four localities (Figure 2.6a). Till beneath a nonglacial silt containing the 2-Ma Huckleberry Ridge ash (Boellstorff, 1978c) (site 9) contains 90% sedimentary clasts whereas the upper till with a normal (?) polarity contains 56% sedimentary lithologies. A till with a reversed polarity overlying a silt unit containing the 1.3-Ma Mesa Falls ash (Boellstorff, 1973) (site 10) has a sedimentary clast content of 66%. No polarity could be assigned to the overlying till but its composition is the same as that of the underlying till. A normal-polarity till that is overlain by the 0.6-Ma Lava Creek ash (site 8) has a sedimentary clast content of 50%. A similar stratigraphic setting (site 4) exposes the 0.6-Ma Lava Creek ash overlying a till unit with a relatively low sedimentary clast

content of (53%). This unit, however, is weakly magnetized, and while its polarity cannot be assigned unequivocally, it appears to be reversed.

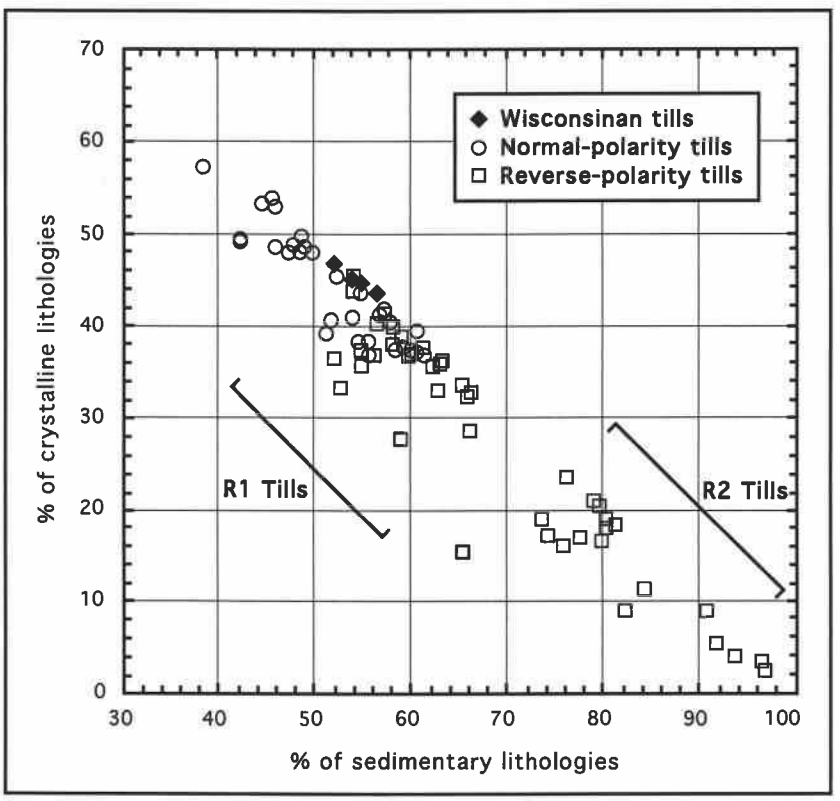

Figure 2.5: Relationship between the clast (4-12.5 mm) content of crystalline and sedimentary lithologies of tills placed in the context of the paleomagnetic results. See text for details on clusters labeled R1 tills and R2 tills. Not every sample sums to 100% because some of the lithologies could not be determined.

Based on relative age of till units determined by stratigraphic superposition in individual outcrops, we also find a consistent decrease in sedimentary lithologies and concomitant increase in crystalline lithologies in younger tills (Figure 2.6b, Table 2.3). At the sites exposing multiple-tills with same polarity, the clast lithology of the lower unit is either similar to or is enriched in sedimentary clasts relative to the overlying unit. Where the unit succession consists of a reverse-polarity till overlain by a normal-polarity till, a similar upward decrease in sedimentary clasts is documented. These results are consistent with the clast composition of the till units present at the volcanic

ash localities described above (Figure 2.6a), and taken together, these results tend to suggest the presence of a compositional trend consisting of a decrease in sedimentary clasts in progressively younger till sequences.

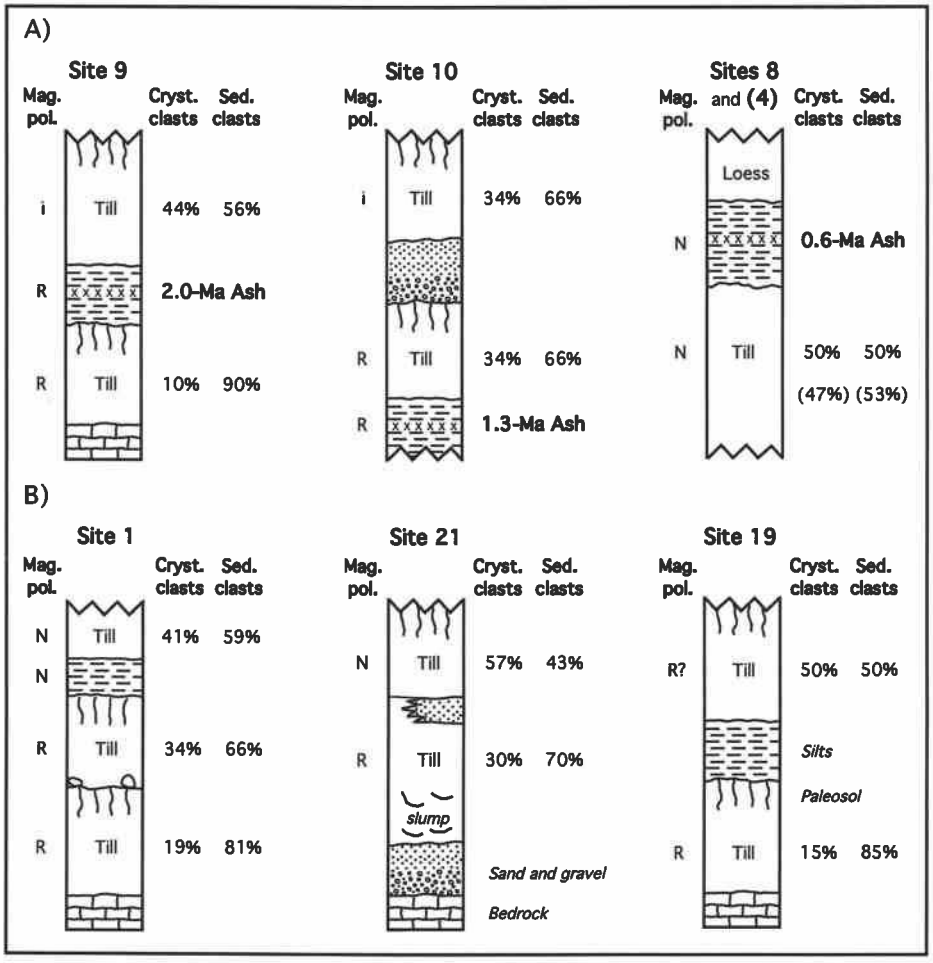

Figure 2.6: Schematic stratigraphic sections showing the increase in crystalline lithologies in progressively younger sedimentary sequences (see text for details). (A) Sites of tills in contact with volcanic ashes. (B) Multiple-till sections containing units of reversed and normal magnetic polarity or units showing significant contrast in composition. Symbols: N, R, and i indicate units with normal, reverse, and indeterminate polarity, respectively.

Table 2.3 Lithological and mineralogical content of tills units

Site	Mag. pol.[‡]	Lithostra-tigraphy	Till Group	Sample number	Clast lithology[§] Sedl.	Cryst.	Clay mineralogy[¶] Kao.	Exp.	Ill.	Chl.	Silt mineralogy[††] Qtz/Felds.	Qtz/Carb.
1	N	Upper till	N	CTY09	58.6	41.4	12.0	56.3	31.7	0.0	0.94	0.51
					58.6	**41.4**					**0.94**	**0.51**
	R	Middle till	R1	CTY08	69.9	30.1	~	~	~	~	~	~
				CTY07	68.1	31.9	~	~	~	~	0.54	0.65
				CTY06	61.4	38.6	~	~	~	~	0.74	0.83
					66.5	**33.5**					**0.64**	**0.74**
	R	Lower till	R2	CTY05	82.1	17.9	~	~	~	~	~	~
				CTY04	81.0	19.0	~	~	~	~	~	~
				CTY03	79.5	20.5	~	~	~	~	0.81	1.01
				CTY02	81.2	18.8	~	~	~	~	0.83	0.79
				CTY01	82.8	17.2	~	~	~	~	0.84	0.89
					81.3	**18.7**					**0.82**	**0.90**
2	R	Upper till	R1	GLW06	63.7	36.3	29.8	48.5	21.7	0.0	1.56	0.36
				GLW07	59.1	40.9	14.8	59.3	25.9	0.0	1.38	0.36
					61.4	**38.6**	**22.3**	**53.9**	**23.8**	**0.0**	**1.47**	**0.36**
	R	Lower till	R1	GLW05	67.0	33.0	16.1	53.2	30.7	0.0	2.51	0.36
				GLW04	59.6	40.4	21.4	50.8	28.6	0.0	1.77	0.37
				GLW03	60.5	39.5	~	~	~	~	~	~
					62.4	**37.6**	**18.8**	**52.0**	**29.6**	**0.0**	**2.14**	**0.37**
3	R	Till	R1	CRS03	60.3	39.7	23.2	46.3	30.4	0.0	1.04	0.41
				CRS02	63.8	36.2	24.0	42.3	34.2	0.0	1.07	0.27
				CRS01	60.5	39.5	26.2	40.0	33.9	0.0	1.39	0.37
					61.5	**38.5**	**24.5**	**42.9**	**32.8**	**0.0**	**1.17**	**0.35**
4	R?	Till	R1	SHM02	55.8	44.2	16.6	42.9	40.4	0.0	1.39	0.40
				SHM05	50.0	50.0	17.5	53.0	28.7	2.1	0.81	0.26
					52.9	**47.1**	**17.0**	**48.0**	**34.6**	**1.0**	**1.10**	**0.33**
5	i	Till	i	MCD03	54.3	45.7	~	~	~	~	1.82	0.49
				MCD02	55.0	45.0	~	~	~	~	1.42	0.45
				MCD01	49.1	50.9	~	~	~	~	1.74	0.42
					52.8	**47.2**					**1.66**	**0.45**
6	R?	Upper till	R1	GRN01	54.5	45.5	~	~	~	~	~	~
				GRN02	60.8	39.2	27.7	37.5	34.8	0.0	1.17	0.79
					57.6	**42.4**	**27.7**	**37.5**	**34.8**	**0.0**	**1.17**	**0.79**
	R?	Lower till	R1	GRN05	59.4	40.6	~	~	~	~	~	~
				GRN06	58.9	41.1	~	~	~	~	1.26	0.73
				GRN07	60.3	39.7	25.8	49.5	24.7	0.0	1.15	0.37
					59.5	**40.5**	**25.8**	**49.5**	**24.7**	**0.0**	**1.20**	**0.55**
7	N	Till	N	THA05	46.0	54.0	~	~	~	~	~	~
				THA04	48.4	51.6	31.8	32.6	33.8	1.8	1.77	0.78
				THA03	59.1	40.9	32.1	33.1	32.8	2.1	1.18	0.66
				THA02	45.5	54.5	26.6	40.8	30.7	1.9	1.16	0.71
				THA01	49.2	50.8	31.7	31.0	35.4	1.9	~	~
					49.6	**50.4**	**30.5**	**34.4**	**33.2**	**1.9**	**1.37**	**0.71**
8	N	Till	N	FLO02	49.2	50.8	~	~	~	~	~	~
				FLO01	50.0	50.0	23.7	37.3	37.3	1.7	0.71	0.27
					49.6	**50.4**	**23.7**	**37.3**	**37.3**	**1.7**	**0.71**	**0.27**
9	i	Upper till	i	AF119	54.6	45.4	~	~	~	~	~	~
			i	AF151	57.9	42.1	~	~	~	~	~	~
					56.3	**43.7**						
	R	Lower till	R2	AF172	90.4	9.6	~	~	~	~	0.91	0.91
					90.4	**9.6**					**0.91**	**0.91**

(continued next page)

Table 2.3 Lithological and mineralogical content of tills units *(continued)*

Site	Mag. pol.‡	Lithostra-tigraphy	Till Group	Sample number	Clast lithology§ Sedi.	Cryst.	Clay mineralogy¶ Kao.	Exp.	Ill.	Chl.	Silt mineralogy†† Qtz/Felds.	Qtz/Carb.
10	i	Upper till	i	DC120	66.1	33.9	~	~	~	~	1.57	0.24
					66.1	**33.9**					**1.57**	**0.24**
	R	Lower till	R1	DC139	65.8	34.2	21.4	40.9	37.7	0.0	2.81	0.38
					65.8	**34.2**	**21.4**	**40.9**	**37.7**	**0.0**	**2.81**	**0.38**
11	N	Till	N	LMR02	46.3	53.7	~	~	~	~	~	~
				LMR01	45.7	54.3	10.6	59.0	27.3	3.1	0.69	0.19
					46.0	**54.0**	**10.6**	**59.0**	**27.3**	**3.1**	**0.69**	**0.19**
12	R?	Till	R1	TUR02	58.5	41.5	~	~	~	~	~	~
				TUR01	59.5	40.5	17.0	50.0	33.0	0.0	0.68	0.46
					59.0	**41.0**	**17.0**	**50.0**	**33.0**	**0.0**	**0.68**	**0.46**
13	R	Till	R1	LOV02	63.7	36.3	~	~	~	~	~	~
				LOV01	58.1	41.9	~	~	~	~	~	~
					60.9	**39.1**						
14	N	Upper till	N	FRE06	61.8	38.2	~	~	~	~	0.61	0.14
				FRE05	62.4	37.6	~	~	~	~	0.24	0.17
				FRE04	61.0	39.0	~	~	~	~	0.82	0.20
					61.7	**38.3**					**0.56**	**0.17**
	N	Lower till	N	FRE07	56.4	43.6	2.1	65.3	30.2	2.4	~	~
				FRE03	60.7	39.3	2.7	68.6	26.3	2.4	0.68	0.26
				FRE02	55.6	44.4	3.4	62.8	31.2	2.5	0.78	0.46
				FRE01	56.6	43.4	2.8	62.9	31.8	2.5	1.30	0.56
					57.3	**42.7**	**2.8**	**64.9**	**29.9**	**2.5**	**0.92**	**0.43**
15	R	Upper till	R1	THU06	62.0	38.0	~	~	~	~	0.78	0.19
				THU05	60.8	39.2	~	~	~	~	1.21	0.20
					61.4	**38.6**					**0.99**	**0.19**
	R	Lower till	R1	THU04	66.1	33.9	23.6	44.0	32.4	0.0	1.47	1.18
				THU03	60.5	39.5	~	~	~	~	1.61	0.37
				THU02	55.2	44.8	21.4	50.0	28.6	0.0	1.73	0.34
					60.6	**39.4**	**22.5**	**47.0**	**30.5**	**0.0**	**1.60**	**0.63**
	R	*Diamicton*	*n.a.*	THU01	*82.9*	*17.1*	~	~	~	~	~	~
16	N	Till	N	STR01	57.7	42.3	11.3	60.9	27.8	0.0	0.69	0.38
					57.7	**42.3**	**11.3**	**60.9**	**27.8**	**0.0**	**0.69**	**0.38**
17	R	Till	R2	ELC03	97.7	2.3	~	~	~	~	0.93	1.53
				ELC02	96.6	3.4	~	~	~	~	0.82	1.46
				ELC01	96.0	4.0	~	~	~	~	0.72	1.24
					96.7	**3.3**					**0.82**	**1.41**
18	R	Till	R1	SEN02	62.0	38.0	29.9	39.8	31.2	0.0	2.20	0.23
				SEN01	67.1	32.9	24.9	38.3	36.8	0.0	1.41	0.26
					64.6	**35.4**	**27.4**	**39.1**	**34.0**	**0.0**	**1.81**	**0.24**
19	R?	Upper till	R1	BEF04	49.4	50.6	27.0	40.8	30.0	3.1	1.16	0.78
				BEF03	50.8	49.2	33.4	37.5	29.1	0.0	1.24	0.74
					50.1	**49.9**	**30.2**	**39.1**	**29.5**	**1.5**	**1.20**	**0.76**
	R	Lower till	R2	BEF02	81.7	18.3	24.3	43.0	32.7	0.0	1.03	1.39
				BEF01	88.2	11.8	23.2	34.2	42.6	0.0	0.77	1.17
					85.0	**15.0**	**23.7**	**38.6**	**37.7**	**0.0**	**0.90**	**1.28**
20	R	Upper till	R2	ATC05	79.0	21.0	~	~	~	~	~	~
				ATC04	76.5	23.5	~	~	~	~	~	~
					77.7	**22.3**						
	R	Lower till	R2	ATC03	81.0	19.0	23.8	41.6	34.7	0.0	0.68	0.35
				ATC02	79.7	20.3	25.1	39.1	35.8	0.0	0.60	0.33
				ATC01	81.6	18.4	26.6	41.7	31.7	0.0	0.75	0.26
					80.8	**19.2**	**25.1**	**40.8**	**34.0**	**0.0**	**0.68**	**0.31**

(continued next page)

Table 2.3 Lithological and mineralogical content of tills units *(continued)*

Site	Mag. pol.‡	Lithostra-tigraphy	Till Group	Sample number	Clast lithology§ Sedi.	Cryst.	Clay mineralogy¶ Kao.	Exp.	Ill.	Chl.	Silt mineralogy†† Qtz/Felds.	Qtz/Carb.
21	N	Upper till	N	WAT05	39.8	60.2	~	~	~	~	~	~
				WAT04	45.9	54.1	~	~	~	~	1.08	0.17
					42.9	**57.1**					**1.08**	**0.17**
21	R	Lower till	R1	WAT03	63.8	36.2	23.0	38.7	38.3	0.0	1.86	0.73
				WAT02	61.9	38.1	27.3	30.9	41.7	0.0	1.94	0.64
					62.8	**37.2**	**25.1**	**34.8**	**40.0**	**0.0**	**1.90**	**0.69**
22	i	Till	i	BET03	94.3	5.7	~	~	~	~	~	~
				BET01	91.1	8.9	~	~	~	~	0.88	2.24
					92.7	**7.3**					**0.88**	**2.24**
23	N	Till	N	MER05	61.3	38.7	~	~	~	~	1.14	0.25
				MER04	58.6	41.4	~	~	~	~	0.89	0.41
				MER03	60.0	40.0	~	~	~	~	0.53	0.21
				MER02	53.4	46.6	23.8	37.3	37.2	1.7	1.06	0.43
					58.3	**41.7**	**23.8**	**37.3**	**37.2**	**1.7**	**0.91**	**0.32**
24	Wisco	Till	Wisc.	WHA02	55.2	44.8	~	~	~	~	~	~
				WHA01	52.8	47.2	~	~	~	~	~	~
					54.0	**46.0**						
25	Wisco	Upper till	Wisc.	ALD06	54.6	45.4	4.3	55.2	36.7	3.9	0.58	0.18
				ALD05	56.6	43.4	3.2	60.5	32.7	3.7	0.52	0.15
					55.6	**44.4**	**3.8**	**57.8**	**34.7**	**3.8**	**0.55**	**0.17**
	N	Middle till	N	ALD04	57.6	42.4	1.9	66.5	29.3	2.4	0.80	0.36
				ALD03	60.3	39.7	1.6	67.2	28.8	2.3	0.82	0.39
					58.9	**41.1**	**1.8**	**66.9**	**29.0**	**2.4**	**0.81**	**0.37**
	N	*Diamicton*	*n.a.*	ALD02	~	~	~	~	~	~	~	~

Notes: †Mean of each till unit is shown in bold and large numbers; ~ = no data.

‡See Table 2 for legend.

§Clast lithological results (4-12.5 mm size-fraction): sedimentary and crystalline lithologies.

¶Clay mineralogical results (<2 μm size fraction): kaolinite, expandable clays, illite, and chlorite.

††Silt mineralogical results (<15 μm size-fraction): quartz/feldspar ratio and quartz to carbonate ratio.

2.6.2 Mineralogy of the clay and silt fractions of tills

The clay mineralogy of tills is sensitive to pedogenic alteration during interglacial periods. For this reason we focused our work on unweathered tills (i.e. tills not affected paleosol development). The X-ray diffraction (XRD) analyses indicate that illite, kaolinite, and interstratified illite/smectite (expandable clays) are the main clay mineral constituents of the <2 μm fraction of tills, along with minor amount of chlorite. Intensity changes in the XRD patterns show variations in the abundance of these minerals among the till samples that, when placed within the context of the paleomagnetic and ash chronology, reveal mineralogical differences between tills of different age (Table 2.3).

The clay mineralogy of the reverse-polarity tills is characterized by a lower abundance of expandable clays and higher abundance of kaolinite compared to that of normal-polarity tills (Figure 2.7). Wisconsinan tills are also distinct from their older counterparts with a composition of 58% expandable clays and 4% kaolinite. The Wisconsinan tills and the normal-polarity tills can also be distinguished from the reverse-polarity tills by the occurrence of minor amounts of chlorite, which is most abundant in the Wisconsinan tills. The content of illite does not vary significantly among the till groups, showing abundances ranging from 32% to 36%. Contrary to the clast lithological content of tills, distinctions cannot be made within the reverse-polarity tills using clay mineralogy. This, however, may be related to the small number (n=5) of R2-till samples analyzed. Nevertheless, the R2 tills are slightly depleted in expandable minerals compared to the R1 tills.

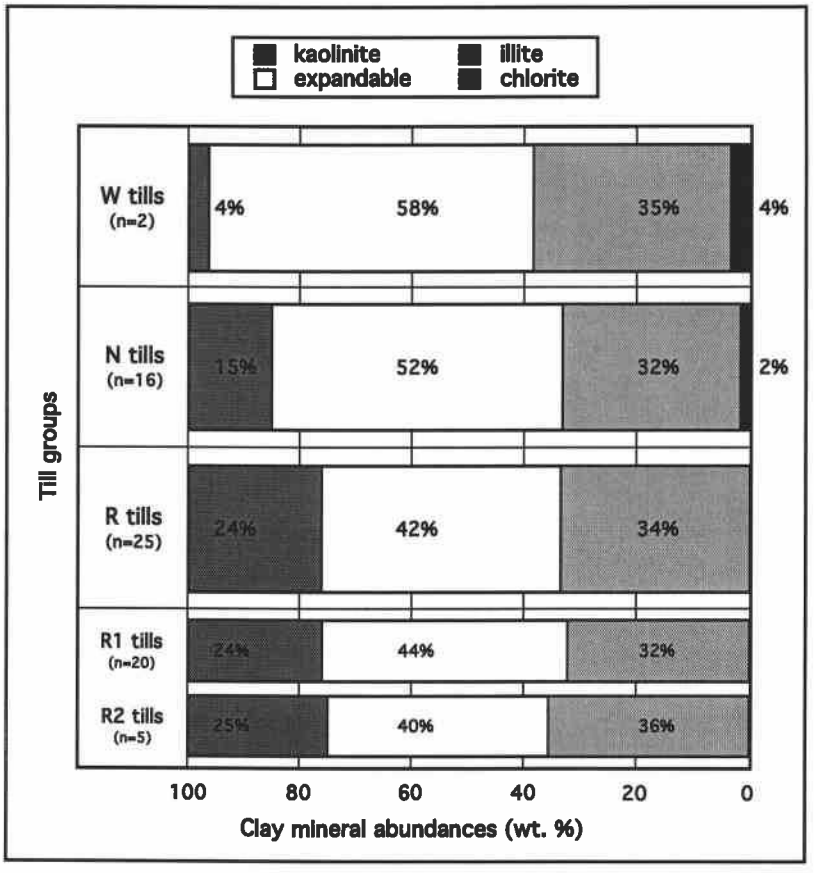

Figure 2.7: Clay mineral abundances (weight %) in the various till groups.

We also find significant mineralogical contrasts in the silt fraction of the different till groups. Semi-quantitative analyses of the mineralogy of the silt fraction are complicated by the wide variety of minerals and the corresponding overlap of their intensity peaks in XRD patterns, and thus prevent the true assessment of mineral abundance. For this reason, we discuss only ratios of the peak areas of quartz relative to the peak areas of calcite and dolomite, and to feldspars. The R2 tills show the largest quartz/carbonate ratio (0.94), followed by the R1 tills (0.51), the normal-polarity tills (0.37), and the Wisconsinan tills (0.17) (Figure 2.8a). This trend can be attributed to some combination of a decrease of quartz and an increase of carbonate minerals in the silt fraction of tills with time.

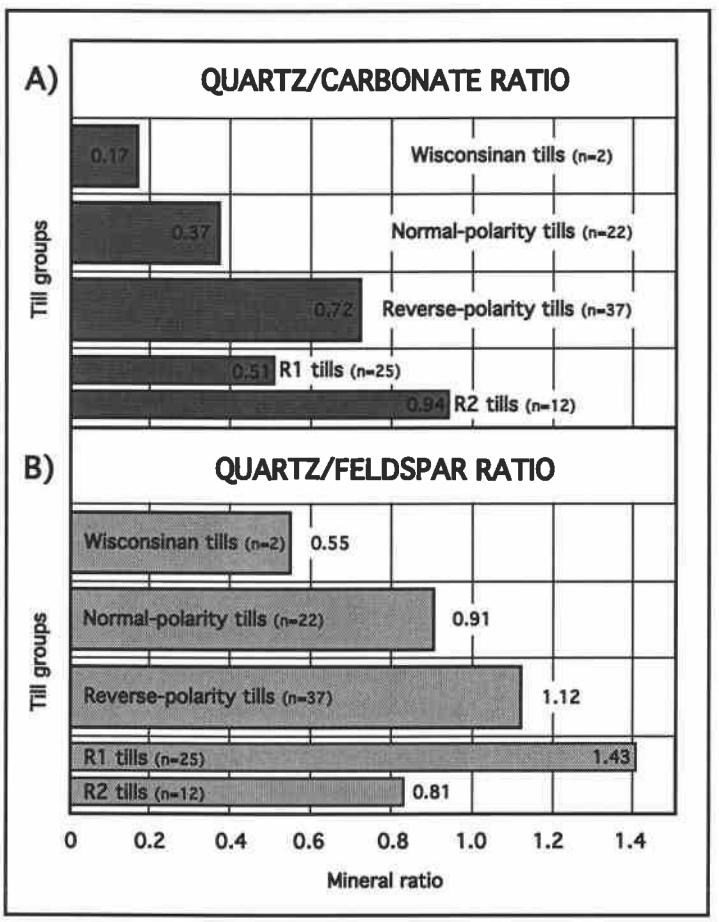

Figure 2.8: Mineral ratios in the silt (<15 μm) fraction of tills derived from the peak areas of minerals. (A) ratio of quartz/calcite+dolomite (quartz/carbonate); (B) ratio of quartz/feldspar.

The group of feldspar minerals shows a wide range in composition, which is reflected in XRD patterns by subtle variations in the position of the individual feldspar peaks. Therefore, in order to obtain information on the "total" feldspar content of samples, we integrated the total area under the segment comprising most of the feldspar peaks in the XRD patterns of samples. The XRD intensities of feldspar peaks are also very sensitive to crystal orientation on the smeared slides, and thus have the potential to produce apparent large intensities if the feldspars of the analyzed samples have any preferred orientation. For these reasons, ratios involving feldspars should be regarded as highly qualitative and attention should only be placed on large changes between the main till groups (i.e. reverse- and normal-polarity tills). Our results reveal significant changes in the till groups and indicate that the reverse polarity tills show the largest quartz/feldspar ratio (1.12), followed by the normal-polarity tills (0.91), and the Wisconsinan tills (0.55) (Figure 2.8b; Table 2.3). This trend is related to some combination of an increase of feldspar and a decrease of quartz in progressively younger glacial sequences.

2.7 Stratigraphic implications

2.7.1 Comparisons to previous work

In this study, we have documented a compositional change in the glacial sedimentary sequences of the midcontinent that is best seen in the clast lithological content of tills, although the mineralogy of the clay and silt fractions of tills also shows significant changes between the reverse- and normal-polarity tills. Boellstorff (1978b) previously established a stratigraphic framework for the study area based on general till compositional variations in younging glacial sequences that are similar to those we describe here. In this framework, Boellstorff (1973, 1978b) used the heavy mineral content of the fine-sand fraction of tills and the lithology of the pebble fraction of tills to distinguish three groups of tills (A, B, and C tills). The A and C tills were further

divided into subunits based on their relations to paleosols and their paleomagnetic signature (Figure 2.2), although these subunits could not be distinguished using their lithological or heavy-mineral content.

Although Boellstorff's stratigraphic framework was not intended for regional use, subsequent stratigraphic studies elsewhere in the midcontinent have correlated till units to those defined by Boellstorff (Hallberg, 1980; Aber, 1991; Kemmis et al., 1992; Rovey and Kean, 1996; Colgan, 1999). In the context of relatively weak geochronological constraints, namely the absence of tephras and the small number of paleomagnetic analyses, these correlations were largely based on till compositional changes. Some of these correlations were also based on clay mineralogy and/or grain size analyses, even though Boellstorff (1973, p. 59) could not distinguish tills on the basis of these two criteria.

Despite the wide use of Boellstorff's framework, the occurrence of different till groups with identical polarity and with nearly similar composition (e.g. B and A4 tills) makes till unit recognition difficult, and this problem is further accentuated on a regional scale. For instance, the validity of A4 till as a separate stratigraphic unit has been questioned in a stratigraphic study in north-central Missouri (Rovey and Kean, 2001). However, all these studies demonstrate a similar stratigraphic succession whereby older tills are distinguished from younger tills by their composition. Some pre-Illinoian till sequences at various locations in the midcontinent region also show a change in polarity, and this provides a chronological marker for regional correlations (Rovey and Kean, 2001). Consequently, these compositional changes and occurrence of magnetic reversals emerge as recurrent characteristics of midcontinent glacial sequences that can be used to improve the regional stratigraphic framework.

2.7.2 Proposed stratigraphic framework

Similar to previous studies (e.g. Aber, 1991; Rovey and Kean, 1996), we have documented compositional criteria that enable the identification of till groups of different age. In particular, our results are in agreement with those of Boellstorff in showing a change in clast lithology with time. We also report a high proportion of expandable clay minerals in normal-polarity tills and a lower proportion of expandable clays in reverse-polarity tills that is consistent with a regional pattern documented in eastern Iowa (Hallberg, 1980; Kemmis et al., 1992) and north-central Missouri (Rovey and Kean, 1996). However, we provide additional mineralogical criteria that, with the clast lithology data and within the context of our extensive paleomagnetic dating control at each site investigated, identify three regionally significant lithostratigraphic units (Figure 2.9, 2.10).

In light of these findings, we propose a simple stratigraphic framework based on the temporal changes in till composition, as constrained by stratigraphic relations of till units to each other, to volcanic ashes, and to the Brunhes/Matuyama magnetic reversal (Figure 2.9). This stratigraphic framework represents a revision of the till stratigraphy proposed by Boellstorff in two ways. First, our intermediate-age till group (R1 tills) includes the B and A4 tills, and our youngest pre-Illinoian till group (N tills) includes the A3, A2, and A1 tills. Secondly, we cannot distinguish regional subgroups by composition alone; paleomagnetic measurements are also needed. These conclusions are based on the results presented above as well as on data we obtained for two sites at which Boellstorff reported B and A4 tills. For instance, Boellstorff interpreted the upper till at site 1 as A4 till despite the lack of paleomagnetic measurements on that unit. Our results, however, indicate that the polarity of this unit is normal, thus ruling out the possibility that this is an A4 till (A4 tills are reversed). Moreover, the composition of this unit is comparable to other normal-polarity tills. In addition, Boellstorff interpreted two tills at site 10 that are separated by highly weathered silts

and fine gravels as B and A4 tills. We are unable to assign a polarity to the upper till, but our results indicate that the lower till is reversed. The absence of compositional differences between these tills suggests that they belong to the same till group (i.e. R1 tills). These results thus indicate that the reverse-polarity B and A4 tills cannot be distinguished from each other by composition.

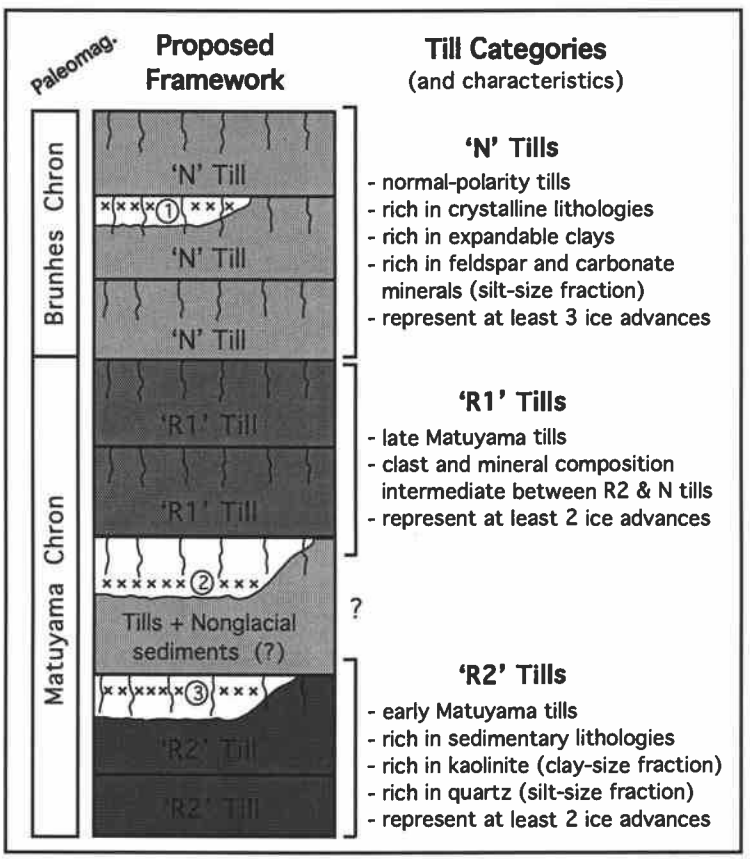

Figure 2.9: Proposed stratigraphic framework for the north-central U.S. region. See text for details. Legend for symbols and tephra ages is the same as in Figure 2.2.

Nevertheless, each of our three till groups contains several till units that are separated by paleosols, thus suggesting, within the present stratigraphic setting, that each of these groups may represent multiple ice advances. However, determining the exact number of advances, their age and duration, and their significance to the regional stratigraphy requires further dating control. Consequently, the main distinction of our proposed framework relative to Boellstorff's is that it indicates that individual pre-

Illinoian lithostratigraphic units cannot be correlated accurately, but instead can simply be regrouped under categories defined by broad chronological constraints.

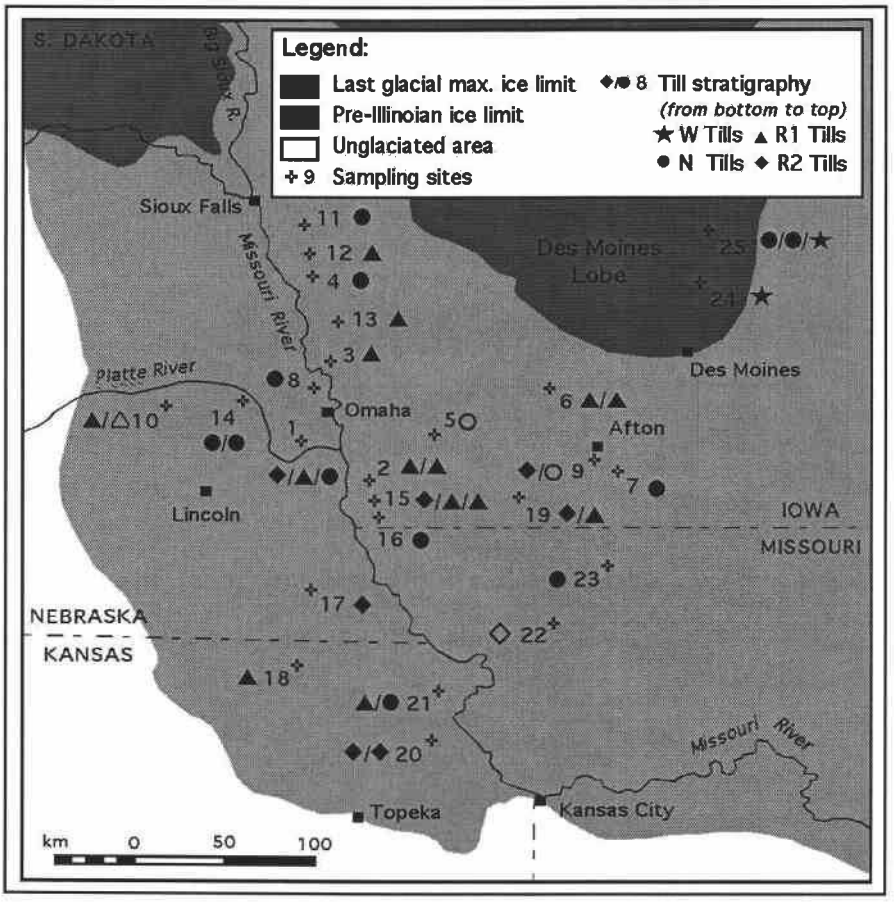

Figure 2.10: Distribution of the various till units at each stratigraphic site with respect to the three till categories identified. Open symbols correspond to till units with indeterminate magnetic polarity but of general clast composition suggesting their belonging to one of the three till groups. Volcanic ash localities: sites 4, 8, 9, and 10.

The oldest till group, **R2 tills**, consists of till units with a reversed polarity and >77% of sedimentary clasts. Low amounts of expandable clays, substantial amounts of kaolinite, and the absence of chlorite characterize the clay mineralogy of R2 tills. The mineralogy of the silt fraction of R2 tills is rich in quartz and depleted in calcite, dolomite, and feldspar. This till group includes a till unit that underlies the 2.0-Ma Huckleberry Ridge ash, thus indicating deposition sometime between ~2.5 Ma (onset of Northern Hemisphere glaciations) (Mix et al., 1995) and 2.0 Ma. Although we do not

know whether the other R2 tills were deposited during this interval, the close compositional affinities of the remaining R2 tills with the >2 Ma unit suggest that the R2 tills may have been deposited during the early part of the Matuyama Chron. The R2 till group is similar in composition to the C tills of Boellstorff (1973, 1978b), and R2 tills were found in all four states investigated.

The intermediate group, **R1 tills**, comprises till units also with a reverse polarity but with a lithological composition ranging from 70% to 55% of sedimentary clasts. The clay mineralogy of R1 tills is similar to that of R2 tills. The silt fraction of R1 tills is slightly richer in carbonate minerals than R2 tills, but contains about the same amount of feldspar as the R2 tills. The R1-till group includes two till units that overlie the 1.3-Ma Mesa Falls ash, thus indicating at least two glaciations between 1.3 Ma and 0.8 Ma. The compositional similarity of the other R1 tills suggest that they may have been deposited during this interval, although further dating control is required to support this assumption. The R1 till group includes the B and A4 till types of Boellstorff (1973, 1978b). R1 tills were found in all states but Missouri.

Finally, the youngest group of pre-Illinoian tills, **N tills**, consists of till units with a normal polarity and with a lithological content of <62% of sedimentary clasts. The clay mineralogy of N tills is characterized by the appearance of minor chlorite, the largest amount of expandable clays and the lowest amount of kaolinite of the three groups of pre-Illinoian tills. N tills also show the greatest amount of feldspar and carbonate minerals in the silt fraction. This group includes at least one till unit overlain by the 0.6-Ma Lava Creek ash, thus suggesting that some of these units were deposited between 0.8-0.6 Ma, but also later, as indicated by two sites with a till overlying the 0.6 Ma ash (Boellstorff, 1973). The N till group is considered to include the A1, A2, and A3 tills of Boellstorff (1973, 1978b). N tills were found in all four states investigated.

2.8 Conclusions

Lithological and mineralogical analyses of pre-Illinoian glacial deposits indicate that the glacial sequences of the north-central U.S. display a wide variation in composition. Paleomagnetism analyses clearly identified units with normal polarity (Brunhes Chron) and reverse polarity (Matuyama Chron). One important contribution of our paleomagnetism study is to remove the ambiguity related to the magnetic polarity of the oldest glacial deposits of the study area. For instance, our data indicate that the till underlying a 2.0-Myr ash-bearing silt unit has a reverse polarity, thus suggesting deposition during the earlier part of the Matuyama Chron. The compositional data indicate that the multiple-till sequences consistently show an upward (younging) increase in the amount of crystalline lithologies in tills. When placed in the context of paleomagnetic data and the three volcanic ashes of known age, however, we find a compositional change whereby clasts in the older (> 0.8 Ma) reversely magnetized tills (Matuyama Chron) contain a relatively high percentage of sedimentary lithologies and a corresponding low percentage of crystalline lithologies, whereas the younger (< 0.8 Ma), normally magnetized tills are relatively depleted in sedimentary lithologies and rich in crystalline rocks. Two groups can be further distinguished within the reverse-polarity tills on the basis of their composition. The changes in the mineralogy of the clay and silt fractions of the reverse- and normal-polarity tills also show significant changes. When compared to the reverse-polarity tills, the clay fraction of the normal-polarity tills is rich in expandable minerals and poor in kaolinite. The silt fraction of the normal-polarity tills is also enriched in carbonate and feldspar minerals, and depleted in quartz with respect to the reverse-polarity tills. Taken together, these data may reflect an unroofing sequence of the Canadian Shield that involved the removal of a former saprolite mantle (weathered rocks) by ice sheet erosion, progressively exposing a greater surface area of fresh crystalline rocks (Clark and Pollard, 1998).

Based on these results and lithostratigraphic considerations, we propose a simple stratigraphic framework in which we divide the pre-Illinoian tills into three groups. The oldest group, R2 tills, consists of reverse-polarity tills having >77% of sedimentary lithologies. The intermediate group, R1 tills, shows a transitional composition between the two other pre-Illinoian till groups, and contains till units that were deposited sometime between 1.3 and 0.8 Ma. The younger group, N tills, is composed of normal-polarity tills which show approximately equal proportions of sedimentary and crystalline lithologies. The low resolution of our chronology prevents the identification of individual ice advances in the study area, but within the present stratigraphic context, the presence of paleosols developed in tills of different age and composition suggest a record of at least seven pre-Illinoian advances of the Laurentide ice sheet to a position south of the Last Glacial Maximum.

2.9 Acknowledgements

We thank Greg Balco, Howard Hobbs, and Charles Rovey for critically reviewing the manuscript. Art Bettis and Joe Mason provided useful discussions in the field and assistance in finding stratigraphic sections. Joe Mason and the drilling crew of the Nebraska Geological Survey were instrumental in obtaining core samples. Supported by the National Science Foundation (ATM 9709684), a Geological Society of America Graduate Research Grant, and the Research Funds in Natural Science of the Province of Quebec (FCAR).

2.10 References

Aber, J.S., 1991, The glaciation of northeastern Kansas: Boreas, 20, p. 297-314.

Aber, J.S., 1999, Pre-Illinoian glacial geomorphology and dynamics in the central United States, west of the Mississippi, *In* Mickelson, D.M., and Attig, J.W., eds., Glacial Processes Past and Present: Boulder, Colorado, Geological society of America Special Paper 327, p. 113-119.

Boellstorff, J., 1973, Tephrochronology, petrology, and stratigraphy of some Pleistocene deposits in the Central Plains, USA [Ph.D. Thesis]: Baton rouge, Louisiana State University, 197 p.

Boellstorff, J., 1976, The succession of late Cenozoic ashes in the Great Plains: a progress report: Guidebook Series 1, Kansas Geological Survey, p. 37-71.

Boellstorff, J., 1978a, A need for redefinition of North American Pleistocene stages: Transactions of the Gulf Coast Association of Geological Societies, Transactions, v. 28, p. 65-74.

Boellstorff, J., 1978b, Chronology of some Late Cenozoic deposits from the central United States and the Ice Ages: Transactions of the Nebraska Academy of Science, v. 6, p. 35-49.

Boellstorff, J., 1978c, North American Pleistocene stages reconsidered in the light of probable Pliocene-Pleistocene continental glaciation: Science, v. 202, p. 305-307.

Clark, P.U. and Pollard, D., 1998, Origin of the middle Pleistocene transition by ice sheet erosion of regolith: Paleoceanography, v. 13, p. 1-19.

Colgan, M.P., 1999, Early middle Pleistocene glacial sediments (780000-620000 BP) near Kansas City area, northeastern Kansas and northwestern Missouri, USA: Boreas, v. 28, p.477-489.

Dort, W. Jr., 1985, Field evidence for more than two early Pleistocene glaciations of the central Plains: Ter-Qua Symposium Series, v. 1, p. 41-51.

Easterbrook, D.J. and Boellstorff, J., 1984, Paleomagnetism and chronology of Early Pleistocene tills in the central United States, *in*: Mahaney, W.C., ed., Correlation of Quaternary Chronologies: Norwich, England, GeoBooks, p. 73-90.

Gansecki, C.A., Mahood, G.A., and McWilliams, M., 1998, New ages for the climatic eruptions at Yellowstone: Single-crystal $^{40}Ar/^{39}Ar$ dating identifies contamination: Geology, v. 26, p. 343-346.

Hallberg, G.R., 1986, Pre-Wisconsinan glacial stratigraphy of the central plains region in Iowa, Nebraska, Kansas, and Missouri: Quaternary Science Reviews, v. 5, p. 11-15.

Hallberg, G.R., 1980, Pre-Wisconsinan stratigraphy in southeast Iowa, *in*: Hallberg, G.R., ed., Illinoian and pre-Illinoian stratigraphy of southeast Iowa and adjacent Illinois: Iowa City, Iowa Geological Survey Technical Information Series 11, p. 1-110.

Hays, J.D., Imbrie, J. and Shackleton, N.J., 1976, Variations in the Earth's orbit: Pacemaker of the ice ages: Science, v. 194, p. 1121-1132.

Izett, G.A., 1981, Volcanic ash beds: Recorders of upper Cenozoic silicic pyroclastic volcanism in the western United States: Journal of Geophysical Research, v. 86, p. 10200-10222.

Kemmis, T.J. Bettis, E.A. III, and Hallberg, G.H., 1992, Quaternary Geology of Conklin Quarry: Guidebook Series no. 13, Iowa Department of Natural Resources, 41 p.

Kirschvink, J.L., 1980, The least-squares line and plane and the analysis of paleomagnetic data: Geophysical Journal of the Royal Astronomical Society, v. 62, p. 699-718.

Mix, A.C., Pisias, N.G., Rugh, W., Wilson, J., Morey, A. and Hagelberg, T.K., 1995, Benthic foraminifer stable isotope record from site 849 (0-5 Ma): Local and global

climate changes: N.G. Pisias et al. eds., Procedures of Ocean Drilling Program Scientific Results, v. 138, p. 371-342.

Richmond, G.M. and Fullerton, D.S., 1986a, Introduction to Quaternary glaciations in the United States of America: Quaternary Science Reviews, v. 5, p. 3-10.

Richmond, G.M. and Fullerton, D.S., 1986b, Summation of Quaternary glaciations in the United States of America: Quaternary Science Reviews, v. 5, p. 183-196.

Reed, E.C., Dreezen, V.H., 1965, Revision of the classification of the Pleistocene deposits of Nebraska: Nebraska Geological Survey Bulletin, v. 23, 65 p.

Reynolds, Jr., R.C., 1985, NEWMOD© A computer program for the calculation of one-dimensional diffraction patterns of mixed-layered clays: R.C. Reynolds, Jr., 8 Brook Dr., Hanover, NH.

Rovey, C.W. II, Kean, W.F., 1996, Pre-Illinoian stratigraphy in north-central Missouri: Quaternary Research, v. 45, p. 17-29.

Rovey, C.W. II, Kean, W.F., 2001, Paleomagnetism of the Moberly formation, northern Missouri, confirms a regional magnetic datum within the pre-Illionian glacial sequence of the midcontinental USA: Boreas, v. 30, p. 53-60.

CHAPTER 3

Geochemical constraints on the regolith hypothesis for the middle Pleistocene transition

M. Roy [†], P.U. Clark [†], G.M. Raisbeck [‡], F. Yiou [‡]

[†]Department of Geosciences,
Oregon State University, Corvallis, OR 97331-5506, USA

[‡]Centre de Spectrométrie Nucléaire et de Spectrométrie de Masse,
IN2P3-CNRS, Bât. 108, 91405, Orsay Cedex, France

To be submitted to Earth and Planetary Science Letters.

3.1 Abstract

We examined the composition of glacial deposits from the north-central U.S. to evaluate the hypothesis that the middle Pleistocene transition (MPT) occurred by erosion of a regolith and subsequent exposure of the underlying Canadian Shield rocks by the Laurentide Ice Sheet. The petrology, mineralogy, and geochemistry of the silicate fraction of tills spanning the past 2 Ma indicate that late Pliocene tills are depleted in crystalline lithologies, unstable minerals, and major-element oxides (CaO, MgO, Na_2O) derived from feldspars and ferromagnesians, and enriched in kaolinite, quartz (SiO_2), iron oxides (FeO) and TiO_2-bearing resistates, and meteoric ^{10}Be. In contrast, early and middle Pleistocene tills show a gradual enrichment in crystalline lithologies, stable minerals, and major-oxides derived from feldspars and ferromagnesians, and depletion in meteoric ^{10}Be, whereas late Pleistocene tills show major-element concentrations closely resembling that of the shield rocks. Marine isotope records of Sr, Os, and Hf show significant changes around the MPT that support the removal of a regolith and the exhumation of fresh silicate rocks. These results thus indicate that ice sheets initially expanded on a highly weathered bedrock and progressively excavated a much fresher rock source with time, thereby suggesting that a change in subglacial substrate during the late Cenozoic best explains the geological constraints on the MPT that are imposed by records of ice volume and ice sheet extent. Specifically, the regolith favored the development of thin but areally extensive ice sheets that responded linearly to the dominant (23 and 41 kyr) orbital forcing. The subsequent unroofing of crystalline bedrock by glacial erosion gave rise to the MPT and allowed the edification of larger volume ice sheets of similar extent that responded nonlinearly to forcing, and which experienced rapid deglaciation ~100 kyr following mechanisms intrinsic to the dynamics of large ice sheets.

3.2 Introduction

Oxygen isotope ($\delta^{18}O$) records preserved in deep-sea sediments indicate that following the development of Northern Hemisphere ice sheets at ~2.4 Ma, global ice volume waxed and waned at periodicities (23, 41, 100 ka) similar to the variations of the Earth's orbital parameters (precession, tilt, eccentricity) (Hays et al., 1976; Imbrie et al., 1984; Mix et al., 1995). High-resolution $\delta^{18}O$ records, however, show a transition in the middle Pleistocene (~1.2 Ma) from small ice-volume fluctuations that varied largely at 41-kyr cycles to larger ice-volume fluctuations that varied predominantly at 100-kyr cycles despite the fact that radiation forcing remained unchanged across that interval (Pisias and Moore, 1981; Ruddiman et al., 1989; Imbrie et al., 1993; Mix et al., 1995).

A number of hypotheses have been proposed to explain this middle Pleistocene transition (MPT), but a consensus on its origin has yet to emerge (Imbrie et al., 1993; Elkibbi and Rial, 2001). Here we address this issue by testing a hypothesis stipulating that the MPT is related to a change from ice sheets underlain entirely by soft beds to ice sheets underlain by a mixture of hard and soft beds (Clark and Pollard, 1998). This hypothesis is based on the $\delta^{18}O$ record that indicates a large increase in global ice volume after the MPT, whereas continental records of glaciations indicate a similar areal extent of ice sheets before and after the MPT (Figure 3.1), thus indicating that the MPT also involves a change from thin to thick ice sheets. Studies of modern and former ice sheets indicate that ice-sheet size and dynamics are strongly dictated by the geology of the subglacial substrate (Boulton and Jones, 1979; Alley et al., 1986, Clark et al., 1999). These observations thus suggest that glaciological processes may have played a significant role in the origin of the MPT as well as in the mechanisms that produced the 100-kyr cycle (Clark et al., 1999).

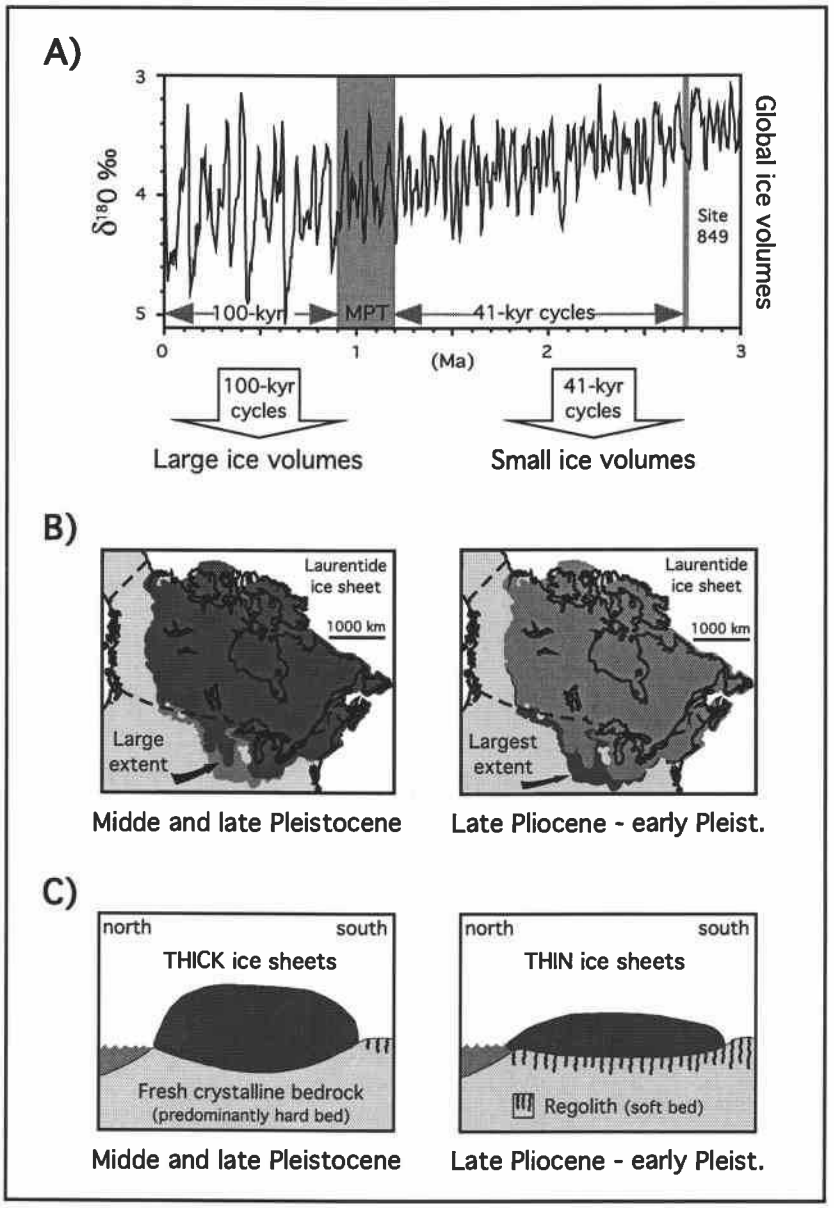

Figure 3.1: A) Oxygen isotope record showing the middle Pleistocene transition (MPT). The MPT is change in the amplitude and frequency of ice volumes reflecting a shift from small volume to large volume ice sheets ($\delta^{18}O$ data from Mix et al., 1995). B) Maximum extent of the Laurentide ice sheet. The areal extent of the small volume (pre-MPT) ice sheets is similar or greater than the larger volume (post-MPT) ice sheets. C) These observations indicate that the MPT also represents a change from thin to thick ice sheets. The change in ice sheet thickness may reflect the glacial erosion of a regolith (wiggly lines) which maintained thin ice sheets prior to the MPT.

3.3 Strategy

Clark and Pollard (1998) proposed that the change in basal boundary conditions of ice sheets responsible for the MPT resulted from the glacial erosion of a thick regolith mantle that had developed through prolonged chemical weathering of crystalline bedrock prior to the onset of late Cenozoic Northern Hemisphere glaciation. Before the MPT, the regolith favored the development of thin ice sheets that responded linearly to the 41-kyr orbital forcing. Successive glaciations eventually gave rise to the MPT through the erosion of the regolith and unroofing of unweathered crystalline bedrock, thereby providing hard-bed conditions that caused a fundamental change in the response of ice sheets to orbital forcing.

Our strategy in evaluating the regolith hypothesis for the MPT is based on the fact that the bulk mineralogy and geochemistry of the regolith will be substantially distinct from that of the parent bedrock (Goldich, 1938; Nesbitt and Young, 1989; Setterholm and Morey, 1995). Accordingly, tills derived from erosion of the regolith should have a compositional signature that is distinct from tills derived largely from unweathered bedrock. Here we document the geochemical, mineralogical, and petrographic composition of late Pliocene-Pleistocene glacial sedimentary sequences of the north central U.S. (Figure 3.2) to evaluate whether a compositional change occurs, and to determine whether this change reflects a shift from erosion of a regolith to a fresh bedrock source during the middle Pleistocene.

3.4 Late Cenozoic glacial stratigraphy of the midcontinent

The midcontinent region is underlain by upper Pennsylvanian limestone, shale, and sandstone bedrock; most sections investigated lie directly on carbonate bedrock. This region preserves extensive sedimentary sequences that record evidence of late Pliocene and Pleistocene advances of the Laurentide ice sheet (LIS). The midcontinent

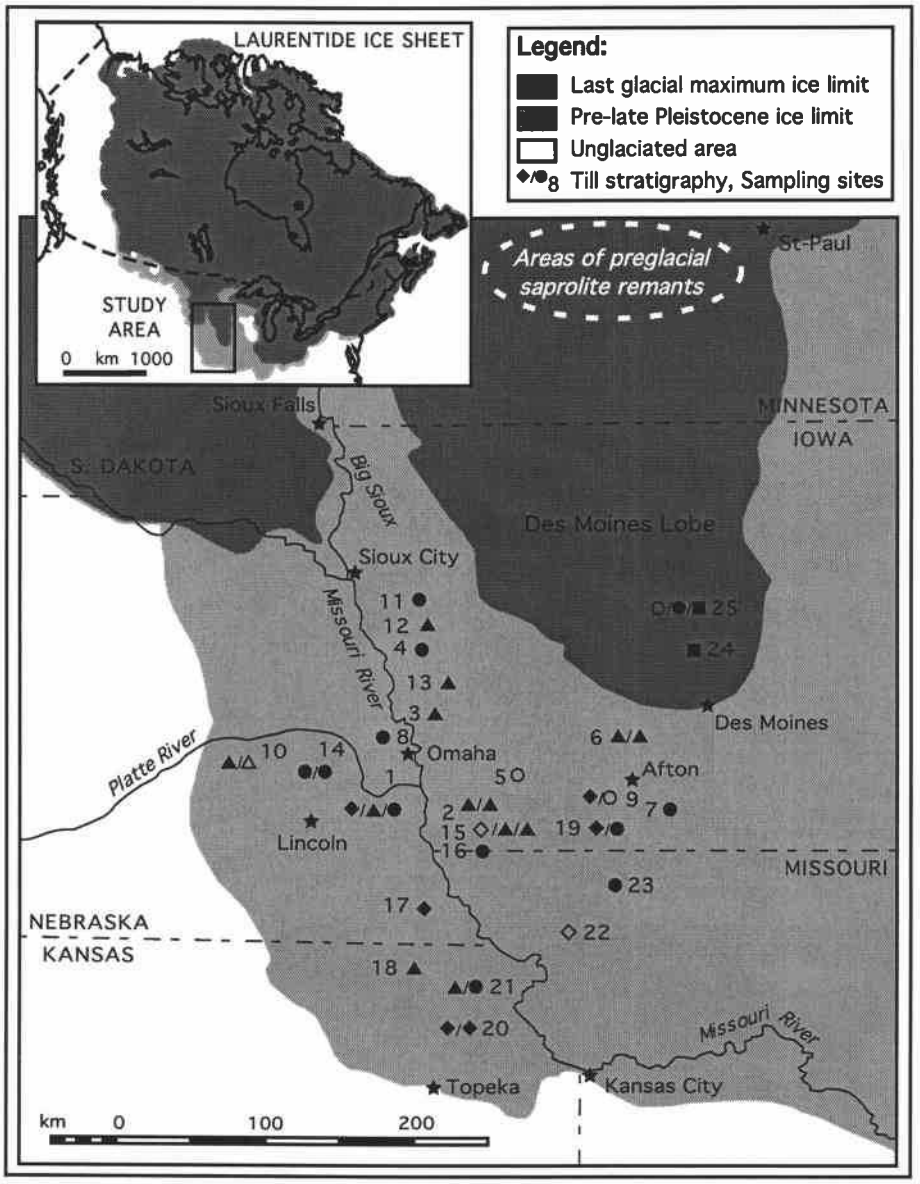

Figure 3.2: Location of the stratigraphic sections investigated and maximum extent the late Pliocene – early Pleistocene (pre-Illinoian) and last glacial maximum (LGM) ice sheets. Symbols correspond to the till stratigraphy exposed at each site (from bottom to top): ◆ are late Pliocene 'R2 tills'; ▲ are early Pleistocene 'R1 tills'; ● are middle Pleistocene 'N tills'; ■ are late Pleistocene 'LGM tills'. Open symbols correspond to till units with uncertain magnetic polarity but of lithological composition suggesting their belonging to one of the four till groups (*see* text for explanations on till groups). Volcanic ash localities: sites 4, 8, 9, and 10.

stratigraphy consists of multiple tills interbedded with paleosols and three volcanic ashes derived from eruptions of the Yellowstone caldera in Wyoming: Huckleberry

Ridge ash bed (2.003 Ma), Mesa Falls ash bed (1.293 Ma), and Lava Creek ash bed (0.602 Ma) (Izett, 1981; Gansecki et al., 1998). A till underlying an ash-bearing silt unit indicates that the oldest glacial deposit is more than 2.0 Ma (Boellstorff, 1978b). Since then, the LIS has advanced southward across the area on at least seven other occasions (Roy et al., 2003). Stratigraphic considerations indicate that ice advances younger than ~200 ka have not reached the area (Hallberg, 1986). Minimum age estimates from cosmogenic dating of striated bedrock outcrops in southwestern Minnesota indicate that these striations were made by overriding ice ~575 kyr ago (Bierman et al., 1999), thereby suggesting that the region south of Minnesota was not affected, at least significantly, by subsequent glaciation during marine isotope stage 6. During the last glaciation, however, the Des Moines lobe advanced in the northern sector of the study area (Figure 3.2). Tills are typically fine-grained, compact, and matrix-dominated deposits. The fine-grained nature of the tills prevents groundwater migration, thereby limiting post-glacial weathering.

Roy et al. (2003) developed a chronological framework for the midcontinent glacial sequences based on paleomagnetism of glacial and nonglacial deposits, and the stratigraphic relation of the three volcanic ashes to the composition of till units. Magnetic polarity distinguished tills deposited during the Brunhes Normal Chron from those deposited during the Matuyama Reverse Chron. Glacial deposits exhibit large variations in composition that, when placed in the context of the paleomagnetic and ash chronology, indicate significant lithological and mineralogical differences between tills of different age. From these relations, Roy et al. (2003) identified three pre-Illinoian till groups: an early Matuyama group (**R2 tills**), a late Matuyama group (**R1 tills**), and a middle Pleistocene Brunhes group (**N tills**) (Figure 3.3). Tills deposited around the last glacial maximum (LGM) ~17 ka represent a fourth group (**LGM tills**).

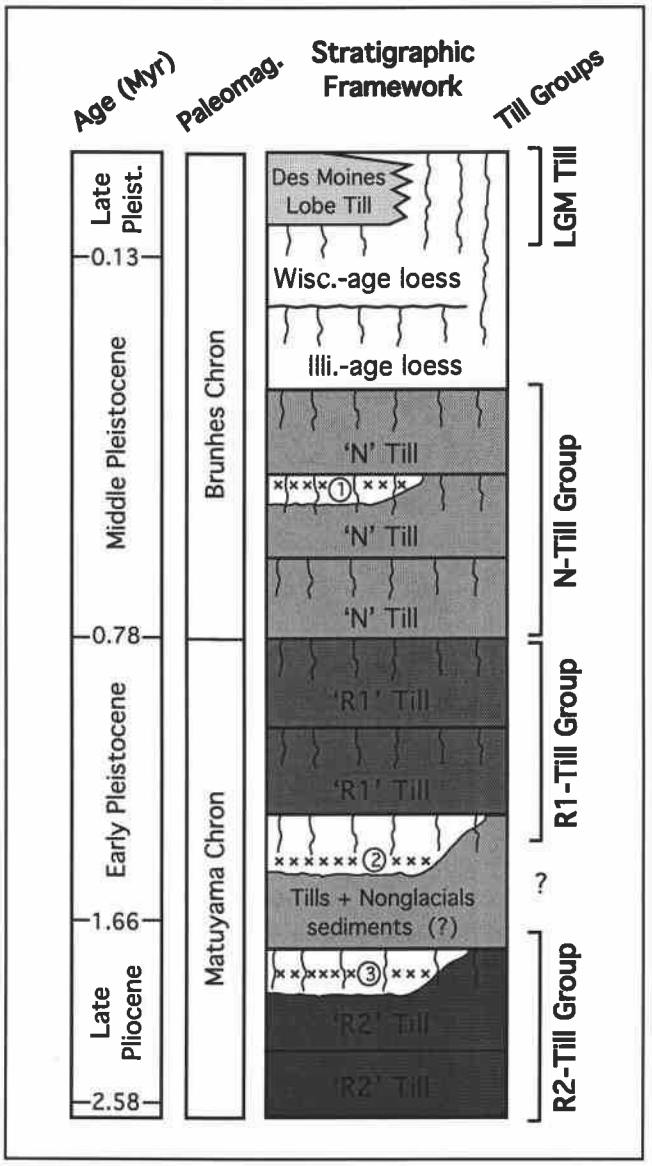

Figure 3.3: Stratigraphic framework for the glacial deposits of the study area (modified from Roy et al., 2003). The current chronological methods do not allow the identification of individual ice advance, thus the till groups may represent more ice advances than physically recognized in the field. Till groups: R2 tills consist in early Matuyama tills representing at least two ice advances; R1 tills are late Matuyama representing at least two ice advances; N tills consist in normal polarity tills representing at least three advances. Paleosols indicated by the wavy vertical lines. Tephras indicated by x's: (1) 0.602-Ma Lava Creek ash; (2) 1.293-Ma Mesa Falls ash; (3) 2.003-Ma Huckleberry Ridge ash (ages after Gansecki et al., 1998). LGM is last glacial maximum, Wisc. and Illi. are Wisconsinan and Illinoian glacial stages, respectively.

3.5 Methods

We investigated the composition of glacial sedimentary sequences located in Iowa, Nebraska, Kansas, and Missouri (Figure 3.2) in order to document geochemical variations that may indicate a change in the erosion of a regolith to fresh bedrock with time. We obtained till samples from 25 stratigraphic sections exposed in rock quarries, roadcuts, and along river banks, and drilled sediment cores at three localities where previous work reported volcanic ashes interbedded with tills (Boellstorff, 1973, 1976, 1978a). Prior to sampling, sediment exposures were cleaned to a width of ~1 m and a depth of ~0.5 m, and fresh, unweathered material was collected for analyses. We also sampled tills deposited during the LGM in order to obtain a more complete range of compositional variations over the spectrum of late Cenozoic glaciations. These deposits allow direct comparisons between the older tills and tills deposited under a fully developed 100-kyr cycle.

Bulk till samples of ~4 kg were sieved for their clast content and the lithology of ~200 clasts (4-12.5 mm size-fraction) of 95 samples was identified under microscope. Clast lithologies were grouped into sedimentary (carbonate, sandstone, shale) and crystalline (igneous and metamorphic) lithologies. The mineralogy of the clay (<2 μm) and silt (<15 μm) fractions of 43 and 61 till samples, respectively, was analyzed using X-ray diffraction (XRD) techniques, and the abundance of the main minerals present in XRD patterns was obtained through computer-assisted semi-quantitative analysis (*see* Appendix A for details). The <2 mm fraction of 28 till samples was leached of its carbonate content and the major and trace elements of the remaining silicate fraction were obtained using X-ray fluorescence (XRF) methods.

3.6 Composition of the weathered and fresh rock source

Changes in the underlying geological substrate that may be responsible for the MPT are presumed to have occurred in the so-called hard-bedded region associated with the igneous and metamorphic rocks of the Canadian Shield (Clark and Pollard, 1998; Clark et al., 1999). We thus use the average composition of the shield bedrock as the fresh rock end-member in the hypothesis. The composition of the Canadian Shield is comparable to the average upper continental crust (AUCC), which is in turn equivalent to that of a granodiorite (Shaw et al., 1967, 1976; Wedepohl, 1995). Accordingly, we infer that the weathered end-member rock source originally developed on an AUCC-type (granodiorite) bedrock.

The long-term effect of weathering will be to change the bulk mineralogy and geochemistry of the parent rock, resulting in the formation of a saprolite (Goldich, 1938; Nesbitt and Young, 1984; 1989; Nesbitt and Markovics, 1997). The overall composition of the weathering profile will reflect the behavior of the original rock-forming minerals in response to weathering. Compositional changes caused by chemical weathering are greatest at the surface and diminish progressively with depth. The resulting upper profile of a saprolite consists of quartz, K-feldspars, and some muscovite, along with minor quantities of resistates (zircon, rutile, garnet, ilmenite). Alteration of the other major minerals gives rise to the formation of a wide range of secondary minerals (Al-rich clays and Fe-oxides). Loss of plagioclase and ferromagnesians causes an increase in the relative abundances of quartz, K-feldspars, magnetite and ilmenite in the upper part of the profile (Goldich, 1938). If the weathering conditions are intense and prolonged, desilication may also occur with the attendant transformation of smectite > kaolinite > gibbsite.

Mineral changes from weathering result in geochemical changes in the soil profile. In a saprolite, aluminosilicates and ferromagnesians will release soluble elements such

as Ca, K, Na, Mg, and K that will eventually be leached from the profile (congruent weathering). On the other hand, the release of elements with a lower solubility, that is primarily Si and Al from aluminosilicates, with minor amounts of Ti, Cr, Mn, Fe, Co, and Ni originating from ferromagnesians, will be preserved in the profile (incongruent weathering), mainly as part of secondary minerals forming the weathering products. In the case of granitoids, element mobility is generally ranked as: Ca > Na > Mg > Fe > K > Si > Al > Ti (Taylor and Eggleton, 2001). The depth at which elements are leached or accumulated is specific to each element (Nesbitt and Markovics, 1997).

Although the development of the regolith generally takes place over large areas and for long periods of time, the compositional changes from fresh rock to weathered products do not necessarily result in a thick and homogenous regolith mantle. Spatial and depth variations in weathering products are likely to be present (Ollier and Pain, 1996), and these irregularities within the regolith mantle have to be accounted for when evaluating the provenance/source of regolith-derived sediments.

In central and western Minnesota, just north of the study area, a deep saprolite developed in Precambrian bedrock is preserved under glacial deposits (Figure 3.4) (Parham, 1970; Setterholm and Morey, 1995). This saprolite averages thickness of about 30 meters, although it reaches a thickness of more than 60 m in some places. Saprolite remnants have also been found in several other locations formerly covered by the LIS, including Quebec and Labrador (Godard, 1979, Bouchard and Godard, 1984; Bouchard, 1985), the Appalachian mountains (LaSalle et al., 1985; Bouchard and Pavich, 1989), the Maritimes of eastern Canada (McKeague et al., 1983; Wang and Ross, 1989), and in the Hudson Bay region of Manitoba (Nielsen et al., 1986).

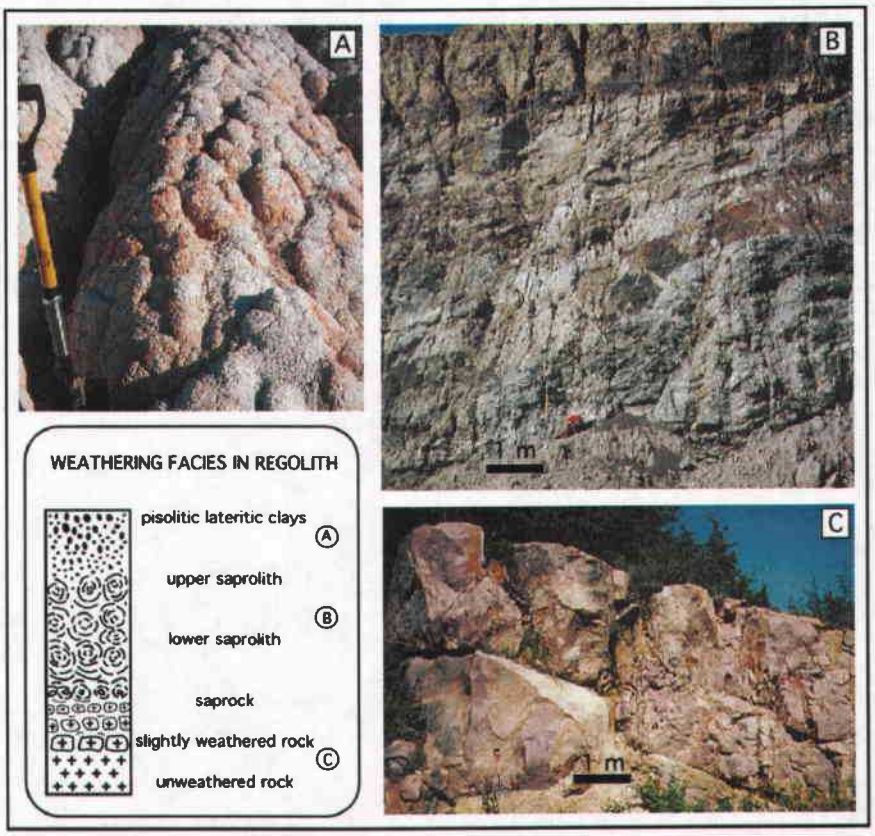

Figure 3.4: Different facies of the saprolite remnant preserved in Minnesota and their corresponding chemical index of alteration (CIA) values. A) Pisolitic lateritic clays (CIA=90); B) Weathered granite rock (saprolite; CIA=70); C) Weathering along joint-fractures isolating segments of fresh granite bedrock (CIA=55). Saprolite profile from Setterholm and Morey (1995). Note CIA values correspond to the ones reported for the till groups (*see* Fig. 6a). CIA method from Nesbitt and Young (1982).

3.7 Till compositional results

3.7.1 Till lithology and mineralogy

A significant change in the composition in the midcontinent glacial deposits is recorded in the lithology of the clast fraction of tills with an increase in the amount of crystalline lithologies in progressively younger till sequences (Boellstorff, 1978a; Roy et al., 2003). The late Pliocene R2 tills are depleted in crystalline lithologies (10-22%; 15% average), the early Pleistocene R1 tills have intermediate proportions (30-45%;

average 37%), and the middle Pleistocene N tills and the LGM tills are enriched in crystalline lithologies (38-60%; average 47%).

The mineralogy of the clay and silt fractions also shows differences among the till groups. The clay fraction of all till groups is dominated by smectite. However, small but significant decreases in kaolinite and increases in chlorite occur in the N and LGM tills relative to R2 and R1 tills (Figure 3.5a). The mineralogy of the silt fraction shows larger contrasts among different-age tills. In particular, the N tills are characterized by increases in calcite, dolomite, and feldspars, with respect to their quartz content, whereas the older reverse-polarity tills (R2 and R1 tills) are enriched in quartz (Figure 3.5b, 3.5c).

Boellstorff (1973) reported changes in the heavy mineral content of the fine-sand fraction of tills from the study area that also indicate systematic changes with age. Specifically, tills equivalent to R2 tills are enriched in weathered products (iron oxides, limonite) and depleted in unstable minerals (hornblende, biotite, apatite), relative to the N tills. Furthermore, Gravenor (1975) identified the presence of fragments of bauxite, a product of prolonged chemical weathering, in the R2-equivalent tills.

3.7.2 Till geochemistry

The major-element chemistry of a saprolite developed on a granodiorite will be largely governed by the weathering of K-feldspars and Na- and Ca-rich plagioclases, which account for ~80% of the minerals susceptible to chemical weathering (Nesbitt and Young, 1984). In addition to feldspar, the weathering products of ferromagnesian minerals will also influence the distribution of major elements in the till groups, despite their much lower abundance in the rock source (~15%). Although some MgO can be partly retained in the saprolite as smectite, most of it is released from the profile (Faure, 1998). In contrast, FeO is largely retained in as secondary iron precipitates such as

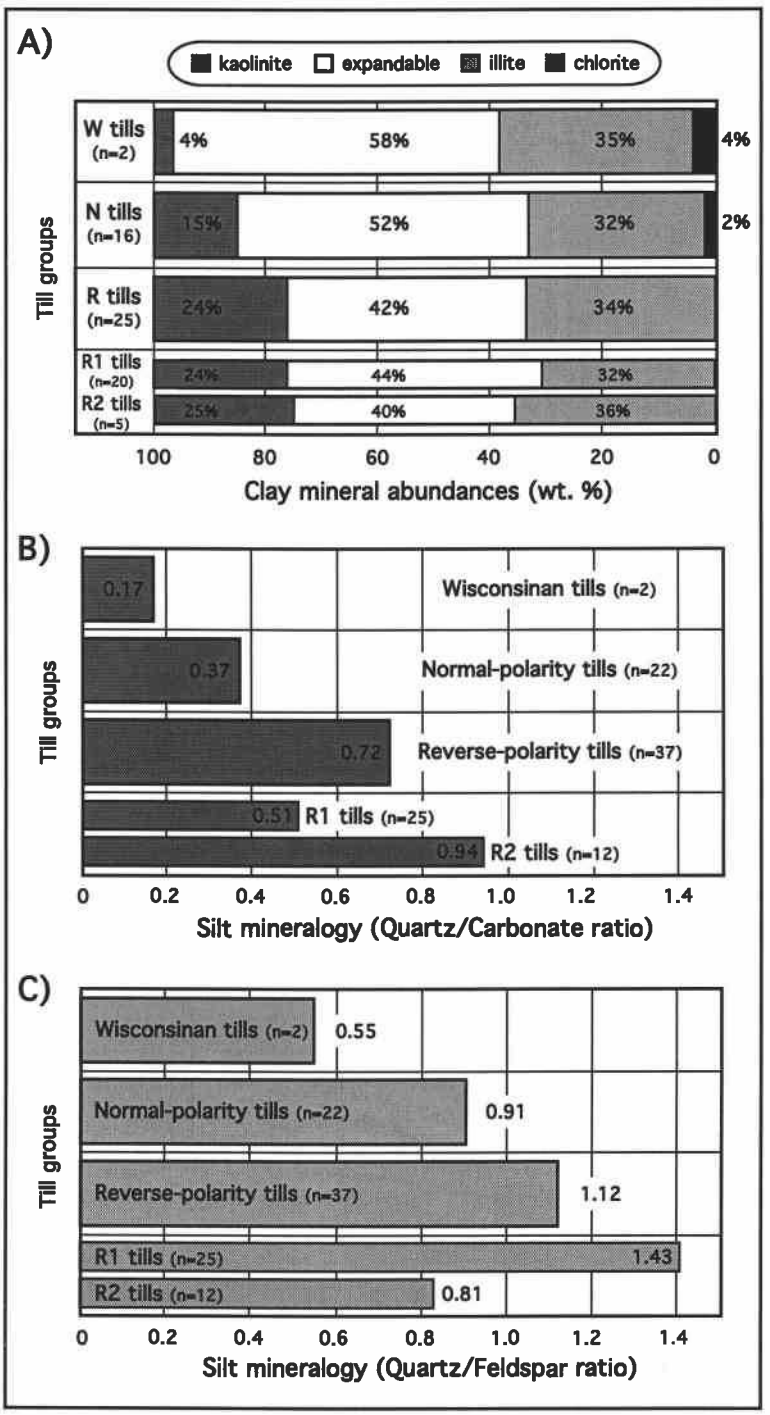

Figure 3.5: A) Mineralogy of the clay fraction (<2 μm) of the four till groups. B) Mineralogy of the silt fraction (<15 μm) of tills; ratio of quartz/calcite+dolomite (carbonate). Mineral ratios derived from the peak areas of minerals in XRD patterns; C) ratio of quartz/feldspar. The lack of differences between the clay mineralogy of R2 tills and R1 tills may be in part related to the small number of samples analyzed in the R2 till group.

goethite and hematite. Similarly, TiO_2 is highly immobile and is often adsorbed by newly formed minerals in the profile. TiO_2 is also found in resistate minerals such rutile and ilmenite. Resistates may become concentrated in the upper profile due to depletion of other mineral phases, and may thus become reliable indicators of source composition (Faure, 1998; Taylor and Eggleton, 2001). For these reasons we focus on geochemical indices that constrain the weathering of feldspars and ferromagnesians, or reflect enrichment in resistate minerals.

We first compare the results of bulk geochemical analyses of the four till groups with the major-oxide concentrations of the average upper continental crust (AUCC). In general, the concentrations of major elements of tills contrast significantly from the composition of the AUCC(Figure 3.6a; Table 3.1). The main difference between the pre-Illinoian tills and the AUCC are losses in FeO, MnO, CaO, MgO, K_2O, and Na_2O, and gains in SiO_2 and TiO_2. In contrast, the LGM tills are enriched in CaO, MnO, MgO, and Na_2O, depleted in TiO_2 and FeO, and are similar in SiO_2 and K_2O with respect to the AUCC. Some variability is observed among the N, R1, and R2 tills, but there is a clear demarcation between these tills and the LGM tills.

The LGM and R2 tills exhibit the largest geochemical differences among the four till groups whereas R1 and N tills have nearly identical compositions. When compared to a saprolite developed on granodiorite rocks from Minnesota (Setterholm and Morey,1995), the R2 tills most closely resemble the upper part of the saprolite (Figure 3.6b; Table 3.1). The remaining till groups show concentrations that are more similar to the composition of the lower saprolite and unweathered rock, with LGM tills being most like fresh granodiorite.

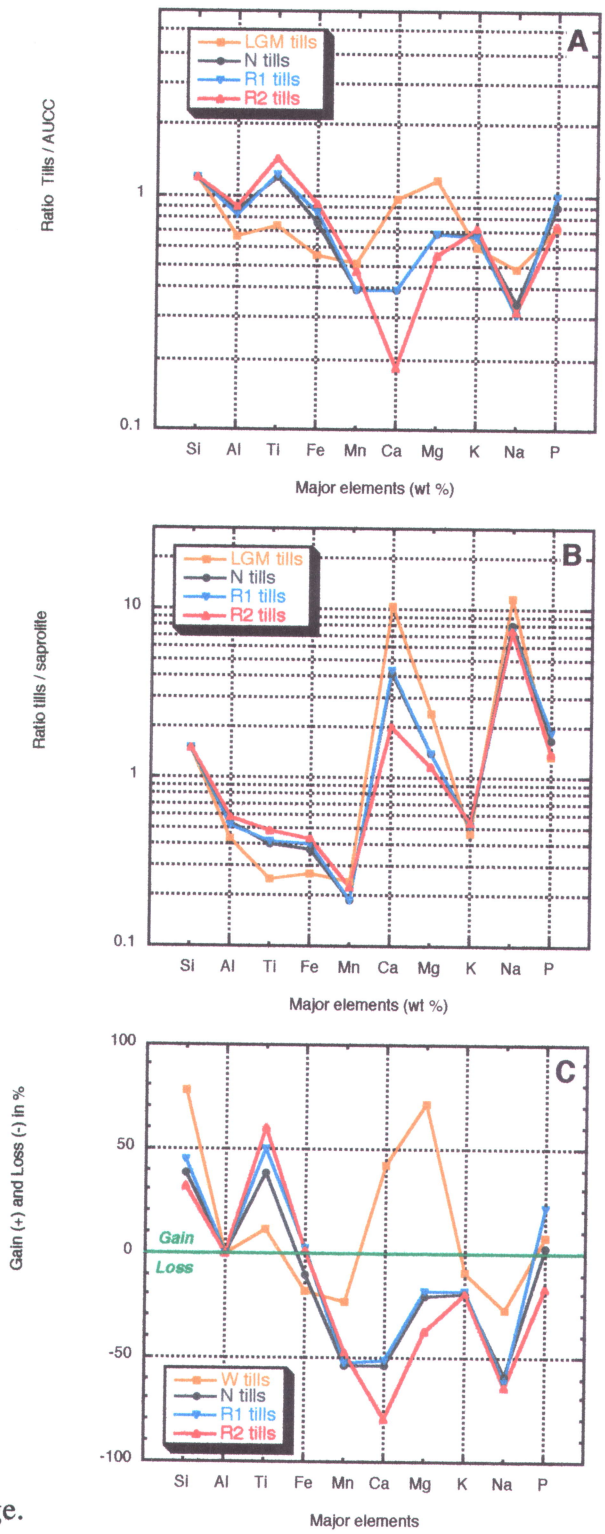

Figure 6:
See caption next page.

Figure 3.6: A) Ratio diagram comparing the average composition in major-element oxides of the four till groups to the bulk composition of the average upper continental crust (AUCC; ~granodiorite). Number of samples: 2 LGM tills, 11 N tills, 8 R1 tills, and 7 R2 tills. B) Ratio diagram comparing the average geochemical composition of till groups to the major-element composition of the upper profile of a preglacial saprolite remnant developed on a granodiorite. AUCC composition from Wedepohl (1995); saprolite composition from Setterholm and Morey (1995). C) Diagram showing net gain and loss % in major-oxides of till groups with respect to the composition of the AUCC. Because major-oxide concentrations expressed in Weight % cause apparent changes in each element that do not reflect true changes, Wt % are corrected to net gain-loss % using the Al_2O_3 concentration, assumed to have remained preserved in the weathering profile (*see* Table 3.1; Appendix B). Original XRF data are presented in Appendix C.

Table 3.1: Net[†] gain (positive) % and loss (negative) % in major-element oxides of till groups and saprolite[‡] when compared to a the composition of a fresh AUCC[§].

Major-element oxides	Till Groups				Saprolite	
	LGM tills Gain-loss (%)	N tills Gain-loss (%)	R1 tills Gain-loss (%)	R2 tills Gain-loss (%)	Up. Profile Gain-loss (%)	Low. Profile Gain-loss (%)
SiO_2	77	38	44	32	-50	-29
Al_2O_3	x	x	x	x	x	x
TiO_2	11	39	50	60	90	34
FeO*	-18	-10	2	1	32	33
MnO	-24	-54	-52	-48	35	12
CaO	42	-55	-52	-79	-94	-92
MgO	71	-21	-18	-38	-69	-65
K_2O	-10	-19	-18	-20	-17	66
Na_2O	-27	-60	-62	-64	-97	-91
P_2O_5	8	3	21	-17	-66	-74

[†]Conversion of Weight % to Net gain-loss % based on the concentration of Al oxides, assumed to have remained unchanged in the profile during weathering processes (see Appendix B for details);

[‡]Saprolite developed on granodiorite rocks (Setterholm and Morey, 1995);

[§]Average upper continental crust, equivalent to a granodiorite (Wadepohl, 1995).

The geochemical differences among till groups are consistent with the regolith hypothesis. The depletion in labile elements (CaO, MgO, and Na_2O) in the older till groups relative to the younger till groups reflects the low resistance of plagioclases and

ferromagnesians to weathering, and thus records the erosion of a progressively less-weathered bedrock source. The differences in the K_2O content of the till groups are less pronounced, which may reflect the greater resistance of K-feldspars to weathering. The slight enrichment of FeO in R2 and R1 tills relative to N and LGM tills indicates that the older till groups derive from the erosion of a source enriched in secondary iron precipitates. Similarly, R2 tills are slightly enriched in TiO_2 compared to the R1 tills and N tills, whereas LGM tills are clearly depleted in TiO_2. The TiO_2 content of the till groups indicates the erosion of a source rich in resistate minerals or reflects the low mobility of TiO_2 in the saprolite. The depletion in SiO_2 of R2 tills with respect to the R1 and N tills may also suggest the erosion of the uppermost part of the weathering profile where quartz was affected by pronounced leaching (Table 3.1). The marked increase in SiO_2 of LGM tills points towards a greater input of quartz, likely from the erosion of fresh crystalline rocks. Despite their depletion in SiO_2 concentrations relative to younger tills, R2 and R1 tills still show an enrichment in SiO_2 compared to the AUCC (Table 3.1), suggesting that quartz was a major constituent of the weathered profile.

We next evaluate differences in the geochemistry of the main till groups and their relation to source rock using ternary diagrams (Figure 3.7). These diagrams regroup several major-element constituents at once, thereby documenting the effect of weathering on the composition of the presumed fresh parent rock. The **Al-CaNa-K** diagram mainly depicts the weathering of feldspars and also contains the major elements forming the chemical index of alteration that quantifies the degree of weathering to which silicate minerals have been subjected prior to their erosion (Nesbitt and Young, 1982, 1984). The values of the till groups fall parallel to a mixing line between fresh and weathered granite rock end-members, representing the two rock sources inferred in the hypothesis (Figure 3.7a). LGM tills plot close to the feldspar join, indicative of a fresh bedrock source. The values of R2 tills generally group in a cluster indicative of the erosion of a strongly weathered rock source. R1-tills cluster in

a distribution that is between the LGM tills and the R2 tills, suggesting that R1 tills were derived from the erosion of a rock source slightly less weathered than the R2-till rock source, but not as fresh as the source of LGM tills. We find similar differences between the R2, R1, and LGM tills on the **Mg-Ca-NaK** and **Al-CaNaK-FeMg** diagrams (Figures 3.7b, 3.7c), which show the effect of weathering on ferromagnesians with respect to Ca- and Na-plagioclase, and K-feldspars. The **Si/10-CaMg-NaK** diagram (Figure 3.7d) has the advantage of comparing the geochemistry of all till groups to different rock sources.

In all cases, the distribution of N-till geochemical values overlaps the range spanned by the clusters of R2 and R1 tills. The geochemistry of N tills is, at first hand, surprising since it is opposite to their lithological and mineralogical content which suggest that N tills were derived primarily from the erosion of a fresh crystalline rock source, nearly similar in composition to that of LGM tills. We interpret the geochemical distribution of N-till values to reflect recycling and mixing of older deposits (R2 and R1 tills) as well as incorporation of fresh, unweathered rock.

In the context of the results described above, the data suggest that R2 tills come from the erosion of a highly weathered rock source, whereas R1 tills were still derived from weathered rock, but from material that had originally been lower in the weathering profile and thus less enriched in weathered products. On the other hand, the data of LGM tills suggest that subsequent glacial erosion progressively exposed fresher crystalline bedrock with time. This should have provided a source of unweathered lithologies and mineralogies to N tills, but recycling of preexisting tills may have complicated their geochemical signature by providing a source of weathered material, thereby explaining the inconsistencies in the distribution of N-till geochemical values.

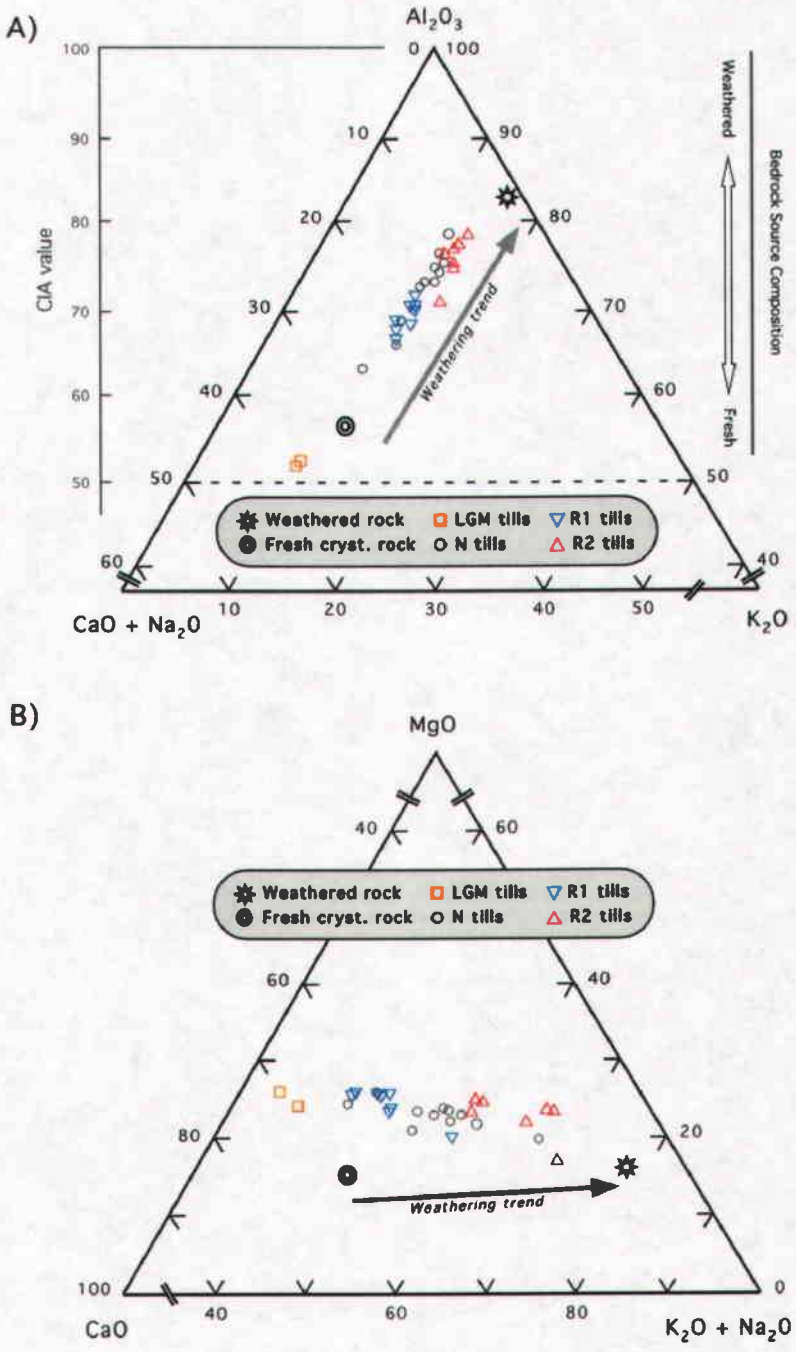

Figure 3.7: Ternary diagrams showing the distribution of the geochemical composition of till groups with respect to the weathering path of a fresh granitoid rock source (AUCC-type rock). A) Diagram depicting the weathering of feldspars. CIA is chemical Index of Alteration (Nesbitt and Young, 1982); high CIA values correspond to highly weathered material; CIA=$[Al_2O_3/(Al_2O_3+CaO^*+Na_2O+K_2O)]x100$, where CaO* is from silicate minerals. B) Weathering of feldspars vs ferromagnesians (*continued next page*).

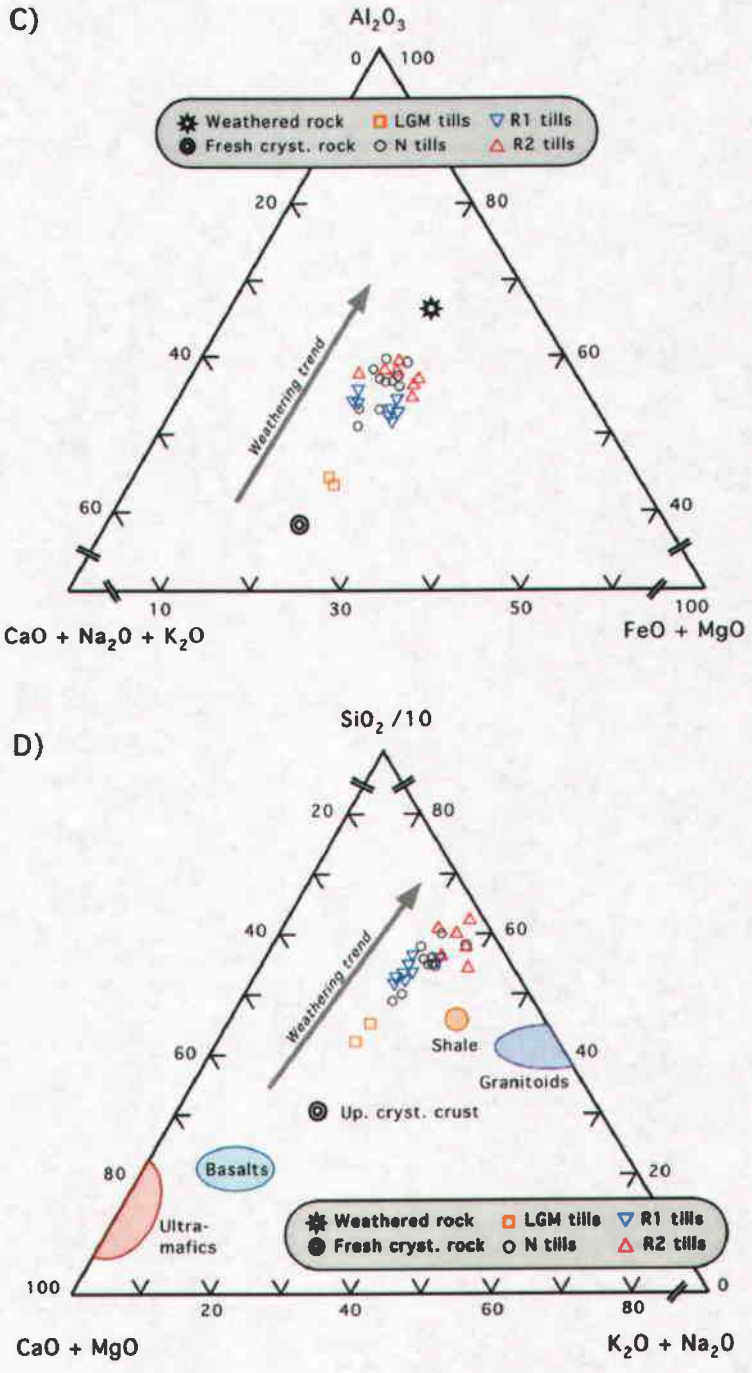

Figure 3.7 (*continued*): Ternary diagrams showing the distribution of the geochemical composition of till groups with respect to the weathering path of a fresh granitoid rock source (AUCC-type rock). C) Weathering of ferrogmagnesians vs Ca-rich feldspars and Na-, K-rich feldspars; D) Composition of till groups vs various rock sources.

An additional factor that may have contributed to the discrepancy between the lithology-mineralogy and the geochemistry of N tills is the duration of interglacials weathering following the MPT and the onset of 100-kyr glaciations. The history of the LIS during the last glaciation suggests that the ice margin remained near the outer boundary of the Canadian Shield for most of the glaciation (i.e. the initial 80 kyr), only advancing to its maximum extent near the end of the glacial cycle (Clark et al., 1999; Dyke et al., 2002). Assuming that this pattern is representative of 100-kyr glaciations in general, then extensive areas of pre-existing glacial deposits from previous glaciations distal to the Canadian Shield would be exposed to long intervals of subareal weathering during these 'extended' interglacial (subareal) conditions. Studies of soil development in granitic moraines (tills) show that interglacial weathering rates follow an exponential decrease (Taylor and Blum, 1995; Blum, 1997), suggesting that 80 kyr-long interglacials can potentially result in weathering rates that are greater by four orders of magnitude than that of shorter interglacials, such as the ones associated with the 41-kyr cycles. Incorporation of this surficial weathered material by subsequent glaciations may thus have provided a source of material depleted in base cations to the N tills. Consequently, the geochemistry of N tills may possibly reflect the occurrence of long periods of subareal exposures during the 100-kyr glaciations as well as recycling of older deposits.

3.7.3 Meteoric ^{10}Be in glacial sedimentary sequences

We further assess the MPT hypothesis by measuring ^{10}Be concentrations in till samples with the best age control. Meteoric ^{10}Be is produced in the upper atmosphere. Precipitation subsequently transfers the ^{10}Be to the Earth's surface, where it is efficiently trapped by soil particles (i.e. clays). Studies of soil chronosequences show that ^{10}Be concentrations increase in soils of increasing age (Pavich et al., 1984), and that a saprolite can yield a large ^{10}Be inventory (i.e. 8.8×10^{11} atoms/gram) (Pavich et al., 1985). In the latter case, most of the high ^{10}Be concentrations were found in the upper

1-5 m of the profile where clays are abundant; below this horizon, ^{10}Be concentrations decrease exponentially with depth. These results suggest that the pre-glacial regolith mantle may have accumulated large amounts of ^{10}Be over time. If correct, tills originating from the erosion of the upper part of this regolith should have higher ^{10}Be concentrations than tills derived from the lower part of the regolith or fresh crystalline bedrock, in which ^{10}Be is virtually absent.

We measured the ^{10}Be concentrations of six till samples with reasonably well-constrained ages (Table 3.2). For this purpose, we grounded the <2 mm fraction of each till sample, added a calibrated spike of ^{9}Be carrier to ~1 g of sample, and then extracted the beryllium using a fusion method (Stone, 1998). After oxidation of the samples to BeO, ^{10}Be/^{9}Be ratios were measured by accelerator mass spectrometry at the Gif-sur-Yvette Tandetron facility.

Table 3.2: Concentrations of meteoric ^{10}Be for 6 till samples of different age

Till group	Sample number	Age constraints of samples†			^{10}Be concentrations (10^7 atoms/gram)			
		maximum age (ky)	minimum age (ky)	average age (ky)	measured conc.	corrected (max.)	corrected (min.)	corrected (avg.)
W	WHA1R	17	17	17	5.62	5.67	5.67	5.67
N	FLO1R	780	600	690	3.97	5.75	5.24	5.49
R1	CRS2R	1300	780	1040	2.29	4.18	3.31	3.72
R1	DC139R	1300	780	1040	3.69	6.73	5.34	5.99
R2	CTY3R	2700	2000	2350	6.32	22.00	15.92	18.72
R2	AF172R	2700	2000	2350	4.54	15.81	11.44	13.45

†Age constraints provided by volcanic ashes (0.6, 1.6, and 2.0 Ma) and the Brunhes/Matuyama magne reversal (~0.8 Ma); see Fig. 3.3 for details.

The ^{10}Be concentrations, corrected for radioactive decay, indicate that the two late Pliocene R2 tills have the highest concentrations (13.45 and 18.72 x 10^7 atoms/g), whereas the younger tills have concentrations that are an order of magnitude lower (3.72 to 5.99 x 10^7 atoms/g) (Table 3.2; Figure 3.8). The ^{10}Be contents of the R2 tills, however, are not as high as might be expected if they represented a source solely

derived from a ^{10}Be-saturated saprolite mantle that had been exposed to weathering and meteoric precipitation for tens of millions of years (i.e. equilibrium value of 2.8 x 10^{12} atoms/cm^2 of Pavich et al., 1985). We interpret these lower concentrations as reflecting the consequences of several factors: loss of ^{10}Be from the uppermost part of the regolith during preglacial times; erosion of the most ^{10}Be-enriched horizons by ice sheets during glaciations that preceded the event that led to the deposition of our older tills; and some combination of the erosion of the uppermost horizon of the regolith and subsequent mixing with ^{10}Be-depleted sediments during glacial transport.

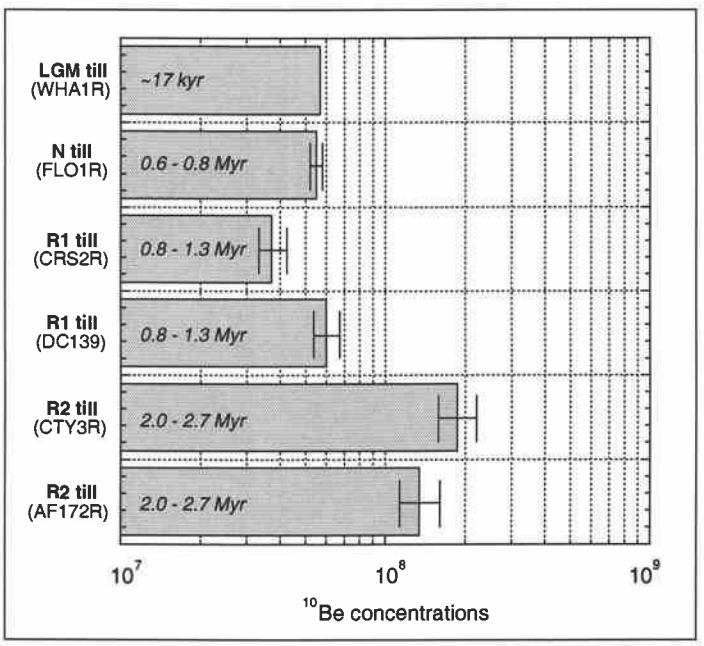

Figure 3.8: ^{10}Be concentrations in tills of different ages, corrected for radioactive decay. Horizontal bars represent mean concentrations with respect to the age constraints of each samples (*see* Table 3.2). Thin vertical lines at the end of each horizontal bar represent concentrations associated with the maximum and minimum age limits.

The lower concentrations among the younger R1 and N tills suggest that the uppermost meters enriched in ^{10}Be of the regolith had been eroded by 1.3 Ma. Accordingly, the ^{10}Be content of tills support the presence of a pre-glacial regolith, and it subsequent erosion during late Pliocene and early Pleistocene glaciations.

3.8 Marine records of strontium, hafnium, and osmium isotopes

Three marine tracers of continental weathering provide further support for removal of a weathered rock mantle and exposure of fresh silicate bedrock of the Canadian Shield during the MPT. The record of $^{87}Sr/^{86}Sr$ of dissolved Sr in seawater over the past 5 Ma is characterized by increasing $^{87}Sr/^{86}Sr$ ratios beginning ~2.6 Ma (Figure 3.9). Although the mechanisms responsible for the changes in seawater $^{87}Sr/^{86}Sr$ during the Cenozoic are still a subject of debate (e.g. Ruddiman, 1997), this increase is generally associated with the onset of Northern Hemisphere glaciation and an attendant increase in the flux of Sr from the continents or in the $^{87}Sr/^{86}Sr$ ratio of riverine Sr (Armstrong, 1971; Capo and DePaolo, 1990; Farrell et al., 1995; Blum and Erel, 1995; Blum, 1997). However, the marine Sr record is also characterized by two subsequent changes in the rate of increase of $^{87}Sr/^{86}Sr$ (Figure 3.9) which we attribute to unroofing of the Canadian Shield by ice sheet erosion of the overlying regolith, and to the subsequent onset of 100-kyr glaciations. By this argument, we attribute the initial increase in $^{87}Sr/^{86}Sr$ between 2.6 and 1.4 Ma at a rate of 0.033 p.p.m. kyr^{-1} to an increased flux of radiogenic Sr to the oceans derived from glacial erosion of the regolith. Because subsequent exposure of fresh crystalline bedrock would enhance the weathering rate of silicate minerals, we associate the accelerated rise in marine $^{87}Sr/^{86}Sr$ at 1.4 Ma (~0.1 p.p.m. kyr^{-1}) to an increase in the $^{87}Sr/^{86}Sr$ ratio of river waters from enhanced silicate weathering of basement rocks during 41-kyr glaciations, in addition to an increased flux from glacial activity. Finally, we attribute the decelerated rise in marine $^{87}Sr/^{86}Sr$ after 1 Ma (~0.037 p.p.m. kyr^{-1}) to the onset of 100-kyr glaciations, which would result in lower values of riverine $^{87}Sr/^{86}Sr$ relative to those associated with 41-kyr cycles (Blum and Erel, 1995; Blum, 1997). This deceleration can be modeled with an increased riverine $^{87}Sr/^{86}Sr$ ratio resulting from continued silicate weathering of newly exposed crystalline bedrock during 100-kyr glacial cycles (Blum and Erel, 1995; Blum, 1997).

A record of ε_{Hf} in seawater also indicates changes associated with the onset of Northern Hemisphere glaciation. In this case, van de Flierdt et al. (2002) attributed the overall decrease in ε_{Hf} values at ~2.5 Ma to an increase in glacial crushing of zircons, which are the primary reservoir of unradiogenic Hf. Of significance here, however, is the fact that the decrease in ε_{Hf} values accelerated from ~2.5 Ma until sometime between 0.8 and 1.7 Ma, at which point the rate of decrease remained constant to the present. We suggest that this trajectory of ε_{Hf} values reflects enhanced crushing of minerals in response to increasing surface area of exposed Canadian Shield rocks caused by progressive glacial erosion (Clark and Pollard, 1998). Exposure of hard bedrock at the ice-bed interface would induce greater mineral crushing relative to that associated with a soft, regolith-floored substrate (Cuffey and Alley, 1996). Rates of mineral crushing would then remain constant when the entire Shield became exposed, thus delivering a constant, and high, flux of unradiogenic Hf to the ocean.

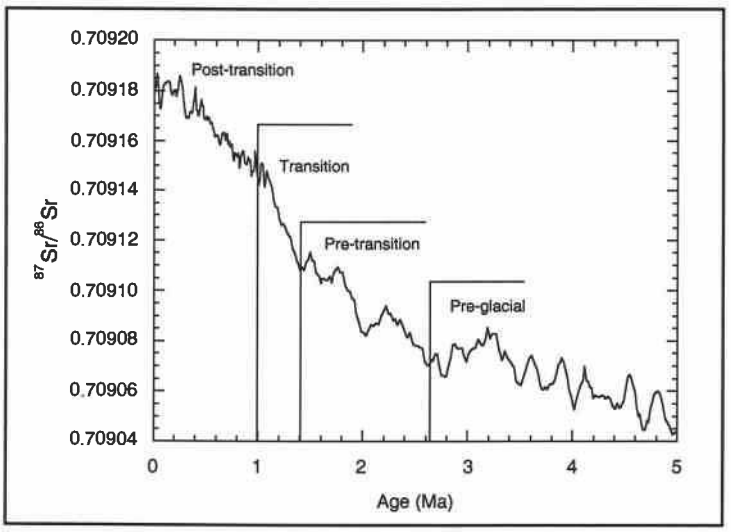

Figure 3.9: Diagram showing the evolution of the marine $^{87}Sr/^{86}Sr$ isotope record for the past 5 Myr in the context of unroofing of fresh crystalline bedrock around the middle Pleistocene transition (data from Farrell et al. (1995), 5-point running average).

Osmium is another tracer of continental weathering, with higher $^{187}Os/^{186}Os$ ratios indicating an increase in silicate weathering rates (Peucker-Ehrenbrink and Blum, 1998). For example, the slightly more radiogenic nature of North Atlantic seawater

compared to other ocean water masses may reflect the enhanced silicate weathering of recently deglaciated shield areas surrounding the North Atlantic Ocean (Peucker-Ehrenbrink and Blum, 1998). Burton et al. (1995) reported a constant $^{187}Os/^{186}Os$ ratio of seawater between 2.5 and 0.9 Ma, followed by a steep increase in the $^{187}Os/^{186}Os$ ratio to the present. Unlike Sr isotopes, the exchangeable fraction of radiogenic Os in highly weathered soils is strongly depleted relative to the bulk soil fraction, so that an increased continental flux of such material would not influence the $^{187}Os/^{186}Os$ ratio of seawater. Accordingly, Peucker-Ehrenbrink and Blum (1998) suggested that the initial period of a constant $^{187}Os/^{186}Os$ ratio reflected regolith erosion by ice sheets, whereas subsequent exposure of unweathered shield bedrock ~0.9 Ma is reflected by an increase in the $^{187}Os/^{186}Os$ of seawater.

3.9 Discussion and conclusions

Because the MPT involved a transition from low-amplitude, higher-frequency (41 kyr) to high-amplitude, lower-frequency (100 kyr) glacial cycles under essentially the same orbital forcing (Pisias and Moore, 1981), most explanations for the MPT invoke some forcing internal to the climate system. Several ice sheet-climate models, for example, have simulated the MPT as a nonlinear response to a prescribed long-term cooling trend, possibly in response to a gradual decrease in atmospheric pCO_2 (Raymo, 1998; Berger et al., 1999; Tziperman and Gildor, 2003). New records, however, suggest that low pCO_2 has existed over the last 25 Myr (Pagani et al., 1999; Pearson and Palmer, 2000), although the resolution and precision of these records may be too low to identify a relatively small decrease in pCO_2 that may induce a threshold from smaller to larger ice sheets with corresponding differences in response to orbital forcing (Berger et al., 1999). Nevertheless, existing ice core records of pCO_2 (Petit et al., 1999) do not support the assumption of the continuation of a 3-Myr linear decrease in pCO_2 over the last 440 ka (Raymo, 1998; Berger et al., 1999). Future ice core records that extend over the last 1 Ma will shed important new information on this issue.

Long-term cooling induced by mechanisms other than pCO_2 would provide a viable candidate for the MPT. For example, one model (Tziperman and Gildor, 2003) simulates an MPT in response to late Cenozoic cooling of deep ocean water (Ruddiman et al., 1989; McIntyre et al., 1999). The relation between any such long-term cooling and the MPT remains unclear, however, particularly since the cooling may instead be a response to events associated with the MPT, such as increased ice sheet size (Ghil and Childress, 1987). According to this scenario, any cooling may then represent an important feedback on subsequent glacial dynamics, but it is not the primary forcing of the MPT.

Perhaps the most important constraint that any mechanism for the MPT must address is the evidence that the volumetric increase in post-MPT ice sheets was accomplished through an increase in the thickness of already areally extensive ice sheets (Figure 3.1) (Clark and Pollard, 1998). Models that simulate the MPT through long-term cooling do so as a consequence of an attendant increase in either ice volume (Berger et al., 1999) or sea ice extent (Tziperman and Gildor, 2003), with a threshold occurring in both cases that triggers the onset of the 100-kyr glacial cycle. Although these models also simulate an increase in the amplitude of glacial cycles, they do not explicitly identify a mechanism that causes a transition from thin, areally extensive ice sheets to thick, areally extensive ice sheets, and thus do not satisfy the spatial-extent constraint required by the geologic record (Boellstorff, 1978a; Joyce et al., 1993; Roy et al., 2003).

The regolith hypothesis for the MPT provides such a mechanism to explain a change from extensive and thin ice sheets to extensive and thick ice sheets with a corresponding spectral change that is seen in the $\delta^{18}O$ record (Figure 3.1) (Clark and Pollard, 1998). Ice sheet thickness is controlled primarily by mechanisms at the base of the ice sheet that control ice motion. Accordingly, an ice sheet underlain by soft,

deformable sediments (regolith) will be thinner than an ice sheet underlain by solid bedrock. The regolith hypothesis states that the MPT occurred by progressive advection of the regolith through shear imposed by the overlying ice sheet, eventually exposing the hard bedrock to cause a change from thinner to thicker ice sheets (Figure 3.1) with a corresponding difference in ice sheet response to orbital forcing.

The regolith hypothesis makes a clear prediction that a fundamental change in the composition of terrestrial and marine sediments should accompany the MPT. Our results on the geochemistry, mineralogy and petrology of midcontinent tills that span the MPT confirm this prediction in documenting an early bedrock source that was highly weathered, followed by a change to a source comprised of less weathered or fresh crystalline bedrock. Specifically, the oldest (R2) tills are depleted in crystalline lithologies and unstable minerals, and enriched in weathered products, as indicated by clay mineralogy and till geochemistry. In contrast, the younger tills show enrichment in crystalline lithologies and stable minerals, and depletion in weathered products. High ^{10}Be concentrations in R2 tills similarly indicate a regolith source for these old tills, whereas lower ^{10}Be concentrations in younger tills indicate that the upper ^{10}Be-enriched horizon of the regolith had been eroded by ~1.3 Ma.

Additional mineralogical evidence for a change in source composition from weathered to unweathered material during the MPT comes from marine sediments core ODP 645B from Baffin Bay, which record the erosion of the northeastern sector of the LIS. In particular, there is a marked decrease in kaolinite and expandable clays and an increase in illite, chlorite and feldspars during the MPT (Thiebault et al., 1989; Andrews, 1993).

Marine records of Sr, Os, and Hf further identify removal of a highly weathered regolith and subsequent unroofing of fresh, unweathered silicate rock during the MPT. Onset of Northern Hemisphere glaciation increased the flux of Sr to the global ocean,

thus initiating a secular increase in the $^{87}Sr/^{86}Sr$ of dissolved Sr in seawater. Subsequent exposure of unweathered silicate rocks at the start of the MPT is reflected by a further increase in $^{87}Sr/^{86}Sr$ resulting from a combination of continued glacial flux and an increase in riverine $^{87}Sr/^{86}Sr$ from silicate weathering. Finally, $^{87}Sr/^{86}Sr$ ratios and $^{187}Os/^{186}Os$ ratios of seawater indicate that complete removal of the regolith and widespread weathering of fresh silicate bedrock was essentially complete by ~1 Ma. At the same time, exposure of the hard rock substrate increased physical crushing of minerals beneath the LIS, causing an increase in the flux of unradiogenic Hf to the ocean. We note that weathering of newly exposed silicate bedrock during the MPT may have provided an important sink of CO_2 (Blum, 1997), with attendant cooling perhaps representing an important feedback to the onset and maintenance of the 100-kyr cycles.

In summary, the MPT is characterized by a change from low-amplitude, high-frequency glacial cycles to high-amplitude, low-frequency glacial cycles in the absence of any change in orbital forcing. The geologic record indicates that this change involved a switch from extensive and thin ice sheets to extensive and thick ice sheets. The regolith hypothesis accommodates these changes by providing an explicit mechanism to cause a transition from thin to thick ice sheets (Clark and Pollard, 1998). Fundamental changes in the petrography and geochemistry of midcontinent tills and the geochemistry of seawater during the MPT are consistent with the prediction of unroofing of Precambrian Shield bedrock by ice sheet erosion of regolith. We thus conclude that regolith erosion and the attendant change in the basal boundary condition of the LIS best explains the geologic constraints on the MPT.

3.10 Acknowledgements

We thank R. Glasmann and R. Barendreg for helpful discussions on data interpretation, and J. Stone and G. Balco for useful suggestions on the ^{10}Be extraction method. This study was supported by the National Science Foundation (ATM 9709684).

3.11 References

Alley, R. B., Blankenship, D.D., Bentley, C.R., and Rooney, S. T., 1986, Deformation of till beneath ice stream B, West Antarctica. Nature, v. 322, p. 57-59.

Armstrong, R.L., 1971, Glacial erosion and the variable isotopic composition of strontium in seawater: Nature, v. 230, p. 132-133.

Andrews, J.T., 1993, Changes in the silt- and clay-size mineralogy of sediments at Ocean Drilling Program site 645B, Baffin Bay: Canadian Journal of Earth Sciences, v. 30, p. 2448-2452.

Berger, A., 1978, Long-term variations in caloric insolation resulting from the Earth's orbital elements: Quaternary Research, v. 9, p. 139-167.

Berger, A., Li, X.S., Loutre, M.F., 1999, Modeling northern hemisphere ice volume over the last 3 Ma: Quaternary Science Reviews, v. 18, p. 1-11.

Blum, J.D., 1997, The effect of late Cenozoic glaciation and tectonic uplift on silicate weathering rates and the marine $^{87}Sr/^{86}Sr$ record, *in* W.F. Ruddiman, ed., Tectonic Uplift and Climate Change: Plenum Press, New York, p. 259-288.

Blum, J.D. and Erel, Y., 1995, A silicate weathering mechanism linking increase in marine $^{87}Sr/^{86}Sr$ with global glaciation: Nature, 373, p. 415-418.

Bierman, P.R., Marsella, K.A., Patterson, C., Davis, P.T., and Caffee, M., 1999, Mid-Pleistocene cosmogenic minimum-age limits for pre-Wisconsinan glacial surfaces in southwestern Minnesota and southern Baffin Island: a multiple nuclide approach: Geomorphology, v. 27, p. 25-39.

Boellstorff, J., 1973, Tephrochronology, petrology, and stratigraphy of some Pleistocene deposits in the Central Plains, USA [Ph.D. Thesis]: Baton rouge, Louisiana State University, 197 p.

Boellstorff, J., 1976, The succession of late Cenozoic ashes in the Great Plains: a progress report: Guidebook Series 1, Kansas Geological Survey, p. 37-71.

Boellstorff, J., 1978a, Chronology of some Late Cenozoic deposits from the central United Stades and the Ice Ages: Transactions of the Nebraska Academy of Science, v. 6, p. 35-49.

Boellstorff, J., 1978b, North American Pleistocene stages reconsidered in the light of probable Pliocene-Pleistocene continental glaciation: Science, v. 202, p. 305-307.

Bouchard, M., 1985, Weathering and weathering residuals on the Canadian Shield: Fennia, v. 163, p. 327-332.

Bouchard, M., Godard, A., 1984, Les alterites du boulcier canadien: premier bilan d'une campagne de reconnaissance: Geographie Physique et Quaternaire, v. 38, p. 149-163.

Bouchard, M., Pavich, M.J., 1989, Characteristics and significance of pre-Wisconsinan saprolites in the northern Appalachians: Z. Geormorphl. N.F., Suppl. Band, v. 72, p. 125-137.

Boulton, G.S. and Jones, A.S., 1979, Stability of temperate ice caps and ice sheets resting on beds of deformable sediments. Journal of Glaciology, v. 24, 29-43.

Burton, K.W., Birck, J.L., Allegre, C.J., O'Nions, R.K., 1995, Fine scale records of seawater $^{187}Os/^{186}Os$: Eos, Transactions, American Geophysical Union, v. 76, Suppl., p.182.

Capo, R.C. and DePaolo, D.J., 1990, Seawater strontium isotopic variations from 2.5 Million years ago to present: Science, v. 249, p. 51-55.

Clark, P.U. and Pollard, D., 1998, Origin of the middle Pleistocene transition by ice sheet erosion of regolith: Paleoceanography, v. 13, p. 1-19.

Clark, P.U., Alley, R. B. and Pollard, D., 1999, Northern Hemisphere ice sheet influences on global climate change: Science, v. 286, p. 1104-1111.

Cuffey, K.M., Alley, R.B., 1996, Is erosion by deforming subglacial sediments significant? (toward till continuity): Annals of Glaciology, v. 22, p. 17-24.

Dyke, A.S., Andrews, J.T., Clark, P.U., England, J.H., Miller, G.H., Shaw, J., Veillette, J.J., 2002, The Laurentide and Innuitian ice sheets during the last glacial maximum, Quaternary Science Reviews, v. 21, p. 9-31.

Elkibbi, M., Rial, J.A., 2001, An outsider's review of the astronomical theory of the climate: is the eccentricity-driven insolation the main driver of the ice ages?: Earth-Science Reviews, v. 56, p. 161-177.

Faure, G., 1998, Principles and applications of geochemistry, 2nd ed. Prentice-Hall, 600 p.

Farrell, J.W., Clemens, S.C. and Gromet, L.P., 1995, Improved chronostratigraphic reference curve of late Neogene seawater $^{87}Sr/^{86}Sr$: Geology, v.23, p. 403-406.

Gansecki, C.A., Mahood, G.A., and McWilliams, M., 1998, New ages for the climatic eruptions at Yellowstone: Single-crystal $^{40}Ar/^{39}Ar$ dating identifies contamination: Geology, v. 26, p. 343-346.

Ghil, M., Childress, S., 1987, Topics in geophysical fluid dynamics, atmospheric dynamics, dynamo theory, and climate dynamics: Applied Mathematical Sciences, v. 60, Springer, New York-Heidelberg-Berlin, International, 485. p.

Godard, A., 1979, Geomorphological reconnaissance on the north part of Labrador and Nouveau Quebec peninsula: a contribution to the study of basement-rock landform in cold environments: Revue de Géomorphologie Dynamique, v. 28, p. 125-142

Goldich, S.S., 1938, A study in rock weathering: Journal of Geology, v. 46, p. 17-58.

Gravenor, C.P., 1975, Erosion by continental ice sheets: American Journal of Science, v. 275, p. 594-604.

Hallberg, G.R., 1986, Pre-Wisconsinan glacial stratigraphy of the central plains region in Iowa, Nebraska, Kansas, and Missouri: *In*: Quaternary glaciations in the northern hemisphere; Richmond, G.M. and Fullerton, D.S. (eds.), Quaternary Science Reviews, 5, p. 11-15.

Hays, J.D., Imbrie, J. and Shackleton, N.J., 1976, Variations in the Earth's orbit: Pacemaker of the ice ages: Science, v. 194, p. 1121-1132.

Imbrie et al., 1984, The orbital theory of Pleistocene climate: Support for a revised chronology of marine $\delta^{18}O$ record: in Milankovitch and Climate, Part 1, A.L. Berger et al., eds., p. 269-305, D. Reidel, Norwell, Massachusetts.

Imbrie and 17 others, 1993, On the structure and origin of major glaciations cycles, 2, The 100,000-year cycle: Paleoceanography, v. 8, p. 699-735.

Izett, G.A., 1981, Volcanic ash beds: Recorders of upper Cenozoic silicic pyroclastic volcanism in the western United States: Journal of geophysical Research, 86, p. 10200-10222.

Joyce, J.E., Tjalsma, L.R.C., Prutzman, J.M., 1993, North American glacial meltwater history for the past 2.3 My: Oxygen isotope evidence from the Gulf of Mexico: Geology, v. 21, p.483-486.

Lasalle, P., De Kimpe, C.R., LaVerdiere, M.R., 1985, Sub-till saprolites in southeastern Quebec and adjacent New England: erosion, stratigraphic and climatic significance: Geological Society of America Special Paper 197, p. 13-25.

McIntyre, K., Ravelo, A.C., Delaney, M.L., 1999, North Atlantic intermediate waters in the late Pliocene to early Pleistocene: Paleoceanography, v. 14. p. 324-335.

McKeague, J.A., Grant, D.R., Kodama, H., Beke, G.J., Wang, C., 1983, Properties and genesis of a soil and the underlying gibbsite-bearing saprolite, Cape Breton Island, Canada: Canadian Journal of Earth Sciences, v. 20, p. 37-48.

Mix, A.C., Pisias, N.G., Rugh, W., Wilson, J., Morey, A. and Hagelberg, T.K., 1995, Benthic foraminifer stable isotope record from site 849 (0-5 Ma): Local and global climate changes: N.G. Pisias et al. eds., Procedures of Ocean Drilling Program Scientific Results, v. 138, p. 371-342.

Nielsen, E., Morgan, A.V., Morgan A., Mott, R.J., Rutter, N.W. and Causse, C., 1986, Stratigraphy, paleoecology and glacial history of the Gillam area, Manitoba; Canadian Journal of Earth Sciences, v. 23, p. 1641-1661.

Nesbitt, H.W. and Markovics, G., 1997, Weathering of granodiorite crust, long-term storage of elements in weathering profiles, and petrogenesis of siliciclastic sediments. Geochimica Cosmochemica Acta, v. 61, p. 1653-1670.

Nesbitt, H.W. and Young, G.M., 1982, Early Proterozoic climates and plate motions inferred from major element chemistry: Nature, v. 299, p. 715-717.

Nesbitt, H.W. and Young, G.M., 1984, Prediction of some weathering trends of plutonic and volcanic rocks based on thermodynamic and kinetic considerations: Geochimica Cosmochemica Acta, v. 48, p. 1523-1534.

Nesbitt, H.W. and Young, G.M., 1989, Formation and diagenesis of weathering profiles: Journal of Geology, v. 97, p. 129-147.

Ollier, C. and Pain., C., 1996, Regolith, soil and landforms. Chichester, New York : John Wiley & Sons, 309 p.

Pagani, M., Arthur, M.A., Freeman, K.H., 1999, Miocene evolution of atmospheric carbon dioxide: Paleoceanography, v. 14, p. 273-292.

Parham, W.E., 1970, Clay mineralogy and geology of Minnesota kaolin's clay: Special Publication Series, Minnesota Geological Survey, SP-10, 142 pp.

Pavich, M.J., Brown, L., Klein, J., Middleton, R., 1984, Beryllium-10 accumulation in a soil chronosequence: Earth and Planetary science Letters, v. 68, p. 198-204.

Pavich, M.J., Brown, L., Valette-Silver, N.J., Klein, J., Middleton, R., 1985, ^{10}Be analysis of a Quaternary weathering profile in the Virginia Piedmont; Geology, v. 13, p. 39-41.

Pearson, P.N., Palmer, M.R., 2000, Estimating Paleogene atmospheric pCO_2 using boron isotope analysis of Foraminifera: *In*: Early Paleogene warm climates and biosphere dynamics, Short papers and extended abstracts, Schmitz, B., Sundquist, B., Andreasson, F.P. (eds.), Geological Society of Sweden, Stockholm, Sweden, v. 122, p. 127-128.

Petit, J.R., and 16 others, 1999, Climate and atmospheric history of the past 420,000 years from the Vostok ice core, Antarctica: Nature, v. 399, p. 429-436.

Peucker-Ehrenbrink, B., Blum, J.D., 1998, Re-Os isotope systematics and weathering of Precambrian crustal rocks: implications for the marine osmium isotope record: Geochimica et Cosmochimica Acta, v. 62, p. 3193-3203.

Pisias, N. G., Moore, T.C. Jr., 1981, The evolution of the Pleistocene Climate: A time series approach. Earth Planetary Science Letters, v. 52, p. 450-458.

Raymo, M.E., 1998, Glacial Puzzles: Science, v. 281, p. 1467-1468.

Reynolds, Jr., R.C., 1985, NEWMOD© A computer program for the calculation of one-dimensional diffraction patterns of mixed-layered clays: R.C. Reynolds, Jr., 8 Brook Dr., Hanover, NH.

Roy, M., Clark, P.U., Barendregt, R.W., Glasmann, J.R., Enkin, R.J., (*in press*), Glacial stratigraphy and paleomagnetism of late Cenozoic deposits in the north-central U.S. Geological Society of America Bulletin.

Ruddiman, W.F., 1997, Tectonic Uplift and Climate Change: Ruddiman, ed., Plenum Press, New York, 535 p.

Ruddiman, W.F. et al., 1989, Pleistocene evolution: Northern hemisphere ice sheets and North Atlantic Ocean: Paleoceanography, v. 4, p. 353-412.

Shaw, D.M., Reilly, G.A., Muysson, J.R., Pattenden, G.E., Campbelll, F.E., 1967, An estimate of the composition of the Canadian Precambrian Shield. Canadian Journal of Earth Sciences, v. 4, p. 829-853.

Shaw, D.M., Dostal, J., Keys, R.R., 1976, Additional estimates of continental surface Precambrian shield composition in Canada. Geochimica Cosmochemica Acta, v. 40, p. 73-84.

Setterholm, D.R. and Morey, G.B., 1995, An extensive pre-Cretaceous weathering profile in east-central and southwestern Minnesota: U.S. Geological Survey Bulletin 1989, p. H1-H29.

Stone, J.O., 1998, A rapid fusion method for separation of beryllium-10 from soils and silicates; Geochimica Cosmochemica Acta, v. 62, pp. 555-561.

Taylor, A. and Blum, J.D., 1995, Relation between soil age and silicate weathering rates determined from the chemical evolution of a glacial chronosequence: Geology, v. 23, p. 979-982.

Taylor, G. and Eggleton, R.A., 2001, Regolith geology and geomorphology. John Wiley & Sons, 375 p.

Thiebault, F., Cremer, M., Bebrabant, P., Foulon, J., Nielson, O.B. and Zimmerman, H., 1989, Analysis of sedimentary facies, clay mineralogy, and geochemistry of the Neogene-Quaternary sediments in site 645, Baffin Bay: Procedures of Ocean Drilling Program Scientific Results, v. 105, p. 83-100.

Tziperman, E., Gildor, H., 2003, On the mid-Pleistocene transition to 100-kyr glacial cycles and the asymmetry between glaciation and deglaciation times, Paleoceanography, v. 18, 1001, doi:10.1029/2001PA000627.

van der Flierdt, T., Frank, M., Lee, D., Halliday, A.N., 2002, Glacial weathering and the hafnium isotope of seawater. Earth and Planetary science Letters, v. 198, p. 167-175.

Wang, C., Ross, G.J., 1989, Granitic saprolites: their characteristics, identification and influence on soil properties in the Appalachian region of Canada: Z. Geormorphl. N.F., Suppl. Band, v. 72, p. 149-161.

Wedepohl, K.H., 1995, The composition of the continental crust. Geochimica Cosmochemica Acta, v. 59, p. 1217-1232.

CHAPTER 4

Provenance of glacial deposits from the north-central U.S. based on $^{40}Ar/^{39}Ar$ dating of K-feldspar grains of tills

M. Roy [†], P.U. Clark [†], R.A. Duncan [‡], J. Huard [‡]

[†]Department of Geosciences,
Oregon State University, Corvallis, OR 97331-5506, USA

[‡]College of Oceanic and Atmospheric Sciences,
Oregon State University, Corvallis, OR 97331-5503, USA.

To be submitted to Geology.

4.1 Abstract

The glacial sedimentary sequences of the north-central U.S. record multiple ice advances of the Laurentide ice sheet (LIS) dating back to > 2.0 Ma. These sequences display a compositional change that indicates an increase with time of material derived from the erosion of unweathered crystalline bedrock. This compositional change may reflect either a temporal change in the composition of a single bedrock source region or a change in provenance induced by changes in ice sheet configuration and attendant shifts in flow line trajectories. Here we constrain till provenance by determining 504 $^{40}Ar/^{39}Ar$ ages of individual K-feldspar grains retrieved from 14 till samples that span the last 2 Ma. Most samples analyzed show a large population of grains with $^{40}Ar/^{39}Ar$ ages identical to that of numerical ages of the Churchill province of the Canadian Shield, indicating till deposition by ice originating from the western (Keewatin) sector of the LIS. These results thus indicate that the till compositional changes can be attributed to a change in the composition of the bedrock source region, and that the Keewatin ice dispersal center is a long-lived feature of the LIS.

4.2 Introduction

The north-central U.S. encompasses the southernmost region once covered by the Laurentide ice sheet (LIS) (Figure 4.1). The glacial stratigraphy of this region indicates that the LIS has repeatedly advanced into this area since the late Pliocene. Ice flow directional data indicate that southward flowing ice lobes deposited tills forming these glacial sedimentary sequences (e.g. Aber, 1999). Nevertheless, the composition of midcontinent deposits exhibits a marked temporal change in their lithological and mineralogical composition consisting of older tills enriched in sedimentary clasts, quartz, and kaolinite to younger tills enriched in crystalline clasts, feldspar, and expandable (mixed-layered) clays (Boellstorff, 1973, 1978; Aber, 1991; Rovey and Kean, 1996; Colgan, 1999; Roy et al., 2003a).

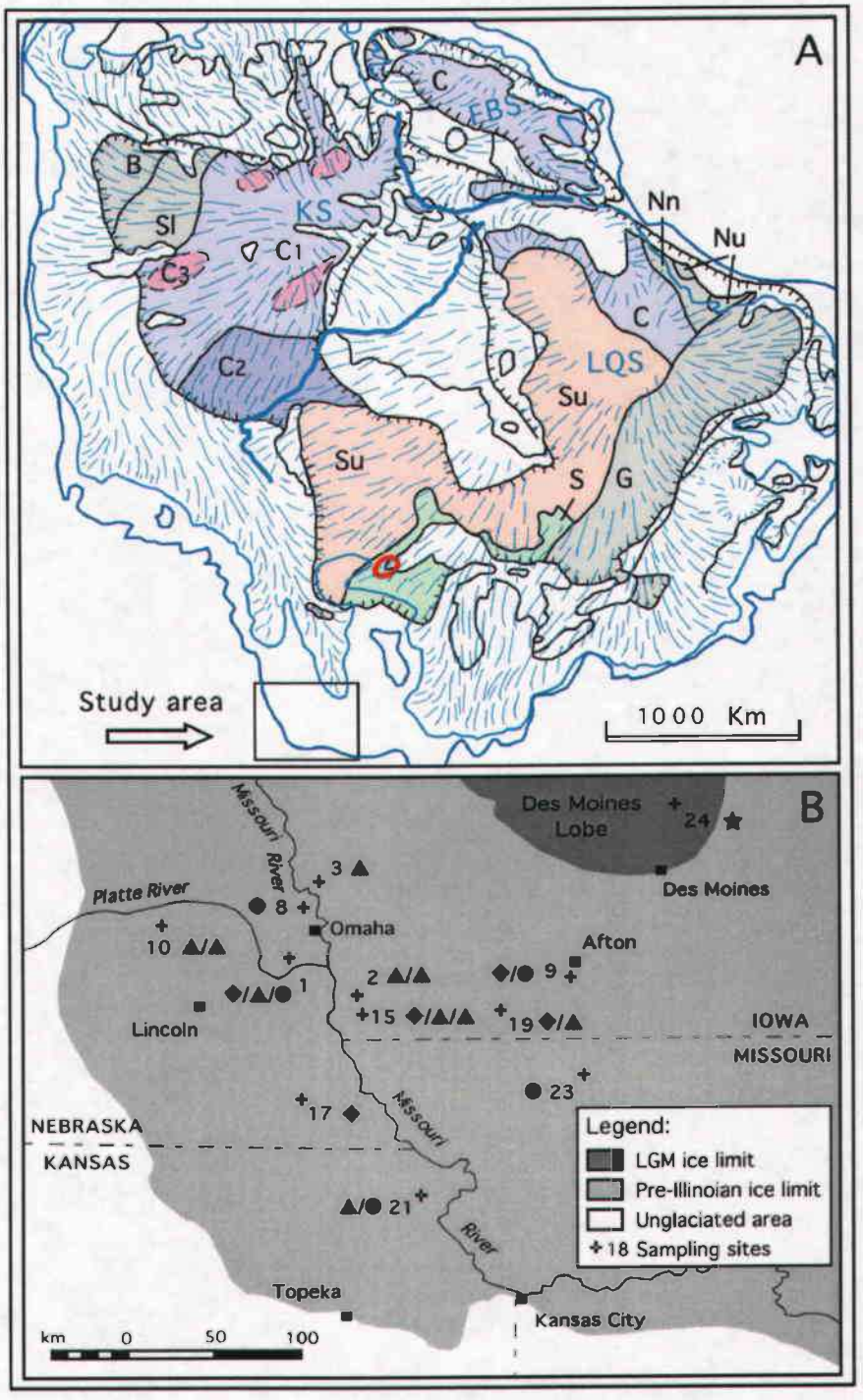

Figure 4.1: (A) Distribution of the main geological provinces of the Canadian shield underlying the Laurentide ice sheet (LIS) at the last glacial maximum (LGM). Dark blue line is the LIS maximum extent during earlier glaciations. The thin and discontinuous lines within LIS represent flow lines emanating from the main ice dispersal centers: KS, Keewatin Sector; LQS, Labrador/Quebec Sector; FBS, Foxe/Baffin Sector. Colored provinces represent the potential rock sources for the midcontinent tills. Geological provinces (modified from Hoffman, 1989; Goodwin,

1996): B, Bear; C, Churchill (C1, Hearne and Rae blocks; C2 Trans-Hudson Orogen; C3, Volcanic and sedimentary cover-sequences); G, Grenville; Nn-Nu, Nain, Nutak; S, Southern; Sl, Slave; Su, Superior. (**B**) Locations of the sampling sites in the study area (see Appendix D for geographic coordinates). Symbols represent the till stratigraphy exposed at each sites (from Roy et al., 2003a): ◆ are late Pliocene 'R2 tills' (~2.5-2.0 Ma); ▲ are early Pleistocene 'R1 tills' (~2.0-0.8 Ma); ● are middle Pleistocene 'N tills' (~0.8-0.5 Ma); and ★ are 'LGM tills' (~18 ka).

These compositional changes may be explained by a change in the composition of a fixed source region related to the progressive glacial erosion of a widespread regolith mantle and subsequent unroofing of the unweathered bedrock of the Canadian Shield (Clark and Pollard, 1998; Roy et al., 2003b). Alternatively, a temporal shift in the composition of late Cenozoic tills may record a change in provenance associated with the glacial erosion of multiple source regions and their attendant compositional characteristics. Such changes in source region would indicate significant changes in the trajectory of ice flowlines feeding the southern LIS lobes, such as occurred during the last deglaciation (Dyke and Prest, 1987).

Here we constrain provenance of midcontinent tills by measuring $^{40}Ar/^{39}Ar$ ages on K-feldspar grains retrieved from tills that span the last 2 Ma. We evaluated two probable ice flow trajectories originating from the main centers of dispersal of the LIS: a western source associated with the Keewatin ice divide, and an eastern source associated with the Labrador/Quebec ice divide (Figure 4.1). The path of each flow line linking the potential source regions to the study area involves the erosion of bedrock of the Canadian Shield with significantly different ages: bedrock of the Churchill Province (predominantly 2.00-1.75 Ga) in the west, and bedrock of the Superior Province (>2.60 Ga) in the east. Similar $^{40}Ar/^{39}Ar$ studies have successfully identified source terrains for the ice-rafted debris associated with Heinrich layers in the North Atlantic (Gwiazda et al., 1996; Hemming et al., 1998, 2000a, 2000b).

The bedrock geology of the North American midcontinent consists of upper Pennsylvanian limestone, shale, and sandstone, and upper Cretaceous shale; most sections investigated here lie directly on carbonate bedrock. The nearest outcrops of crystalline bedrock occur ~350 km north of the study area in southeastern Minnesota where most feldspar-bearing lithologies are Archean in age (>2.65 Ga). The presence of igneous and metamorphic clasts in the midcontinent tills suggests that the tills were derived in part from crystalline bedrock located up-ice from the study area, and their feldspar content should thus represent source regions associated with the main geological divisions of the Canadian Shield.

The Canadian Shield consists of an amalgam of structural provinces that were assembled during various orogens (Hoffman, 1989; Goodwin, 1996) (Figure 4.1). Each province carries a characteristic radiometric imprint that records the last major orogenic event that affected the province. As a result, these provinces contain rocks of different ages, and can be distinguished accordingly. The Superior and Churchill provinces are of particular interest because they were the loci of the Labrador/Quebec and Keewatin ice centers, respectively (Figure 4.1), which were the primary dispersal centers of the LIS during the last glaciation.

The Superior province consists primarily of large gneissic domains that are > 3.00 Ga (Hoffman, 1989; Goodwin, 1996). Less common metavolcanic and metasedimentary subprovinces are arranged in subparallel belts with ages of 2.70-2.80 Ga. Intrusions are associated with the Kenoran orogen (2.73-2.65 Ga), which left a strong tectonic imprint (~2.65 Ga) on some sectors of the Superior province.

The Churchill province largely comprises a complex aggregate of juvenile late Archean crust that has been thoroughly metamorphosed during the early Proterozoic Trans-Hudson orogen (~1.8 Ga) (Lewry et al., 1985; Hoffman, 1989; Goodwin, 1996). Basement rocks are found locally and have been reclassified as the late Archean Hearne and Rae provinces (Hoffman, 1990). These small structural entities, which bear a

Hudsonian imprint, consist primarily of felsic volcanics and granitoids, with minor areas of metasedimentary rocks (Lewry et al., 1985; Cavell et al., 1992). Hearne and Rea gneisses record at least four thermotectonic events, including metamorphism at ~2.3 and 2.0 Ga (Crocker et al., 1993; Bickford et al., 1994).

The southern half of the western Churchill province comprises intensively reworked rocks of the Trans-Hudson terrains, which form a suture zone between the Churchill and the Superior provinces. These rocks, which are dated between 2.0 and 1.8 Ga, consist primarily of gneiss representing recrystallized Archean basement, but also include areas of early Proterozoic crust. Post- and anorogenic intrusions (1.80-1.60 Ga) also occupy extensive areas in the south-central Churchill province. Abundant early Proterozoic remnants of reddish sedimentary platform-shelf sequences and turbidite-volcanic rock sequences (1.75-1.60 Ga) fill cratonic basins that cover vast areas in the central Churchill province. The Churchill intra-cratonic basins and Hudsonian plutons are transected in places by the northwest trending Mackenzie dyke swarms (1.32 Ga).

The Southern province, which makes up the southern periphery of the shield (Hoffman, 1989; Goodwin, 1996), shows a wide range of ages (2.65-1.09 Ga) (Sims et al., 1993). This province consists predominantly of accreted juvenile late Archean crust that bears an imprint from the Penokean orogen (1.86-1.80 Ga).

4.4 Sampling methods and analytical precedures

Roy et al. (2003a) constrained the ages of pre-Illinoian tills based on the paleomagnetism of glacial and nonglacial deposits and the relation of tills to three volcanic ashes derived from dated eruptions of the Yellowstone caldera (Izett, 1981). Based on these constraints, the tills were grouped into a late Pliocene till group (R2 tills), an early Pleistocene till group (R1 tills), and a middle Pleistocene till group (N tills). A fourth group of tills that was deposited by the Des Moines lobe around the last

glacial maximum (14-21 ka; LGM tills) occur in the northern sector of the study area (Figure 4.1).

We sampled 14 till units from 11 stratigraphic sections (Figure 4.1). We dated 33 to 38 K-feldspar grains from each till sample by the $^{40}Ar/^{39}Ar$ total fusion method for a total of 504 age determinations. One LGM till sample was analyzed whereas at least four samples were analyzed from each of the three other till groups (Table 4.1).

We sieved bulk till samples of ~4 kg and recovered the 1-2 mm size fraction from which we hand-picked translucide grains showing facets and cleavage under a binocular microscope. Most grains were angular to subangular, but some subrounded grains were also present. We extracted the K-feldspars from the light mineral fraction of each sample using a heavy-density liquid (Na-polytungstate) adjusted to a density of 2.6. The floating grains were subsequently recovered and washed thoroughly in distilled water. We then selected ~50 grains showing clear and typical K-feldspar mineral attributes. Each grain was gently crushed in a mortar, passed through a sieve, and 4 fragments were taken from the 100-150 um size fraction. These four grain fragments were later wrapped together in Cu foil and stacked in a quartz tube, which was then evacuated and sealed prior to irradiation with fast neutrons for 6 hours in the core of the TRIGA reactor at Oregon State University. One irradiated fragment of each grain was then mounted in a Cu block with shallow wells.

We used single step laser heating to measure the $^{40}Ar/^{39}Ar$ total fusion age of each grain fragment. The stage containing the irradiated grain fragments was loaded in the laser extraction system and each fragment was fused using a 10W CO_2 continuous laser (Duncan, 2002). The argon isotopes (^{40}Ar, ^{39}Ar, ^{38}Ar, ^{37}Ar, and ^{36}Ar) were measured on a MAP 215-50 mass spectrometer and each isotope was corrected for interference due to nuclear reactions on Ca, K, and Cl, and for mass fractionation. The reported ages of the glacially-derived grains represent the time elapsed since the last major

thermotectonic event (orogen, metamorphism) or cooling of the host rock through a specific temperature, generally ~250°C for feldspars.

Because of the scale of this geochronological study (ages for >500 grains) we chose to use the total fusion method rather than extensive multiple-step heating experiments. A single heating step can potentially mask a complex thermal history that could involve crystallization, multiple metamorphic events, and low temperature alteration. In order to investigate potential difficulties in using total fusion ages to identify source bedrock, we conducted four incremental heating experiments of 10-17 steps on single grains from one till sample (MER03). Three of the experiments produced plateau ages comprising a majority of the gas released, which we interpret as crystallization ages or the age of complete metamorphic resetting (Figure 4.2). In these cases the plateau ages and the total fusion ages, formed by adding all step gas compositions together, are indistinguishable. In the fourth example, a high temperature plateau comprising 44% of the total gas defines the crystallization age, while lower temperature steps reveal a mild Ar-loss profile. However, the total gas age is still 94% of the plateau age. On the basis of these results, we conclude that the total fusion ages for the optically clear feldspar grains are good estimates of the crystallization/metamorphic ages of the crystalline bedrock source.

4.5 Results – Discussions

The $^{40}Ar/^{39}Ar$ total fusion ages of K-feldspars range from ~0.6 Ga to ~2.4 Ga, with the majority of ages occurring between 1.4 and 2.4 Ga (Figure 4.3; Appendix D). These results thus indicate that the source terrain of glacial deposits is primarily early Proterozoic (2.5-1.6 Ga), with a few grains in each sample also showing ages suggesting a middle Proterozoic and younger source (1.3-0.6 Ga).

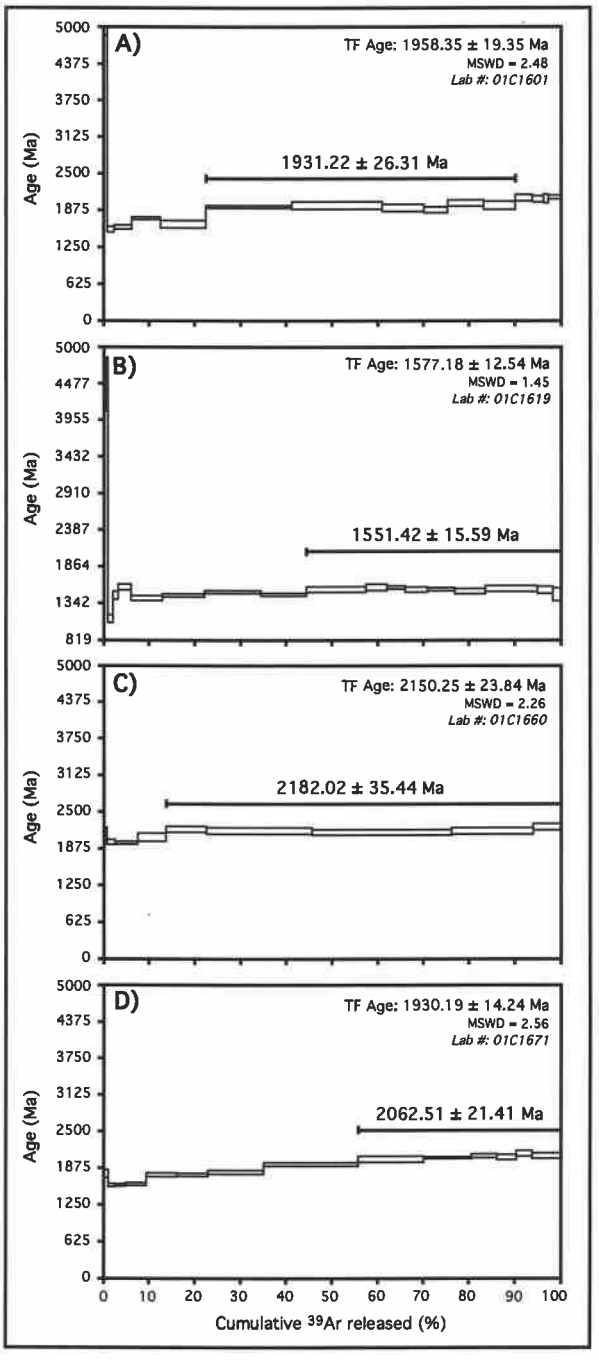

Figure 4.2: $^{40}Ar/^{39}Ar$ incremental heating experiments on single feldspar grains of till sample MERO3 (site 23). The bold horizontal line in each diagram corresponds to the weighted plateau age. Plateau ages are similar to the total fusion ages, which were obtained by adding all step gas composition together. Total fusion (TF) ages are shown on the upper part of each diagram. Ages were calculated using biotite monitor FCT-3 (28.04 Ma) and the following decay constants: $\lambda\varepsilon = 0.58E\text{-}10/yr$, $\lambda\beta = 4.963E\text{-}10/yr$. Age errors are 2σ. MSWD is an F-statistic of within-step variability divided by between-step variability and is significant <2.6.

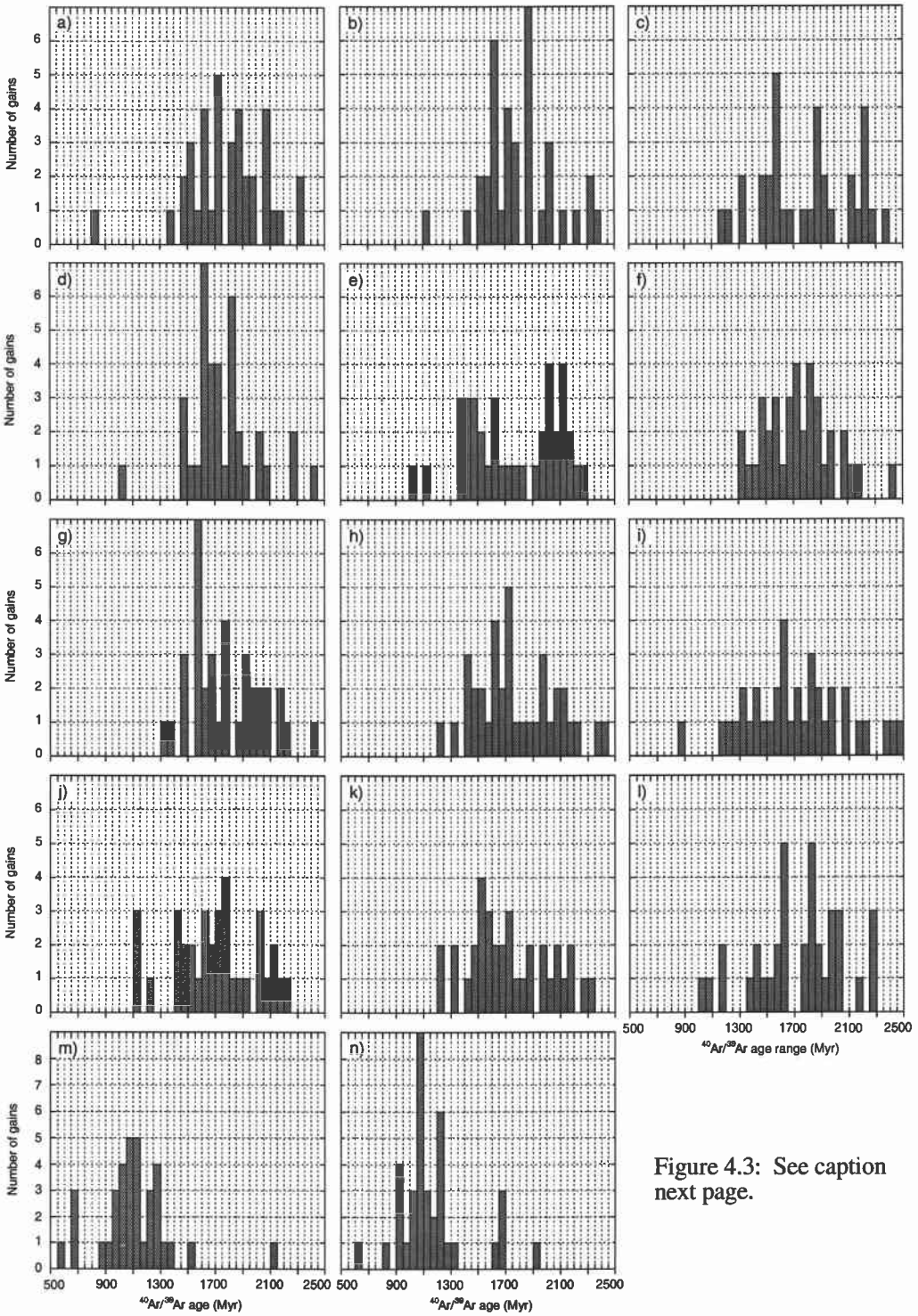

Figure 4.3: See caption next page.

Figure 4.3: Histograms showing the distribution of $^{40}Ar/^{39}Ar$ ages of K-feldspars of tills with respect to the potential rock sources investigated. The following groups are based on the major divisions of the Canadian Shield (Figure 4.2), and were established to facilitate data interpretation: The 'Superior' group (not identified here) comprises Archean lithologies of the greater Superior province with ages >2.6 Ga. 'Hearne-Rae' group comprises the areally restricted blocks of unworked late Archean basement of the Churchill province with various tectonic imprints of ~ < 2.5 to 2.0 Ga; 'Trans-Hudson' group comprises the intensively reworked Churchill rocks with ages from 2.0 to 1.8 Ga that were involved in the Trans-Hudson orogen; 'Churchill cover sequences' group comprises the sedimentary and volcanic rock-cover sequences with ages from 1.8 to 1.6 Ga. This group also includes post- and anorogenic Hudsonian intrusions of this age; 'Churchill various' group comprises lithologies with ages between 1.6-1.3 Ga and includes the Mackenzie dykes (~1.3 Ga). Important periods of anorogenic magmatism occurred between 1.5-1.3 Ga in the North American craton, and anorthosite plutons of this age are common in the eastern Rae and Nain provinces of the Labrador region. Although intrusions of this age have not been documented in the Churchill province, the abundance of such plutons elsewhere in similar basement terrains suggests that 1.5-1.3 Ga plutons may be present in the Churchill province; 'Others' group comprises lithologies with ages (1.30-0.55 Ga). Results of the LGM till: (**A**) sample WHA1-(site) 24, number of grains (n)=37. N tills: (**B**) AF151-9, n=36; (**C**) CTY09-1, n=33; (**D**) WAT05-4, n=37; (**E**) BEF03-19, n=38; (**F**) FLO01-8, n=37. R1 tills: (**G**) GLW03-2, n=36; (**H**) CRS02-3, n=37; (**I**) DC139-10, n=36; (**J**) WAT02-17, n=35. R2 tills: (**K**) AF172-9, n=36; (**L**) BEF02-19, n=36; (**M**) CTY02-1, n=34; (**N**) ELC02-2, n=37.

With the exception of two samples, the distribution of K-feldspar ages is nearly identical in each sample regardless of the age of the till group (Figure 4.3). On average, a typical population of 36 grains consists of 8 'Rae-Hearne' grains, 7 'Trans-Hudson' grains, 10 'Churchill cover sequences' grains, 9 'Churchill intrusive-various' grains, and 2 'Others' (Table 4.1). The wide range of ages is consistent with the different stages of the complex geological history of the Churchill province, that is: formation of late juvenile Archean crust, early Proterozoic deformation, post-orogenic intra-cratonic sedimentation (volcanic and sedimentary), and anorogenic magmatism. The overall range covered by the $^{40}Ar/^{39}Ar$ ages of K-feldspar grains is thus characteristic of the main geological divisions of the terrains that comprise the Churchill province (Figure 4.1). These results thus indicate that deposition of the midcontinent tills occurred by ice originating from the Keewatin sector of the LIS. In contrast, the absence of grains from the Superior province (>2.6 Ga) indicates that an eastern source from the Labrador/Quebec sector of the LIS did not contribute to the deposition of these tills.

Table 4.1: Summary of $^{40}Ar/^{39}Ar$ ages of glacially-derived feldspars in samples

Site	Sample number	Clast content‡ Sed. (%)	Cryst. (%)	Number of grains in each geologic divisions† Superior	Rae & Hearne	Trans-Hudson	Churchill cov. seq.	Churchill various	Others	Total grains
LGM Till										
24	WHA01	54.0	46.0	0	8	11	10	7	1	37
N Tills										
9	AF151	56.3	43.7	0	8	8	14	5	1	36
1	CTY09	58.6	41.4	0	9	8	3	11	2	33
21	WAT05	42.9	57.1	0	6	9	16	4	1	36
19	BEF03	50.1	49.9	0	14	4	6	12	2	38
8	FLO01	49.6	50.4	0	5	10	10	12	0	37
R1 Tills										
3	CRS02	61.5	38.5	0	9	6	12	9	1	37
2	GLW03	62.4	37.6	0	8	6	10	12	0	36
10	DC139	65.8	34.2	0	7	8	8	9	4	36
17	WAT02	62.8	37.2	0	8	3	12	8	4	35
R2 Tills										
9	AF172	90.4	9.6	0	8	5	8	12	2	35
19	BEF02	85.0	15.0	0	7	11	7	7	4	36
1	CTY02	81.3	18.7	0	1	0	0	3	31	35
17	ELC02	96.7	3.3	0	0	1	4	1	31	37

† See caption of Fig. 1 for age and definition of geologic divisions

‡ Lithological data from Roy et al. (2003a); sedimentary and crystalline clasts (4-12.5 mm size fraction).

Two samples (ELC02, CTY02) differ from the 12 others in having a large number of grains (31 grains in each sample) with ages between 1300 and 550 Myr, with the majority of grains being 1300-950 Myr (Figure 4.3m, 4.3n; Table 4.1). Middle Proterozoic rock sources are virtually absent in the Keewatin and Labrador/Quebec source regions. However, rocks of this age crop out in the southwestern sector of the Lake Superior region where volcanic rocks associated with the Midcontinent Rift System are dated around this interval (1.11-1.09 Ga), thereby suggesting a possible source for these two tills (Figure 4.1).

The flow path that would produce such a provenance signal implies deposition by southwestwardly flowing ice that traversed the Lake Superior basin, an area also largely underlain by Archean rocks of the 'Superior' group. The absence of grains of Archean age in these samples is thus surprising, and indicates either selective erosion of middle

Proterozoic lithologies from this source region, or another source terrain yet to be identified. Such a flow line could not explain the high content of sedimentary clasts in these two samples (Table 4.1), since deposition by a Lake Superior lobe would favor deposition of tills rich in crystalline clasts. Furthermore, virtually no metavolcanic clasts were found in the fraction of these two till samples. For these reasons, we currently consider these two samples as undiagnostic of source region.

4.6 Conclusions

Most $^{40}Ar/^{39}Ar$ ages of individual detrital K-feldspar grains from pre-Illinoian and LGM tills in the midcontinent are similar (~2.4-1.6 Ga) to numerical ages of the main tectonic terrains forming the Churchill province, thus identifying a source of these tills from the Keewatin ice center. The absence of grains with Archean ages (>2.6 Ga) rules out a Superior province bedrock source, and thus a source from the Labrador/Quebec ice center. Two samples yielded a grain population that is distinct from the 12 other samples in having younger ages and a narrow age distribution (~1.3-0.9 Ga). These ages may suggest a source from the Lake Superior region, but additional information is needed to confirm this source.

Most of the $^{40}Ar/^{39}Ar$ data provide support for deposition by ice originating from the Keewatin ice center. In particular, the distribution of feldspar ages is nearly identical in each sample, thereby identifying the Keewatin sector as a long-lived feature of the LIS. These results also suggest that the till compositional changes documented from these midcontinent glacial sequences (Roy et al., 2003a, 2003b) reflect changes in the Keewatin source region during late Cenozoic rather than a change in provenance.

4.7 Acknowledgements

The NSF Earth System History program provided funding for this study.

4.8 References

Aber, J.S., 1991, The glaciation of northeastern Kansas: Boreas, 20, p. 297-314.

Aber, J.S., 1999, Pre-Illinoian glacial geomorphology and dynamics in the central United States, west of the Mississippi, *In* Mickelson, D.M., and Attig, J.W., eds., Glacial Processes Past and Present: Boulder, Colorado, The Geological Society of America Special Paper 327, p. 113-119.

Bickford et al., 1994, Crustal history of the Rae and Hearne provinces, southwestern Canadian Shield, Saskatchewan: constraints from geochronological and isotopic data: Precambrian Research, v. 68, p. 1-28.

Boellstorff, J., 1973, Tephrochronology, petrology, and stratigraphy of some Pleistocene deposits in the Central Plains, USA [Ph.D. Thesis]: Baton Rouge, Louisiana State University, 197 p.

Boellstorff, J., 1978, Chronology of some Late Cenozoic deposits from the central United States and the Ice Ages: Transactions of the Nebraska Academy of Science, v. 6, p. 35-49.

Calvell, P.A., Wijbrans, J.R., Baadsgaard, H., 1992, Archean magmatism in Kaminak Lake area, District of Keewatin, Northwest Territories: ages of the carbonatite-bearing alkaline complex and some host granitoid rocks: Canadian Journal of Earth Sciences, v. 29, p. 896-917.

Clark, P.U. and Pollard, D., 1998, Origin of the middle Pleistocene transition by ice sheet erosion of regolith: Paleoceanography, v. 13, p. 1-19.

Colgan, M.P., 1999, Early middle Pleistocene glacial sediments (780000-620000 BP) near Kansas City area, northeastern Kansas and northwestern Missouri, USA: Boreas, v. 28, p.477-489.

Croker et al, 1993, Sm-Nd, U-Pb and Rb-Sr geochronology and lithostructural relationships in the southwestern Rae Province: constraints on crustal assembly in the western Canadian Shield: Precambrian Research, v. 61, p. 27-50.

Duncan, R.A., 2002, A time frame for the construction of the Kerguelen Plateau and Broken Ridge: Journal of Petrology, v. 43, p. 1109-1119.

Dyke, A.S., Prest, V.K., 1987, Late Wisconsinan and Holocene history of the Laurentide ice sheet: Géographie Physique et Quaternaire, v. 41, p. 237-263.

Goodwin, A.M., 1996, Principles of Precambrian Geology: Academic Press, 322 pp.

Gwiazda, R.H., Hemming, S.R., Broecker, W.S., 1996, Evidence from $^{40}Ar/^{39}Ar$ ages for Churchill province source of ice-rafted amphiboles in Heinrich layer 2: Journal of glaciology, v. 42, p. 440-446.

Hemming, S.R., Broecker, W.S., Sharp, W.D., Bond, G.C., Gwiazda, R.H., McManus, J.F., Klas, M., Hajdas, I., 1998, Provenance of Heinrich layers in core V28-82, northeastern Atlantic: $^{40}Ar/^{39}Ar$ ages of ice-rafted hornblende, Pb isotopes in feldspar grains, and Nd-Sr-Pb isotopes in the fine sediment fraction, Earth and Planetary Science Letters, v. 164, p. 317-333.

Hemming, S.R., Bond, G.C., Broecker, W.S., Sharp, W.D., 2000a, Evidence from $^{40}Ar/^{39}Ar$ ages of individual hornblende grains for varying Laurentide sources of iceberg discharges 22,000 to 10,500 yr B.P., Quaternary Research, v. 54, p. 372-383.

Hemming, S.R., Gwiazda, R.H., Andrews, J.T., Broecker, W.S., Jennings, A.E., Onstott, T., 2000b, $^{40}Ar/^{39}Ar$ and Pb-Pb study of individual hornblende and feldspar grains from southeastern Baffin Island glacial sediments: implications for the provenance of Heinrich layers, Canadian Journal of Earth Sciences, v. v. 37, p. 879-890.

Hoffman, P.H., 1989, Precambrian geology and tectonic history: *In* Bally, A.W. and Palmer, A.R., eds., The Geology of North America – An Overview, Geological Society of America, v. A, p. 447-512.

Hoffman, P.H., 1990, Subdivisions of the Churchill province and extent of the Trans-Hudson orogen: *In* Lewry, J.F. and Stauffer, M.R., eds, The Early Proterozoic Trans-Hudson Orogen of North America, The Geological Association of Canada, Special Paper 37, p. 15-40.

Izett, G.A., 1981, Volcanic ash beds: Recorders of upper Cenozoic silicic pyroclastic volcanism in the western United States: Journal of geophysical Research, 86, p. 10200-10222.

Lewry et al., 1985, Variations in character of Archean rocks in the western Churchill province and its significance: *In* Evolution of Archean Supracrustal Sequences, Ayres et al., eds, The Geological Association of Canada, Special Paper 28, p. 239-261.

Rovey, C.W. II, Kean, W.F., 1996, Pre-Illinoian stratigraphy in north-central Missouri: Quaternary Research, v. 45, p. 17-29.

Roy, M., Clark, P.U., Barendregt, R.W., Glassmann, J.R., Enkin, R.J., (*in Press*). Glacial stratigraphy and paleomagnetism of late Cenozoic deposits in the north-central U.S.: Geological Society of America Bulletin.

Roy, M., Clark, P.U., Raisbeck, G.M., Yiou, F., 2003b. Geochemical constraints on the origin of the middle Pleistocene transition from the glacial sedimentary record of the north-central U.S.: (*To be submitted to Earth and Planetary Sciences Letters*).

Sims, P.K., and others, 1993, The Lake Superior region and Trans-Hudson orogen: *In* Precambrian Conterminous U.S., Reed, J.C. et al., eds, The Geology of North America, Geological Society of America, v. C-2, p. 11-120.

CHAPTER 5

Conclusions

The north-central U.S. region preserves extensive glacial sedimentary sequences that record the southernmost advances of continental ice sheets in low mid-latitudes since the onset of Northern Hemisphere glaciation in the late Pliocene ~2.4 Ma. Paleomagnetic measurements on the glacial and nonglacial deposits forming the midcontinent sequences allowed the recognition of tills deposited during the Brunhes Normal Chron and Matuyama Reversed Chron. In addition to the Brunhes/Matuyama magnetic reversal (~0.78 Ma), chronological constraints are also provided by the presence of three volcanic ashes of different ages (2.003 Ma, 1.293 Ma, and 0.602 Ma) derived from eruptions of the Yellowstone caldera in Wyoming. Compositional analyses on the glacial deposits indicate that the midcontinent glacial sequences display a wide variation in their lithological and mineralogical content, which is characterized by an increase in crystalline materials in progressively younger tills. Based on these results and lithostratigraphic considerations, the midcontinent tills can be grouped under three categories. Two older groups of reverse-polarity tills, the late Pliocene 'R2 tills' and the early Pleistocene 'R1 tills', which contain a low and intermediate amount of clasts and minerals originating from crystalline bedrock, respectively; and one younger group of normal-polarity tills, the middle Pleistocene 'N tills', enriched in crystalline materials. N tills have also a composition nearly similar to the one of late Pleistocene tills that were deposited by the Des Moines lobe around the Last Glacial Maximum (LGM). The documented petrographic and mineralogic changes are indicative of an increase with time in the areal distribution of unweathered igneous and metamorphic source bedrock. The current chronology prevents the identification of individual ice advance, but within the present stratigraphic context, the presence of paleosols

developed in tills of different age and composition suggest that the midcontinent sequences record at least seven advances of the Laurentide ice sheet to a position south of the LGM.

The bulk geochemistry of the silicate fraction of the different till groups was used to bring additional constraints on the nature of the petrographic and mineralogic changes documented in the midcontinent till sequences, and to evaluate the hypothesis that the middle Pleistocene transition (MPT) is a consequence of the erosion of an extensive regolith mantle and subsequent exposure of the underlying fresh crystalline bedrock of the Canadian Shield by the Laurentide Ice Sheet. In general, the geochemistry of the till groups shows a discrepancy with the average composition of the Canadian Shield rocks from which they should derive, and this difference decreases in progressively younger till groups. Late Pliocene R2 tills are depleted in major-element oxides (CaO, MgO, Na_2O) derived from feldspars and ferromagnesians, and enriched in $Si0_2$ (quartz), FeO (iron oxides) and TiO_2 (ilmenite and other resistates), whereas the early Pleistocene R1 tills and middle Pleistocene N tills show a gradual enrichment in CaO, MgO, and Na_2O, and depletion in SiO_2, FeO, and TiO_2. In contrast, LGM tills show major-element oxides concentrations resembling the most that of the shield rocks. The content of meteoric ^{10}Be in different-age tills indicate that the late Pliocene R2 tills have the highest ^{10}Be concentrations, and that the ^{10}Be concentrations of younger tills show a marked decrease by ~1.3 Ma. This suggests the disappearance of the uppermost ^{10}Be-enriched horizon of the regolith and attendant exhumation of ^{10}Be-depleted crystalline rocks at the onset of the MPT. Marine isotope records of Sr, Os, and Hf also show significant changes around the MPT that can be explained by the removal of a regolith and the progressive exhumation of fresh silicate rocks. Consequently, these results support the regolith hypothesis and suggest that a change in subglacial substrate during the late Cenozoic best explains the geological constraints on the MPT that are imposed by records of ice volume and ice sheet extent.

A total of 504 $^{40}Ar/^{39}Ar$ ages were obtained from individual K-feldspar grains retrieved from 14 till samples that span the last 2 Ma in order to constrain the provenance of midcontinent tills, and shed light on the origin of the till compositional changes described above. Most samples analyzed show a large population of grains with $^{40}Ar/^{39}Ar$ ages (~2.4-1.6 Ga) similar to that of numerical ages of the main tectonic terranes forming the Churchill province of the Canadian Shield. These results provide support for deposition by ice originating from Keewatin ice dispersal center of the western sector of the LIS. The absence of grains with Archean ages (>2.6 Ga) rules out a Superior province bedrock source, and thus deposition by ice originating from the Labrador/Quebec ice center of the eastern sector of the LIS. The distribution of feldspar ages is nearly identical in each sample, thereby identifying the Keewatin sector as a long-lived feature of the LIS. These results thus suggest that the till compositional changes documented from the midcontinent glacial sequences reflect changes in the Keewatin source region during late Cenozoic rather than a change in provenance.

BIBLIOGRAPHY

Aber, J.S., 1991, The glaciation of northeastern Kansas: Boreas, 20, p. 297-314.

Aber, J.S., 1999, Pre-Illinoian glacial geomorphology and dynamics in the central United States, west of the Mississippi, *In* Mickelson, D.M., and Attig, J.W., eds., Glacial Processes Past and Present: Boulder, Colorado, Geological society of America Special Paper 327, p. 113-119.

Alley, R. B., Blankenship, D.D., Bentley, C.R., and Rooney, S. T., 1986, Deformation of till beneath ice stream B, West Antarctica: Nature, v. 322, p. 57-59.

Andrews, J.T., 1993, Changes in the silt- and clay-size mineralogy of sediments at Ocean Drilling Program site 645B, Baffin Bay: Canadian Journal of Earth Sciences, v. 30, p. 2448-2452.

Armstrong, R.L., 1971, Glacial erosion and the variable isotopic composition of strontium in seawater: Nature, v. 230, p. 132-133.

Berger, A., 1978, Long-term variations in caloric insolation resulting from the Earth's orbital elements: Quaternary Research, v. 9, p. 139-167.

Berger, A., Li, X.S., Loutre, M.F., 1999, Modeling northern hemisphere ice volume over the last 3 Ma: Quaternary Science Reviews, v. 18, p. 1-11.

Bickford et al., 1994, Crustal history of the Rae and Hearne provinces, southwestern Canadian Shield, Saskatchewan: constraints from geochronological and isotopic data: Precambrian Research, v. 68, p. 1-28.

Bierman, P.R., Marsella, K.A., Patterson, C., Davis, P.T., and Caffee, M., 1999, Mid-Pleistocene cosmogenic minimum-age limits for pre-Wisconsinan glacial surfaces in southwestern Minnesota and southern Baffin Island: a multiple nuclide approach: Geomorphology, v. 27, p. 25-39.

Blum, J.D., 1997, The effect of late Cenozoic glaciation and tectonic uplift on silicate weathering rates and the marine $^{87}Sr/^{86}Sr$ record, *in* W.F. Ruddiman, ed., Tectonic Uplift and Climate Change: Plenum Press, New York, p. 259-288.

Blum, J.D. and Erel, Y., 1995, A silicate weathering mechanism linking increase in marine $^{87}Sr/^{86}Sr$ with global glaciation: Nature, 373, p. 415-418.

Boellstorff, J., 1973, Tephrochronology, petrology, and stratigraphy of some Pleistocene deposits in the Central Plains, USA [Ph.D. Thesis]: Baton rouge, Louisiana State University, 197 p.

Boellstorff, J., 1976, The succession of late Cenozoic ashes in the Great Plains: a progress report: Guidebook Series 1, Kansas Geological Survey, p. 37-71.

Boellstorff, J., 1978a, A need for redefinition of North American Pleistocene stages: Transactions of the Gulf Coast Association of Geological Societies, Transactions, v. 28, p. 65-74.

Boellstorff, J., 1978b, Chronology of some Late Cenozoic deposits from the central United States and the Ice Ages: Transactions of the Nebraska Academy of Science, v. 6, p. 35-49.

Boellstorff, J., 1978c, North American Pleistocene stages reconsidered in the light of probable Pliocene-Pleistocene continental glaciation: Science, v. 202, p. 305-307.

Bouchard, M., 1985, Weathering and weathering residuals on the Canadian Shield: Fennia, v. 163, p. 327-332.

Bouchard, M., Godard, A., 1984, Les alterites du boulcier canadien: premier bilan d'une campagne de reconnaissance: Geographie Physique et Quaternaire, v. 38, p. 149-163.

Bouchard, M., Pavich, M.J., 1989, Characteristics and significance of pre-Wisconsinan saprolites in the northern Appalachians: Z. Geormorphl. N.F., Suppl. Band, v. 72, p. 125-137.

Boulton, G.S. and Jones, A.S., 1979, Stability of temperate ice caps and ice sheets resting on beds of deformable sediments: Journal of Glaciology, v. 24, 29-43.

Broecker, W.S., and 7 others, 1989, Routing of meltwater from the Laurentide ice sheet during the Younger Dryas cold episode: Nature, v. 341, p. 318-321.

Burton, K.W., Birck, J.L., Allegre, C.J., O'Nions, R.K., 1995, Fine scale records of seawater $^{187}Os/^{186}Os$: Eos, Transactions, American Geophysical Union, v. 76, Suppl., p.182.

Calvell, P.A., Wijbrans, J.R., Baadsgaard, H., 1992, Archean magmatism in Kaminak Lake area, District of Keewatin, Northwest Territories: ages of the carbonatite-bearing alkaline complex and some host granitoid rocks: Canadian Journal of Earth Sciences, v. 29, p. 896-917.

Capo, R.C. and DePaolo, D.J., 1990, Seawater strontium isotopic variations from 2.5 Million years ago to present: Science, v. 249, p. 51-55.

Clark, P.U., 1994, Unstable behavior of the Laurentide ice sheet over deforming sediments and its implications for climate change: Quaternary Reseach, v. 41, p. 19-25.

Clark, P.U. and Pollard, D., 1998, Origin of the middle Pleistocene transition by ice sheet erosion of regolith: Paleoceanography, v. 13, p. 1-19.

Clark, P.U., Alley, R. B. and Pollard, D., 1999, Northern Hemisphere ice sheet influences on global climate change: Science, v. 286, p. 1104-1111.

Colgan, M.P., 1999, Early middle Pleistocene glacial sediments (780000-620000 BP) near Kansas City area, northeastern Kansas and northwestern Missouri, USA: Boreas, v. 28, p.477-489.

Croker et al, 1993, Sm-Nd, U-Pb and Rb-Sr geochronology and lithostructural relationships in the southwestern Rae Province: constraints on crustal assembly in the western Canadian Shield: Precambrian Research, v. 61, p. 27-50.

Cuffey, K.M., Alley, R.B., 1996, Is erosion by deforming subglacial sediments significant? (toward till continuity): Annals of Glaciology, v. 22, p. 17-24.

Dort, W. Jr., 1985, Field evidence for more than two early Pleistocene glaciations of the central Plains: Ter-Qua Symposium Series, v. 1, p. 41-51.

Duncan, R.A., 2002, A time frame for the construction of the Kerguelen Plateau and Broken Ridge: Journal of Petrology, v. 43, p. 1109-1119.

Dyke, A.S., Prest, V.K., 1987, Late Wisconsinan and Holocene history of the Laurentide ice sheet: Géographie Physique et Quaternaire, v. 41, p. 237-263.

Dyke, A.S., Andrews, J.T., Clark, P.U., England, J.H., Miller, G.H., Shaw, J., Veillete, J.J., 2002, The Laurentide and Innuitian ice sheets during the last glacial maximum, Quaternary Science Reviews, v. 21, p. 9-31.

Easterbrook, D.J. and Boellstorff, J., 1984, Paleomagnetism and chronology of Early Pleistocene tills in the central United States, *in*: Mahaney, W.C., ed., Correlation of Quaternary Chronologies: Norwich, England, GeoBooks, p. 73-90.

Elkibbi, M., Rial, J.A., 2001, An outsider's review of the astronomical theory of the climate: is the eccentricity-driven insolation the main driver of the ice ages?: Earth-Science Reviews, v. 56, p. 161-177.

Faure, G., 1998, Principles and applications of geochemistry, 2nd ed. Prentice-Hall, 600 p.

Farrell, J.W., Clemens, S.C. and Gromet, L.P., 1995, Improved chronostratigraphic reference curve of late Neogene seawater $^{87}Sr/^{86}Sr$: Geology, v.23, p. 403-406.

Gansecki, C.A., Mahood, G.A., and McWilliams, M., 1998, New ages for the climatic eruptions at Yellowstone: Single-crystal $^{40}Ar/^{39}Ar$ dating identifies contamination: Geology, v. 26, p. 343-346.

Ghil, M., Childress, S., 1987, Topics in geophysical fluid dynamics, atmospheric dynamics, dynamo theory, and climate dynamics: Applied Mathematical Sciences, v. 60, Springer, New York-Heidelberg-Berlin, International, 485. p.

Godard, A., 1979, Geomorphological reconnaissance on the north part of Labrador and Nouveau Quebec peninsula: a contribution to the study of basement-rock landform in cold environments: Revue de Géomorphologie Dynamique, v. 28, p. 125-142

Goldich, S.S., 1938, A study in rock weathering: Journal of Geology, v. 46, p. 17-58.

Goodwin, A.M., 1996, Principles of Precambrian Geology: Academic Press, 322 pp.

Gravenor, C.P., 1975, Erosion by continental ice sheets: American Journal of Science, v. 275, p. 594-604.

Gwiazda, R.H., Hemming, S.R., Broecker, W.S., 1996, Evidence from $^{40}Ar/^{39}Ar$ ages for Churchill province source of ice-rafted amphiboles in Heinrich layer 2: Journal of glaciology, v. 42, p. 440-446.

Hallberg, G.R., 1986, Pre-Wisconsinan glacial stratigraphy of the central plains region in Iowa, Nebraska, Kansas, and Missouri: Quaternary Science Reviews, v. 5, p. 11-15.

Hallberg, G.R., 1980, Pre-Wisconsinan stratigraphy in southeast Iowa, *in*: Hallberg, G.R., ed., Illinoian and pre-Illinoian stratigraphy of southeast Iowa and adjacent Illinois: Iowa City, Iowa Geological Survey Technical Information Series 11, p. 1-110.

Hays, J.D., Imbrie, J. and Shackleton, N.J., 1976, Variations in the Earth's orbit: Pacemaker of the ice ages: Science, v. 194, p. 1121-1132.

Hemming, S.R., Broecker, W.S., Sharp, W.D., Bond, G.C., Gwiazda, R.H., McManus, J.F., Klas, M., Hajdas, I., 1998, Provenance of Heinrich layers in core V28-82, northeastern Atlantic: $^{40}Ar/^{39}Ar$ ages of ice-rafted hornblende, Pb isotopes in feldspar grains, and Nd-Sr-Pb isotopes in the fine sediment fraction, Earth and Planetary Science Letters, v. 164, p. 317-333.

Hemming, S.R., Bond, G.C., Broecker, W.S., Sharp, W.D., 2000a, Evidence from $^{40}Ar/^{39}Ar$ ages of individual hornblende grains for varying Laurentide sources of iceberg discharges 22,000 to 10,500 yr B.P., Quaternary Research, v. 54, p. 372-383.

Hemming, S.R., Gwiazda, R.H., Andrews, J.T., Broecker, W.S., Jennings, A.E., Onstott, T., 2000b, $^{40}Ar/^{39}Ar$ and Pb-Pb study of individual hornblende and feldspar grains from southeastern Baffin Island glacial sediments: implications for the

provenance of Heinrich layers, Canadian Journal of Earth Sciences, v. v. 37, p. 879-890.

Hoffman, P.H., 1989, Precambrian geology and tectonic history: *In* Bally, A.W. and Palmer, A.R., eds., The Geology of North America – An Overview, Geological Society of America, v. A, p. 447-512.

Hoffman, P.H., 1990, Subdivisions of the Churchill province and extent of the Trans-Hudson orogen: *In* Lewry, J.F. and Stauffer, M.R., eds, The Early Proterozoic Trans-Hudson Orogen of North America, The Geological Association of Canada, Special Paper 37, p. 15-40.

Imbrie et al., 1984, The orbital theory of Pleistocene climate: Support for a revised chronology of marine _^{18}O record: in Milankovitch and Climate, Part 1, A.L. Berger et al., eds., p. 269-305, D. Reidel, Norwell, Massachusetts.

Imbrie et al., 1992, On the structure and origin of major glaciation cycles, 1. Linear response to Milankovich forcing: Paleoceanography, v. 7, p. 701-738.

Imbrie and 17 others, 1993, On the structure and origin of major glaciations cycles, 2, The 100,000-year cycle: Paleoceanography, v. 8, p. 699-735.

Izett, G.A., 1981, Volcanic ash beds: Recorders of upper Cenozoic silicic pyroclastic volcanism in the western United States: Journal of geophysical Research, 86, p. 10200-10222.

Izett, G.A., 1981, Volcanic ash beds: Recorders of upper Cenozoic silicic pyroclastic volcanism in the western United States: Journal of Geophysical Research, v. 86, p. 10200-10222.

Joyce, J.E., Tjalsma, L.R.C., Prutzman, J.M., 1993, North American glacial meltwater history for the past 2.3 My: Oxygen isotope evidence from the Gulf of Mexico: Geology, v. 21, p.483-486.

Kemmis, T.J. Bettis, E.A. III, and Hallberg, G.H., 1992, Quaternary Geology of Conklin Quarry: Guidebook Series no. 13, Iowa Department of Natural Resources, 41 p.

Kirschvink, J.L., 1980, The least-squares line and plane and the analysis of paleomagnetic data: Geophysical Journal of the Royal Astronomical Society, v. 62, p. 699-718.

Lasalle, P., De Kimpe, C.R., LaVerdiere, M.R., 1985, Sub-till saprolites in southeastern Quebec and adjacent New England: erosion, stratigraphic and climatic significance: Geological Society of America Special Paper 197, p. 13-25.

Lewry et al., 1985, Variations in character of Archean rocks in the western Churchill province and its significance: *In* Evolution of Archean Supracrustal Sequences, Ayres et al., eds, The Geological Association of Canada, Special Paper 28, p. 239-261.

Licciardi, J.M., Teller, J.T., Clark, P.U., 1999, Freshwater routing of the Laurentide ice sheet during the last deglaciation, In Mechanisms of Global Climate Change at Millenial Time Scales, P.U. Clark, R.S. Webb, Keigwin, L.D., eds, Geophysical Monograph, American Gephysical Union, Washington, DC, p. 177-200.

Lowell, T.V., Hayward, R.K., Denton, G.H., 1999, Role of climate oscilations in determining ice margin positions: hypothesis, examples and implications: In Mickelson, D.M. and Attig, J.W., eds, Glacial Processes Past and Present: Special Paper, Boulder, CO, Geological Society of America, p. 193-203.

MacAyeal, D.R., 1993a, A low-order model of growth/purge oscilations of Heinrich-event cycle: Paleoceanography, v. 8, p 767-773.

MacAyeal, D.R., 1993b, Binge/purge oscilations of the Laurentide Ice Sheet as a cause of North Atlanctic Heinrich events: Paleoceanography, v. 8, p 767-773.

McIntyre, K., Ravelo, A.C., Delaney, M.L., 1999, North Atlantic intermediate waters in the late Pliocene to early Pleistocene: Paleoceanography, v. 14. p. 324-335.

McKeague, J.A., Grant, D.R., Kodama, H., Beke, G.J., Wang, C., 1983, Properties and genesis of a soil and the underlying gibbsite-bearing saprolite, Cape Breton Island, Canada: Canadian Journal of Earth Sciences, v. 20, p. 37-48.

Mix, A.C., Pisias, N.G., Rugh, W., Wilson, J., Morey, A. and Hagelberg, T.K., 1995, Benthic foraminifer stable isotope record from site 849 (0-5 Ma): Local and global climate changes: N.G. Pisias et al. eds., Procedures of Ocean Drilling Program Scientific Results, v. 138, p. 371-342.

Nesbitt, H.W. and Markovics, G., 1997, Weathering of granodiorite crust, long-term storage of elements in weathering profiles, and petrogenesis of siliciclastic sediments. Geochimica Cosmochemica Acta, v. 61, p. 1653-1670.

Nesbitt, H.W. and Young, G.M., 1982, Early Proterozoic climates and plate motions inferred from major element chemistry: Nature, v. 299, p. 715-717.

Nesbitt, H.W. and Young, G.M., 1984, Prediction of some weathering trends of plutonic and volcanic rocks based on thermodynamic and kinetic considerations: Geochimica Cosmochemica Acta, v. 48, p. 1523-1534.

Nesbitt, H.W. and Young, G.M., 1989, Formation and diagenesis of weathering profiles: Journal of Geology, v. 97, p. 129-147.

Nielsen, E., Morgan, A.V., Morgan A., Mott, R.J., Rutter, N.W. and Causse, C., 1986, Stratigraphy, paleoecology and glacial history of the Gillam area, Manitoba; Canadian Journal of Earth Sciences, v. 23, p. 1641-1661.

Ollier, C. and Pain., C., 1996, Regolith, soil and landforms. Chichester, New York : John Wiley & Sons, 309 p.

Pagani, M., Arthur, M.A., Freeman, K.H., 1999, Miocene evolution of atmospheric carbon dioxide: Paleoceanography, v. 14, p. 273-292.

Parham, W.E., 1970, Clay mineralogy and geology of Minnesota kaolin's clay: Special Publication Series, Minnesota Geological Survey, SP-10, 142 pp.

Pavich, M.J., Brown, L., Klein, J., Middleton, R., 1984, Beryllium-10 accumulation in a soil chronosequence: Earth and Planetary science Letters, v. 68, p. 198-204.

Pavich, M.J., Brown, L., Valette-Silver, N.J., Klein, J., Middleton, R., 1985, ^{10}Be analysis of a Quaternary weathering profile in the Virginia Piedmont; Geology, v. 13, p. 39-41.

Paterson, W.S.B., 1994, The Physics of Glaciers, 3rd ed.: Pergamon Press, Tarrytown, NY, 380 p.

Pearson, P.N., Palmer, M.R., 2000, Estimating Paleogene atmospheric pCO_2 using boron isotope analysis of Foraminifera: *In*: Early Paleogene warm climates and biosphere dynamics, Short papers and extended abstracts, Schmitz, B., Sundquist, B., Andreasson, F.P. (eds.), Geological Society of Sweden, Stockholm, Sweden, v. 122, p. 127-128.

Petit, J.R., and 16 others, 1999, Climate and atmospheric history of the past 420,000 years from the Vostok ice core, Antarctica: Nature, v. 399, p. 429-436.

Peucker-Ehrenbrink, B., Blum, J.D., 1998, Re-Os isotope systematics and weathering of Precambrian crustal rocks: implications for the marine osmium isotope record: Geochimica et Cosmochimica Acta, v. 62, p. 3193-3203.

Pisias, N. G., Moore, T.C. Jr., 1981, The evolution of the Pleistocene Climate: A time series approach. Earth Planetary Science Letters, v. 52, p. 450-458.

Raymo, M.E., 1994, The initiation of northern hemisphere glaciation: Annual Review of Earth Planetary Science, v. 22, p. 353-383.

Raymo, M.E., 1998, Glacial Puzzles: Science, v. 281, p. 1467-1468.

Reed, E.C., Dreezen, V.H., 1965, Revision of the classification of the Pleistocene deposits of Nebraska: Nebraska Geological Survey Bulletin, v. 23, 65 p.

Reynolds, Jr., R.C., 1985, NEWMOD© A computer program for the calculation of one-dimensional diffraction patterns of mixed-layered clays: R.C. Reynolds, Jr., 8 Brook Dr., Hanover, NH.

Richmond, G.M. and Fullerton, D.S., 1986a, Introduction to Quaternary glaciations in the United States of America: Quaternary Science Reviews, v. 5, p. 3-10.

Richmond, G.M. and Fullerton, D.S., 1986b, Summation of Quaternary glaciations in the United States of America: Quaternary Science Reviews, v. 5, p. 183-196.

Rovey, C.W. II, Kean, W.F., 1996, Pre-Illinoian stratigraphy in north-central Missouri: Quaternary Research, v. 45, p. 17-29.

Rovey, C.W. II, Kean, W.F., 2001, Paleomagnetism of the Moberly formation, northern Missouri, confirms a regional magnetic datum within the pre-Illionian glacial sequence of the midcontinental USA: Boreas, v. 30, p. 53-60.

Roy, M., Clark, P.U., Barendregt, R.W., Glasmann, J.R., Enkin, R.J., (*in press*), Glacial stratigraphy and paleomagnetism of late Cenozoic deposits in the north-central U.S. Geological Society of America Bulletin.

Roy, M., Clark, P.U., Raisbeck, G.M., Yiou, F., 2003b. Geochemical constraints on the origin of the middle Pleistocene transition from the glacial sedimentary record of the north-central U.S.: (*To be submitted to Earth and Planetary Sciences Letters*).

Ruddiman, W.F., 1997, Tectonic Uplift and Climate Change: Ruddiman, ed., Plenum Press, New York, 535 p.

Ruddiman, W.F. et al., 1989, Pleistocene evolution: Northern hemisphere ice sheets and North Atlantic Ocean: Paleoceanography, v. 4, p. 353-412.

Shaw, D.M., Reilly, G.A., Muysson, J.R., Pattenden, G.E., Campbelll, F.E., 1967, An estimate of the composition of the Canadian Precambrian Shield. Canadian Journal of Earth Sciences, v. 4, p. 829-853.

Shaw, D.M., Dostal, J., Keys, R.R., 1976, Additional estimates of continental surface Precambrian shield composition in Canada. Geochimica Cosmochemica Acta, v. 40, p. 73-84.

Setterholm, D.R. and Morey, G.B., 1995, An extensive pre-Cretaceous weathering profile in east-central and southwestern Minnesota: U.S. Geological Survey Bulletin 1989, p. H1-H29.

Sims, P.K., and others, 1993, The Lake Superior region and Trans-Hudson orogen: *In* Precambrian Conterminous U.S., Reed, J.C. et al., eds, The Geology of North America, Geological Society of America, v. C-2, p. 11-120.

Stone, J.O., 1998, A rapid fusion method for separation of beryllium-10 from soils and silicates; Geochimica Cosmochemica Acta, v. 62, pp. 555-561.

Taylor, A. and Blum, J.D., 1995, Relation between soil age and silicate weathering rates determined from the chemical evolution of a glacial chronosequence: Geology, v. 23, p. 979-982.

Taylor, G. and Eggleton, R.A., 2001, Regolith geology and geomorphology. John Wiley & Sons, 375 p.

Thiebault, F., Cremer, M., Bebrabant, P., Foulon, J., Nielson, O.B. and Zimmerman, H., 1989, Analysis of sedimentary facies, clay mineralogy, and geochemistry of the Neogene-Quaternary sediments in site 645, Baffin Bay: Procedures of Ocean Drilling Program Scientific Results, v. 105, p. 83-100.

Tziperman, E., Gildor, H., 2003, On the mid-Pleistocene transition to 100-kyr glacial cycles and the asymmetry between glaciation and deglaciation times, Paleoceanography, v. 18, 1001, doi:10.1029/2001PA000627.

van der Flierdt, T., Frank, M., Lee, D., Halliday, A.N., 2002, Glacial weathering and the hafnium isotope of seawater. Earth and Planetary science Letters, v. 198, p. 167-175.

Wang, C., Ross, G.J., 1989, Granitic saprolites: their characteristics, identification and influence on soil properties in the Appalachian region of Canada: Z. Geormorphl. N.F., Suppl. Band, v. 72, p. 149-161.

Wedepohl, K.H., 1995, The composition of the continental crust. Geochimica Cosmochemica Acta, v. 59, p. 1217-1232.

Appendices

APPENDIX A

Procedures for semi-quantitative analysis of clay mineral assemblages

A.1 Procedures for semi-quantitative analysis of clay mineral assemblages

The mineralogy of the clay (<2 μm) and silt (<15 μm) fraction of till was analyzed using standard X-ray diffraction (XRD) techniques performed on a Phillips XRG3100 equipped with a focussing monochromater (Cu Kα radiation, 0.02° 2 theta/step, 1 sec. count/step). The mineral content of the samples was based upon the interpretation of weighted intensities of XRD pattern basal reflections which were determined using the JADE+ software. The quantitative analysis of the clay mineralogy of a sample is complicated by variations in the chemical composition of clay minerals, as well as their polytypic form and their order-disorder which all have profound effects on the XRD intensities. For these reasons, we used semi-quantitative analysis based on the comparisons (profile fitting) of peak area measurements of unknown samples to the peak areas of internal standards with known mineral composition. The composition of minerals present in five different XRD patterns, which best represent the variety of XRD patterns obtained in this study, was modeled using the computer program NEWMOD (Reynolds, 1985). The XRD patterns were then compared to the modeled XRD patterns in order to identify which of the modeled patterns most closely resembled the mineral content of the samples. The peak areas of the samples were then measured. Knowing the content of each mineral phase present in the modeled patterns, comparisons of the peak areas of the sample with the modeled patterns allowed the determination of the amount of mineral phases present in each sample. The clay mineral abundances of the <2 μm fraction of tills were then normalized to 100% and expressed as weight % values.

APPENDIX B

Conversion of geochemical concentrations from weight % to Net gain-loss %

B.1 Conversion of geochemical concentrations from weight % to Net gain-loss %

The changes caused by chemical weathering on the composition of the rock source are evaluated by comparing the concentrations of the major-element oxides of the till groups to the ones of the average upper continental crust, assumed to be the fresh end-member. Element concentrations from the XRF data are expressed in weight %, i.e. the sum of the concentrations of each element in a sample is equal to 100. Consequently, a 'true' change in one element causes 'apparent' changes in all other elements in the sample. Therefore, a correction must be made to the concentrations of all major elements so the actual gains and losses caused by chemical weathering can be identified. This conversion can be made by recalculating the concentrations of all elements with respect to the concentration of one element assumed to have remained constant during the process of chemical weathering (despite the fact that the raw concentration of this element may appear to change). Al_2O_3 is often chosen as the main conservative elements since it is common in aluminosilicates and because its low solubility favors its preservation within the weathering profile after incongruent weathering (Faure, 1998). This assumption is also confirmed by field observations of a saprolite developed on granitoids just north of the study area (Goldich, 1938). A correction factor can be established based on the change in Al_2O_3 concentrations of the fresh rock source compared to the one of a till sample. For example, the Al_2O_3 concentration[†] in the AUCC and N tills is 14.60% and 12.47%, respectively. This apparent decrease in Al_2O_3 must be related to a gain in the weight of the rock (probably due to a combination of the weathering processes and incorporation of new material during glacial transport). This gain can be defined by:

$$(14.60g / 12.47g) * 100 = 1.17g$$

which means that 17g of material was added to the original 100g of material analyzed. Knowing this fact, the amount of the other elements in the sample can now be corrected by multiplying their concentrations (wt.) in the sample by a 'weight factor' (wt factor) derived from the ratio of the constant oxide in fresh and weathered sampled:

$$\text{wt factor} = (Al_2O_3)_{AUCC} / (Al_2O_3)_{tills} = 1.17.$$

Once the 'real amount' of each element is determined, the actual gain and loss of each element can be calculated by subtracting the 'real amount' of the element to its concentration found in the AUCC. Finally, the proportion of the actual loss and gain of an element is expressed in percent as follow:

element gain or loss (%) = [amount of gain-loss (g) / amount AUCC (g)] *100.

Results of this conversion are presented in Table 1.

([†]the concentration of an element in wt % is equivalent to an amount in grams per 100g of rock or sediments.)

APPENDIX C

Major-oxide concentrations of tills

Table C.1: Major-oxide concentrations of tills[†].

Sample no.	Site[‡] no.	Longitude	Latitude	SiO_2 wt. %	Al_2O_3 wt. %	TiO_2 wt. %	FeO* wt. %	MnO wt. %	CaO wt. %	MgO wt. %	K_2O wt. %	Na_2O wt. %	P_2O_5 wt. %	LOI %
LGM tills														
WHA01	24	42°01'45"	93°35'48"	78.14	9.50	0.370	2.34	0.035	3.66	2.31	1.83	1.72	0.100	5.66
ALD05	25	42°31'33"	93°22'15"	76.30	10.09	0.407	2.51	0.037	4.16	2.75	1.93	1.69	0.117	7.09
N tills														
ALD03	25	42°31'33"	93°22'15"	76.94	11.47	0.533	2.86	0.019	2.65	1.98	1.97	1.48	0.091	6.57
CTY09	1	41°04'27"	95°57'50"	78.52	12.17	0.598	2.96	0.014	0.80	1.13	2.15	1.60	0.064	5.80
FLO01	8	41°22'21"	95°56'51"	75.43	13.55	0.671	3.92	0.027	1.49	1.43	2.23	1.07	0.183	6.66
FRE02	14	41°23'59"	96°31'24"	75.59	13.31	0.652	4.00	0.044	1.41	1.50	2.29	1.04	0.173	7.39
FRE05	14	41°23'59"	96°31'24"	75.55	12.63	0.616	3.45	0.048	2.18	1.96	2.24	1.18	0.132	6.93
LMR01	11	42°50'25"	96°08'56"	75.58	14.12	0.670	3.41	0.017	1.27	1.40	2.27	1.11	0.152	5.80
MER03	23	40°30'31"	93°28'55"	76.41	13.04	0.648	3.38	0.016	1.44	1.42	2.14	1.38	0.135	5.99
THA02	7	40°59'38"	94°02'25"	78.55	11.79	0.607	3.18	0.018	1.46	1.35	1.96	0.97	0.120	4.93
STR01	16	40°45'05"	95°42'45"	80.08	10.28	0.509	2.62	0.038	1.74	1.34	1.99	1.28	0.113	4.17
SHM04	4	41°51'20"	95°59'13"	75.85	13.35	0.664	3.94	0.028	1.32	1.42	2.27	0.99	0.161	6.84
BEF04	19	40°40'24"	94°15'02"	76.61	13.38	0.712	4.03	0.034	1.02	1.12	2.06	0.92	0.123	6.89
R1 tills														
CRSO2	3	41°20'59"	95°53'46"	76.19	11.72	0.682	3.97	0.033	2.30	1.84	2.11	0.98	0.178	8.47
DC141	10	41°14'59"	97°10'00"	75.43	12.61	0.629	4.11	0.035	2.01	1.77	2.23	0.99	0.187	8.01
GLW04	2	41°06'09"	95°49'20"	76.98	12.01	0.627	3.76	0.031	1.78	1.64	2.05	0.95	0.171	7.00
THU03	15	40°51'24"	95°45'30"	78.33	11.06	0.600	3.67	0.029	1.74	1.46	2.00	0.96	0.169	6.33
THU05	15	40°51'24"	95°45'30"	78.82	11.10	0.534	2.50	0.019	2.00	1.61	2.07	1.24	0.104	5.77
GRN02	6	41°27'32"	94°25'51"	76.79	11.73	0.630	3.69	0.033	2.18	1.80	2.00	1.00	0.150	6.64
TUR01	12	42°03'46"	95°59'13"	79.05	11.33	0.566	2.60	0.016	1.50	1.26	2.14	1.45	0.095	4.95
WAT01	21	39°44'34"	94°56'38"	76.33	12.09	0.634	3.98	0.033	1.95	1.73	2.12	0.96	0.184	6.90
R2 tills														
AF172	9	40°59'46"	94°12'16"	78.63	11.68	0.737	3.91	0.023	0.87	1.23	1.96	0.88	0.097	5.12
ATC02	20	39°32'29"	95°10'09"	75.96	12.75	0.709	4.59	0.033	1.12	1.38	2.33	0.96	0.178	5.49
CTY04	1	41°04'27"	95°57'50"	81.96	10.08	0.584	2.36	0.016	0.65	0.85	2.00	1.42	0.069	3.91
ELC01	17	40°15'56"	96°09'37"	75.70	13.80	0.705	3.35	0.023	0.70	1.50	2.56	1.57	0.079	6.25
BEF02	19	40°40'24"	94°15'02"	78.12	12.27	0.749	3.55	0.080	0.73	1.15	2.02	1.26	0.079	5.50
SEN01	18	39°49'37"	96°03'09"	74.07	14.34	0.769	4.88	0.032	1.04	1.45	2.45	0.79	0.178	6.82
BET01	22	40°17'32"	94°00'13"	76.32	13.62	0.795	3.61	0.022	0.57	1.31	2.26	1.39	0.103	5.26

[†]Results obtained from XRF analysis; < 2mm size-fraction of tills; carbonate content of sediment was leached prior to analysis; normalized results (Weight %); with total Fe expressed as FeO.

[‡]See Figure 3.2 for location; site coordinates given for latitude north and longitude west.

APPENDIX D

Results of $^{40}Ar/^{39}Ar$ ages of K-feldspar grains of tills

Table D.1: $^{40}Ar/^{39}Ar$ ages of glacially-derived feldspars in till sample WHA01

Sample: WHA01			Site 24 latitude: N 42°01'45"		
Till group: LGM Till			longitude: W 93°35'48"		
Lab No.	Age (Ma)	± 2σ (Ma)	40Ar (%)	K/Ca	± 2σ
02C2053	834.39	± 28.42	98.86	1.518	± 0.359
02C2048	1371.91	± 8.94	100.00	0.000	± 0.000
02C2056	1460.66	± 15.64	99.84	16.229	± 11.236
02C2041	1469.65	± 22.37	99.40	3.112E-21	± 0.000
02C2069	1522.61	± 12.82	99.82	79.589	± 312.573
02C2072	1534.32	± 23.17	99.78	121.159	± 777.643
02C2034	1547.63	± 10.05	99.80	63.610	± 265.787
02C2044	1557.26	± 15.99	99.94	2.67E-18	± 0.000
02C2060	1603.47	± 16.70	99.87	10.517	± 4.845
02C2066	1611.52	± 17.46	99.74	4.23E-08	± 0.000
02C2051	1638.53	± 12.09	99.95	1.34E-16	± 0.000
02C2064	1643.84	± 18.65	99.61	4.897	± 1.416
02C2076	1678.24	± 22.13	99.83	115.570	± 829.289
02C2046	1703.97	± 15.31	99.81	0.000	± 0.000
02C2062	1707.87	± 17.19	100.00	25.814	± 39.998
02C2063	1727.77	± 17.34	99.87	1.120E-10	± 0.000
02C2043	1732.40	± 20.53	99.93	384.854	± 12432.435
02C2035	1741.84	± 34.83	99.68	21.152	± 37.529
02C2037	1810.04	± 12.15	99.82	24.440	± 27.136
02C2067	1811.49	± 14.54	99.86	27.969	± 35.585
02C2042	1845.02	± 23.48	100.00	574.829	± 20807.587
02C2050	1852.50	± 15.79	99.82	9.694	± 4.446
02C2055	1856.29	± 15.79	99.89	7.701E-15	± 0.000
02C2039	1860.69	± 10.32	99.85	13.134	± 7.587
02C2045	1878.44	± 21.55	99.89	2.667E-18	± 0.000
02C2052	1921.81	± 27.43	99.83	51.276	± 101.631
02C2073	1932.60	± 31.80	100.00	37.426	± 119.729
02C2068	1982.95	± 12.94	100.00	28.216	± 41.899
02C2074	1995.89	± 17.41	99.80	1.496E-03	± 0.000
02C2036	2063.79	± 13.97	99.60	12.627	± 8.287
02C2070	2065.53	± 14.31	99.92	45.925	± 96.950
02C2075	2075.62	± 16.15	99.88	17.527	± 13.451
02C2059	2080.59	± 23.62	100.00	2.962E-12	± 0.000
02C2038	2135.36	± 25.61	99.88	12.973	± 8.910
02C2058	2193.00	± 32.89	99.82	19.959	± 29.185
02C2049	2308.89	± 25.88	100.00	2.667E-18	± 0.000
02C2057	2344.26	± 23.92	100.00	61.295	± 294.227

Table D.2: $^{40}Ar/^{39}Ar$ ages of glacially-derived feldspars in till sample AF151

Sample: AF151			Site 9 latitude: N 40°59'46"		
Till group: N Till			longitude: W 94°12'16"		
Lab No.	Age (Ma)	± 2σ (Ma)	40Ar (%)	K/Ca	± 2σ
02C1783	1133.50	± 12.32	99.78	47.361	± 50.978
02C1770	1436.75	± 12.39	99.45	24.838	± 12.648
02C1799	1511.12	± 17.24	99.65	36.667	± 34.121
02C1781	1543.50	± 13.38	99.83	49.259	± 60.547
02C1786	1551.61	± 15.36	99.63	92.008	± 317.49
02C1785	1595.58	± 22.29	99.89	0.868	± 0.052
02C1788	1604.10	± 25.63	99.69	6.377E-19	± 0.000
02C1795	1605.05	± 22.72	99.97	45.596	± 47.293
02C1771	1623.79	± 13.47	99.69	51.290	± 39.037
02C1798	1626.36	± 19.46	99.88	18.199	± 8.220
02C1777	1640.88	± 14.47	99.83	43.429	± 36.997
02C1772	1642.25	± 11.97	99.72	17.589	± 6.533
02C1767	1685.25	± 17.70	99.92	20.967	± 8.115
02C1776	1700.25	± 16.58	99.68	62.114	± 78.637
02C1762	1709.50	± 10.61	99.91	42.917	± 28.837
02C1773	1715.68	± 15.22	99.89	29.437	± 26.542
02C1782	1743.63	± 27.04	99.89	28.392	± 18.230
02C1763	1760.94	± 17.58	99.80	13.306	± 4.365
02C1775	1769.00	± 16.36	99.80	5.490E-34	± 0.000
02C1793	1796.77	± 12.53	99.87	112.987	± 420.871
02C1802	1850.69	± 27.38	99.85	17.713	± 7.920
02C1768	1862.15	± 29.08	99.86	38.720	± 42.042
02C1787	1872.25	± 14.01	99.77	0.000	± 0.000
02C1766	1880.90	± 22.21	99.83	11.916	± 2.725
02C1805	1882.33	± 20.84	99.83	50.446	± 154.186
02C1794	1891.29	± 14.78	99.88	3.899E-11	± 0.000
02C1765	1896.95	± 16.36	99.92	14.958	± 9.976
02C1803	1971.35	± 16.83	99.95	17.636	± 5.250
02C1780	2023.80	± 11.19	99.69	25.632	± 18.807
02C1792	2030.65	± 22.50	99.74	39.898	± 55.898
02C1807	2046.00	± 14.93	99.94	11.840	± 5.325
02C1761	2102.56	± 20.73	99.72	15.267	± 4.829
02C1791	2246.20	± 17.83	99.94	247.490	± 1642.694
02C1806	2302.29	± 15.91	100.00	23.134	± 19.810
02C1789	2319.13	± 18.73	99.85	26.307	± 20.622
02C1800	2355.25	± 28.85	99.91	15.417	± 6.665

Table D.3: $^{40}Ar/^{39}Ar$ ages of glacially-derived feldspars in till sample CTY09

Sample: CTY09			Site 1	latitude: N 41°04'27"	
Till group: N Till				longitude: W 95°57'50"	
Lab No.	Age (Ma)	± 2σ (Ma)	40Ar (%)	K/Ca	± 2σ
02C2588	1198.14	± 32.74	99.99	3.816	± 3.098
02C2581	1224.29	± 10.48	99.88	2.893	± 0.977
02C2568	1301.37	± 89.21	99.74	8.385E-22	± 0.000
02C2584	1305.79	± 17.07	99.84	8.104	± 5.739
02C2585	1475.43	± 17.47	99.87	16.078	± 19.464
02C2586	1491.57	± 22.12	99.90	6.396	± 5.663
02C2573	1504.63	± 9.30	99.78	2.669E-19	± 0.000
02C2555	1531.12	± 14.67	99.83	5.065	± 2.851
02C2559	1554.44	± 17.82	99.81	7.307	± 3.306
02C2553	1569.46	± 18.75	99.98	2.034E-34	± 0.000
02C2583	1570.45	± 11.40	99.97	9.514	± 6.863
02C2560	1579.61	± 13.71	99.89	7.143	± 3.670
02C2558	1595.04	± 22.82	99.77	5.525	± 1.191
02C2578	1617.84	± 25.11	99.82	1.141E-16	± 0.000
02C2582	1686.34	± 12.19	99.74	4.287	± 2.515
02C2549	1776.37	± 17.05	100.00	2.034E-34	± 0.000
02C2564	1834.14	± 15.26	99.89	55.926	± 203.784
02C2569	1855.32	± 12.70	99.88	38.517	± 109.273
02C2557	1894.70	± 33.38	99.85	2.734	± 0.922
02C2548	1897.09	± 26.16	99.85	13.456	± 31.435
02C2565	1898.32	± 17.25	99.86	11.421	± 10.163
02C2562	1917.14	± 16.77	99.79	11.252	± 13.222
02C2580	1945.88	± 15.19	99.96	10.092	± 11.296
02C2575	1978.32	± 25.13	99.84	2.669E-19	± 0.000
02C2556	2101.75	± 19.62	99.89	10.078	± 5.401
02C2547	2132.05	± 24.50	99.81	9.115	± 10.262
02C2566	2162.78	± 22.68	99.85	8.555	± 7.330
02C2576	2207.40	± 49.90	99.71	1.529	± 0.932
02C2571	2207.61	± 17.90	99.95	2.669E-19	± 0.000
02C2567	2234.68	± 13.41	99.89	8.230	± 7.731
02C2574	2247.92	± 25.22	100.00	2.669E-19	± 0.000
02C2572	2267.91	± 11.66	99.97	2.669E-19	± 0.000
02C2552	2398.17	± 12.17	99.87	2.034E-34	± 0.000

Table D.4: $^{40}Ar/^{39}Ar$ ages of glacially-derived feldspars in till sample WAT05

Sample: WAT05			Site 21 latitude: N 40°15'56"		
Till group: N Till			longitude: W 96°09'37"		
Lab No.	Age (Ma)	±2σ (Ma)	40Ar (%)	K/Ca	±2σ
02C2321	1004.13	± 60.57	100.00	0.309	± 0.081
02C2291	1455.71	± 19.77	99.35	5.142	± 2.232
02C2323	1463.94	± 25.39	99.98	34.403	± 116.967
02C2292	1484.98	± 15.00	99.70	9.279	± 4.342
02C2300	1511.33	± 18.29	99.69	2.744E-17	± 0.000
02C2309	1577.29	± 21.92	99.64	2.744E-17	± 0.000
02C2285	1606.47	± 24.91	100.00	1.693E-21	± 0.000
02C2314	1624.07	± 18.50	99.95	2.744E-17	± 0.000
02C2283	1626.90	± 16.45	100.00	20.301	± 23.884
02C2320	1628.52	± 17.41	100.00	18.728	± 35.159
02C2318	1631.29	± 17.36	100.00	27.580	± 61.662
02C2298	1636.66	± 19.22	99.87	2.744E-17	± 0.000
02C2299	1639.23	± 21.87	99.73	2.744E-17	± 0.000
02C2294	1650.93	± 22.36	99.94	10.764	± 8.221
02C2311	1675.31	± 24.60	99.91	2.744E-17	± 0.000
02C2293	1678.06	± 16.42	99.72	4.977	± 1.173
02C2306	1697.02	± 25.04	99.75	2.744E-17	± 0.000
02C2308	1700.69	± 18.90	99.79	2.744E-17	± 0.000
02C2290	1721.11	± 14.19	99.53	4.782	± 1.764
02C2302	1737.83	± 19.11	99.70	0.000	± 0.000
02C2286	1744.66	± 9.80	100.00	43.623	± 134.473
02C2307	1755.41	± 23.21	99.91	2.744E-17	± 0.000
02C2303	1813.59	± 14.43	100.00	2.744E-17	± 0.000
02C2316	1813.96	± 13.91	100.00	2.410E-05	± 0.000
02C2322	1819.38	± 14.43	100.00	63.586	± 342.344
02C2317	1821.00	± 14.52	99.96	16.931	± 15.569
02C2284	1830.37	± 21.92	99.99	38.642	± 67.711
02C2312	1830.94	± 19.58	99.72	2.744E-17	± 0.000
02C2301	1864.01	± 25.78	99.97	2.744E-17	± 0.000
02C2296	1875.94	± 17.25	99.29	2.744E-17	± 0.000
02C2282	1912.75	± 25.03	99.63	11.849	± 12.224
02C2315	2025.48	± 47.74	100.00	17.641	± 31.598
02C2289	2049.11	± 17.89	99.86	8.535	± 4.012
02C2319	2083.99	± 19.54	100.00	16.166	± 19.287
02C2310	2263.76	± 31.62	99.91	2.744E-17	± 0.000
02C2304	2285.79	± 21.38	99.97	2.744E-17	± 0.000
02C2287	2425.83	± 26.91	100.00	15.569	± 18.719

Table D.5: $^{40}Ar/^{39}Ar$ ages of glacially-derived feldspars in till sample BEF03

Sample: BEF03			Site 19 latitude: N 40°40'24"		
Till group: N Till			longitude: W 94°15'02"		
Lab No.	Age (Ma)	± 2σ (Ma)	40Ar (%)	K/Ca	± 2σ
02C1995	1012.88	± 22.17	99.77	54.011	± 101.046
02C1969	1143.84	± 17.18	99.53	2.728E-15	± 0.000
02C1965	1351.06	± 9.96	99.83	33.200	± 35.252
02C1984	1388.87	± 15.17	99.67	10.276	± 1.863
02C1970	1391.67	± 12.21	99.79	122.635	± 686.417
02C1985	1401.39	± 10.75	99.77	21.237	± 11.424
02C1960	1409.07	± 16.30	99.94	6.062E-20	± 0.000
02C1963	1444.43	± 11.75	99.98	111.221	± 476.680
02C1986	1479.46	± 8.70	99.83	21.550	± 9.600
02C1980	1489.02	± 13.82	99.98	120.304	± 515.788
02C1981	1496.74	± 13.19	99.78	6.567E-09	± 0.000
02C1973	1514.31	± 16.56	99.91	12.333	± 5.990
02C1971	1515.84	± 19.95	99.19	9.146E-15	± 0.000
02C1961	1568.00	± 22.28	99.36	6.062E-20	± 0.000
02C1972	1603.47	± 26.31	99.59	9.146E-15	± 0.000
02C1956	1612.54	± 13.68	99.94	2.512E-21	± 0.000
02C1983	1620.34	± 8.73	99.56	16.649	± 7.582
02C1990	1693.46	± 51.33	99.48	2.629	± 0.775
02C1993	1714.40	± 9.39	99.54	17.005	± 13.358
02C1979	1752.33	± 9.60	99.89	14.643	± 8.339
02C1977	1827.14	± 14.67	99.90	12.366	± 6.249
02C1978	1923.47	± 18.47	99.89	16.846	± 10.412
02C1955	1968.12	± 12.33	99.84	133.327	± 810.143
02C1974	1995.56	± 25.44	99.82	16.147	± 9.581
02C1997	2009.64	± 33.93	100.00	0.063	± 0.000
02C1962	2022.91	± 12.51	99.56	6.062E-20	± 0.000
02C1964	2027.26	± 30.63	99.99	9.695E-18	± 0.000
02C1967	2039.29	± 20.18	99.97	197.824	± 1341.009
02C1992	2057.21	± 25.19	99.73	11.685	± 17.008
02C1954	2099.28	± 23.12	99.71	110.711	± 646.724
02C1991	2110.44	± 292.91	93.53	0.846	± 0.730
02C1958	2122.54	± 36.69	99.89	47.304	± 203.844
02C1989	2138.11	± 18.10	99.91	248.281	± 4356.905
02C1976	2146.45	± 22.81	99.84	46.764	± 130.151
02C1996	2157.96	± 54.97	100.00	0.063	± 0.000
02C1957	2174.24	± 23.82	99.99	10.745	± 8.528
02C1953	2203.25	± 17.77	99.95	10.887	± 7.393
02C1987	2294.99	± 23.77	99.86	9.416	± 3.076

Table D.6: $^{40}Ar/^{39}Ar$ ages of glacially-derived feldspars in till sample FLO01

Sample: FLO01			Site 8 latitude: N 41°22'21"		
Till group: N Till			longitude: W 95°56'51"		
Lab No.	Age (Ma)	± 2σ (Ma)	40Ar (%)	K/Ca	± 2σ
02C2864	1320.00	± 4.00	100.00	41.300	± 100.275
02C2882	1323.99	± 5.76	98.66	1.696E-07	± 0.000
02C2858	1376.63	± 8.42	99.58	6.710E-18	± 0.000
02C2886	1427.39	± 15.28	99.99	7.343	± 5.518
02C2885	1454.85	± 11.79	99.62	260.938	± 6376.577
02C2878	1484.12	± 5.74	99.98	1.696E-07	± 0.000
02C2869	1488.38	± 5.64	99.84	12.200	± 7.939
02C2871	1516.74	± 6.51	99.10	8.413	± 6.587
02C2855	1537.59	± 8.19	99.63	259.027	± 3040.100
02C2873	1564.10	± 7.21	99.90	2.484E-09	± 0.000
02C2876	1575.78	± 5.01	99.93	8.442	± 5.336
02C2874	1579.24	± 7.66	99.99	2.484E-09	± 0.000
02C2859	1616.17	± 6.55	99.94	16.165	± 6.624
02C2868	1653.63	± 12.89	99.61	12.400	± 12.148
02C2875	1663.98	± 6.98	99.95	17.575	± 19.450
02C2867	1672.90	± 9.73	99.85	9.929	± 9.668
02C2889	1705.79	± 12.89	100.00	15.952	± 22.026
02C2866	1716.76	± 6.68	99.89	6.128E-12	± 0.000
02C2877	1726.40	± 9.22	99.91	1.696E-07	± 0.000
02C2854	1738.55	± 8.73	99.82	2.845	± 0.412
02C2849	1754.14	± 4.98	99.76	19.144	± 23.209
02C2870	1762.73	± 8.07	98.92	35.454	± 128.163
02C2863	1837.84	± 7.94	99.95	15.486	± 10.141
02C2884	1839.72	± 8.73	99.69	16.996	± 25.300
02C2850	1843.65	± 12.25	99.82	6.354	± 1.549
02C2853	1845.64	± 4.74	99.47	3.713	± 0.781
02C2888	1855.44	± 9.80	99.73	92.267	± 778.224
02C2880	1867.00	± 9.67	99.98	1.696E-07	± 0.000
02C2883	1868.45	± 10.54	99.89	4.686	± 1.946
02C2851	1903.99	± 6.13	99.91	10.448	± 3.821
02C2856	1980.32	± 7.54	99.89	6.121	± 2.049
02C2860	1985.47	± 4.94	99.99	10.527	± 3.334
02C2852	2053.63	± 7.29	99.90	8.772	± 2.447
02C2879	2080.38	± 15.76	100.00	1.696E-07	± 0.000
02C2861	2100.59	± 7.76	99.93	17.496	± 8.516
02C2862	2189.49	± 7.75	99.88	111.249	± 523.529
02C2887	2424.81	± 13.43	99.94	7.616	± 4.251

Table D.7: $^{40}Ar/^{39}Ar$ ages of glacially-derived feldspars in till sample CRS02

Sample: CRS02			Site 3 latitude: N 41°20'59"		
Till group: R1 Till			longitude: W 95°53'46"		
Lab No.	Age (Ma)	± 2σ (Ma)	^{40}Ar (%)	K/Ca	± 2σ
02C2817	1207.16	± 6.07	99.45	13.399	± 8.309
02C2818	1315.34	± 6.50	99.70	18.777	± 17.961
02C2790	1417.45	± 8.42	99.90	6.013	± 3.264
02C2795	1442.05	± 5.60	99.83	3.188	± 0.565
02C2827	1447.98	± 7.04	99.67	1.612E-07	± 0.000
02C2792	1477.28	± 11.64	99.64	6.132	± 2.560
02C2798	1492.79	± 6.10	99.82	6.852	± 1.457
02C2826	1507.38	± 6.35	99.74	1.612E-07	± 0.000
02C2816	1542.86	± 8.34	99.80	21.465	± 21.786
02C2830	1595.18	± 8.80	99.43	5.506	± 2.822
02C2837	1602.26	± 10.44	99.79	5.598	± 3.039
02C2834	1618.08	± 6.79	99.89	13.201	± 15.318
02C2789	1628.64	± 6.45	99.73	5.803	± 1.593
02C2823	1633.24	± 7.12	99.83	4.799	± 1.421
02C2793	1678.33	± 4.83	99.74	2.759	± 0.525
02C2801	1696.96	± 5.37	99.70	5.920	± 1.114
02C2796	1707.45	± 6.81	99.91	3.672	± 0.887
02C2838	1714.11	± 7.42	99.88	10.927	± 9.114
02C2829	1726.26	± 8.64	99.84	1.612E-07	± 0.000
02C2828	1748.14	± 12.96	99.87	1.612E-07	± 0.000
02C2824	1748.74	± 6.06	99.87	8.025	± 4.751
02C2819	1778.31	± 6.19	99.78	5.129	± 1.543
02C2804	1833.45	± 9.65	99.89	8.089	± 2.530
02C2794	1852.25	± 10.87	99.87	5.791	± 1.675
02C2799	1941.24	± 11.35	99.98	5.861	± 1.832
02C2833	1971.08	± 9.10	99.84	7.767	± 7.395
02C2805	1971.86	± 4.46	99.91	5.620	± 1.440
02C2802	1993.72	± 10.09	99.85	5.946	± 3.483
02C2822	2012.49	± 13.05	99.72	6.484	± 2.657
02C2803	2052.09	± 8.78	99.99	6.032	± 1.671
02C2800	2072.34	± 8.36	99.86	4.236	± 0.819
02C2831	2109.52	± 18.78	99.97	7.522E-06	± 0.000
02C2821	2139.95	± 9.22	99.91	122.558	± 1026.776
02C2835	2151.56	± 10.29	99.96	9.646	± 6.513
02C2791	2228.55	± 7.53	99.92	6.688	± 1.866
02C2820	2395.29	± 7.21	99.90	13.185	± 8.908
02C2836	2418.40	± 6.30	99.99	28.166	± 55.955

Table D.8: $^{40}Ar/^{39}Ar$ ages of glacially-derived feldspars in till sample GLW03

Sample: GLW03			Site 2 latitude: N 41°06'09"		
Till group: R1 Till			longitude: W 95°49'20"		
Lab No.	Age (Ma)	± 2σ (Ma)	^{40}Ar (%)	K/Ca	± 2σ
02C2685	1305.63	± 8.94	99.85	123.470	± 1167.094
02C2692	1351.26	± 10.85	99.80	4.131	± 0.993
02C2669	1467.90	± 21.09	99.54	64.074	± 648.756
02C2668	1481.27	± 14.13	99.75	5.525	± 3.741
02C2702	1495.91	± 12.41	99.87	18.090	± 36.550
02C2708	1571.51	± 16.86	99.86	35.100	± 140.364
02C2706	1572.05	± 15.51	99.91	484.222	± 23323.297
02C2707	1573.42	± 23.61	99.85	92.607	± 1618.343
02C2686	1575.96	± 19.10	99.82	1.703E-15	± 0.000
02C2684	1582.25	± 17.65	99.69	1.478E-16	± 0.000
02C2688	1594.22	± 15.91	99.95	1.703E-15	± 0.000
02C2701	1596.95	± 10.27	99.79	7.663	± 5.817
02C2681	1623.85	± 16.48	100.00	313.574	± 9558.372
02C2703	1644.76	± 12.93	99.86	15.955	± 34.345
02C2672	1650.17	± 13.29	99.73	14.874	± 43.577
02C2704	1653.16	± 13.49	99.86	21.095	± 51.163
02C2674	1681.49	± 13.82	99.90	29.137	± 103.849
02C2676	1707.53	± 17.25	99.84	1.277E-21	± 0.000
02C2680	1766.25	± 22.28	99.94	3.719E-20	± 0.000
02C2695	1770.91	± 13.15	100.00	3.972	± 1.772
02C2678	1785.86	± 14.67	100.00	3.719E-20	± 0.000
02C2673	1794.11	± 13.63	99.95	13.668	± 25.807
02C2694	1889.33	± 19.24	99.91	6.031	± 3.409
02C2679	1917.44	± 18.56	100.00	3.719E-20	± 0.000
02C2696	1935.87	± 20.62	99.99	5.584	± 4.057
02C2682	1947.48	± 19.27	99.92	0.000	± 0.000
02C2671	1961.85	± 17.04	99.91	5.927	± 3.794
02C2690	1991.60	± 16.97	99.97	4.420E-15	± 0.000
02C2693	2004.02	± 12.87	99.96	6.650	± 3.336
02C2697	2033.70	± 20.86	99.97	3.682	± 1.215
02C2700	2057.38	± 37.01	99.88	6.532	± 6.352
02C2670	2061.85	± 21.04	99.89	17.455	± 35.522
02C2699	2153.41	± 19.36	99.87	12.921	± 29.178
02C2709	2197.19	± 269.98	96.49	0.273	± 0.161
02C2689	2205.62	± 20.68	99.98	10.958	± 18.087
02C2677	2443.10	± 36.34	100.00	29.021	± 110.907

Table D.9: $^{40}Ar/^{39}Ar$ ages of glacially-derived feldspars in till sample DC139

Sample: DC139			Site 10 latitude: N 41°14'59"		
Till group: R1 Till			longitude: W 97°10'00"		
Lab No.	Age (Ma)	± 2σ (Ma)	^{40}Ar (%)	K/Ca	± 2σ
02C2741	889.03	± 6.86	99.20	2.307E-15	± 0.000
02C2758	1182.29	± 9.55	100.00	168.075	± 2698.040
02C2757	1243.08	± 14.74	99.71	7.112E-08	± 0.000
02C2731	1261.32	± 22.05	99.79	2.307E-15	± 0.000
02C2722	1317.70	± 12.44	99.32	39.367	± 225.575
02C2754	1334.19	± 16.56	100.00	7.112E-08	± 0.000
02C2752	1385.35	± 21.52	100.00	7.112E-08	± 0.000
02C2727	1408.77	± 18.02	99.53	5.071	± 3.486
02C2734	1428.71	± 7.80	99.96	2.307E-15	± 0.000
02C2730	1462.97	± 15.73	99.84	2.307E-15	± 0.000
02C2745	1518.39	± 11.11	99.10	4.535E-09	± 0.000
02C2759	1566.86	± 17.61	99.85	0.457	± 0.000
02C2742	1585.80	± 18.07	99.49	24.113	± 50.513
02C2740	1615.66	± 16.33	99.88	0.000	± 0.000
02C2726	1618.13	± 14.15	99.88	7.143	± 5.087
02C2728	1637.06	± 13.15	99.37	13.299	± 27.847
02C2749	1637.43	± 12.59	100.00	7.112E-08	± 0.000
02C2753	1674.69	± 14.72	100.00	7.112E-08	± 0.000
02C2737	1706.33	± 16.66	99.80	2.307E-15	± 0.000
02C2751	1729.46	± 16.12	99.82	7.112E-08	± 0.000
02C2736	1763.48	± 13.74	99.63	2.307E-15	± 0.000
02C2748	1831.90	± 14.07	99.98	7.112E-08	± 0.000
02C2750	1835.07	± 17.86	99.99	7.112E-08	± 0.000
02C2735	1844.49	± 16.15	99.95	2.307E-15	± 0.000
02C2724	1850.74	± 18.02	99.72	4.603	± 2.845
02C2760	1855.94	± 35.65	99.84	0.457	± 0.000
02C2743	1927.07	± 11.74	99.88	5.500	± 3.167
02C2739	1952.67	± 12.22	99.92	2.307E-15	± 0.000
02C2732	1988.91	± 14.19	99.98	2.307E-15	± 0.000
02C2744	2069.95	± 16.26	99.85	6.605	± 6.762
02C2733	2074.03	± 26.25	99.96	2.307E-15	± 0.000
02C2725	2175.47	± 22.90	99.87	17.338	± 60.538
02C2746	2245.85	± 20.15	99.94	8.235	± 5.649
02C2761	2359.41	± 15.17	99.75	0.457	± 0.000
02C2755	2437.03	± 42.47	99.96	7.112E-08	± 0.000
02C2723	2450.72	± 24.29	99.80	37.235	± 189.875

Table D.10: $^{40}Ar/^{39}Ar$ ages of glacially-derived feldspars in till sample WAT02

Sample: WAT02			Site 17 latitude: N 40°15'56"		
Till group: R1 Till			longitude: W 96°09'37"		
Lab No.	Age (Ma)	± 2σ (Ma)	^{40}Ar (%)	K/Ca	± 2σ
02C2405	1102.64	± 30.50	99.01	3.490	± 4.487
02C2402	1135.72	± 8.93	99.75	6.381E-11	± 0.000
02C2419	1136.46	± 14.34	99.80	0.017	± 0.000
02C2401	1229.01	± 14.58	98.73	6.381E-11	± 0.000
02C2387	1423.32	± 19.61	99.77	10.435	± 6.388
02C2388	1423.33	± 12.16	99.71	1.144E-17	± 0.000
02C2391	1429.64	± 15.04	99.74	1.144E-17	± 0.000
02C2395	1469.56	± 11.19	99.96	19.990	± 34.502
02C2403	1484.79	± 11.85	99.90	6.381E-11	± 0.000
02C2384	1505.91	± 13.29	99.80	189.585	± 2337.894
02C2399	1543.16	± 14.93	99.84	5.485E-13	± 0.000
02C2392	1571.25	± 17.91	100.00	1.144E-17	± 0.000
02C2410	1620.46	± 13.31	99.91	7.872	± 5.493
02C2413	1628.87	± 24.70	99.71	11.126	± 12.179
02C2409	1648.24	± 28.58	99.78	10.484	± 12.929
02C2390	1658.39	± 21.05	99.86	1.144E-17	± 0.000
02C2416	1668.88	± 10.18	99.91	9.291E-05	± 0.000
02C2414	1717.65	± 13.92	99.85	12.575	± 11.174
02C2396	1733.12	± 7.59	99.98	5.485E-13	± 0.000
02C2411	1742.00	± 12.79	99.93	28.617	± 94.173
02C2417	1756.82	± 12.35	99.85	8.859	± 4.833
02C2397	1757.25	± 22.18	99.84	5.485E-13	± 0.000
02C2386	1785.15	± 24.93	99.88	3.797E-19	± 0.000
02C2385	1793.28	± 17.73	99.83	10.130	± 11.186
02C2383	1835.48	± 20.91	99.59	5.698	± 3.240
02C2382	1886.79	± 20.02	99.88	17.816	± 30.502
02C2408	1915.07	± 25.16	99.78	20.433	± 42.323
02C2418	2002.23	± 23.81	99.82	76.990	± 253.872
02C2393	2026.44	± 54.83	99.00	0.879	± 0.709
02C2407	2035.12	± 30.97	99.85	6.992	± 4.219
02C2394	2056.19	± 48.24	99.65	1.586	± 0.790
02C2420	2102.26	± 30.71	99.65	14.253	± 34.929
02C2404	2125.36	± 16.08	99.86	6.381E-11	± 0.000
02C2400	2177.42	± 32.73	99.93	14.701	± 18.032
02C2412	2245.77	± 14.07	99.84	16.741	± 17.814

Table D.11: $^{40}Ar/^{39}Ar$ ages of glacially-derived feldspars in till sample AF172

Sample: AF172			Site 9 latitude: N 40°59'46"		
Till group: R2 Till			longitude: W 94°12'16"		
Lab No.	Age (Ma)	± 2σ (Ma)	^{40}Ar (%)	K/Ca	± 2σ
02C1850	1224.64	± 8.63	99.70	26.270	± 17.688
02C1830	1246.50	± 10.65	97.86	1.105E-22	± 0.000
02C1868	1303.52	± 11.23	99.56	0.283	± 0.000
02C1832	1304.22	± 13.72	99.62	124.880	± 883.988
02C1851	1433.87	± 16.49	99.35	108.130	± 538.256
02C1866	1475.69	± 10.74	99.84	0.064	± 0.000
02C1833	1484.62	± 14.57	98.45	1.600E-19	± 0.000
02C1862	1502.64	± 12.73	99.71	0.001	± 0.000
02C1849	1509.72	± 18.89	100.00	7.883	± 3.725
02C1853	1528.41	± 12.14	99.86	407.043	± 8412.259
02C1867	1529.77	± 19.86	100.00	104.063	± 612.098
02C1858	1575.57	± 27.94	99.95	12.730	± 12.818
02C1834	1589.53	± 13.38	99.88	21.777	± 13.341
02C1831	1594.31	± 19.97	99.57	36.506	± 60.419
02C1864	1622.81	± 13.15	100.00	19.053	± 8.468
02C1865	1625.70	± 20.53	99.90	127.630	± 297.934
02C1848	1670.20	± 25.10	100.00	5.395E-10	± 0.000
02C1856	1680.14	± 14.46	99.65	7.471	± 2.903
02C1857	1724.54	± 14.24	100.00	17.523	± 12.480
02C1854	1736.12	± 14.26	100.00	1.512E-06	± 0.000
02C1843	1745.77	± 10.17	99.96	80.787	± 141.413
02C1828	1763.97	± 10.71	99.57	31.727	± 34.877
02C1837	1816.66	± 15.71	99.76	1.936E-17	± 0.000
02C1827	1855.92	± 9.74	99.90	37.580	± 34.489
02C1844	1899.40	± 25.95	99.74	236.276	± 2323.370
02C1825	1984.13	± 17.20	100.00	0.000	± 0.000
02C1859	1990.16	± 15.75	99.97	59.207	± 130.105
02C1863	2005.79	± 10.45	100.00	0.001	± 0.000
02C1835	2066.47	± 13.54	100.00	17.660	± 13.254
02C1860	2082.30	± 14.74	99.98	74.441	± 207.708
02C1838	2133.67	± 19.43	99.96	134.638	± 664.998
02C1839	2153.36	± 13.96	100.00	67.412	± 193.737
02C1845	2194.94	± 32.88	99.71	6.692	± 6.108
02C1840	2251.29	± 19.23	100.00	38.262	± 59.036
02C1846	2301.05	± 12.82	99.98	29.064	± 29.934

Table D.12: $^{40}Ar/^{39}Ar$ ages of glacially-derived feldspars in till sample BEF02

Sample: BEF02			Site 19 latitude: N 40°40'24"		
Till group: R2 Till			longitude: W 94°15'02"		
Lab No.	Age (Ma)	± 2σ (Ma)	^{40}Ar (%)	K/Ca	± 2σ
02C2232	1013.96	± 15.88	99.83	8.273E-12	± 0.000
02C2230	1084.16	± 4.49	99.74	103.606	± 100.117
02C2253	1160.68	± 24.18	99.44	0.008	± 0.000
02C2217	1192.42	± 5.68	99.58	10.900	± 5.207
02C2252	1371.05	± 8.53	99.22	35.580	± 31.216
02C2224	1413.19	± 6.85	99.79	10.239	± 1.579
02C2251	1425.48	± 12.63	99.89	8.998	± 4.187
02C2235	1481.35	± 6.26	99.25	2.249E-14	± 0.000
02C2240	1527.06	± 11.72	99.67	8.407	± 2.052
02C2255	1580.71	± 5.97	99.89	39.716	± 33.504
02C2238	1595.22	± 6.73	99.89	79.866	± 102.043
02C2236	1622.28	± 7.46	99.78	36.049	± 34.604
02C2218	1628.51	± 6.29	99.69	23.158	± 20.175
02C2248	1638.93	± 7.34	99.80	53.308	± 73.953
02C2234	1641.92	± 7.39	100.00	2.249E-14	± 0.000
02C2246	1646.21	± 8.44	99.92	9.163E-06	± 0.000
02C2220	1775.64	± 21.11	99.73	3.733E-19	± 0.000
02C2214	1782.27	± 11.81	99.76	9.410	± 4.423
02C2250	1821.09	± 11.00	99.99	3.939E-04	± 0.000
02C2229	1821.82	± 11.84	99.95	3.345	± 0.252
02C2254	1831.54	± 14.46	99.70	0.008	± 0.000
02C2244	1840.96	± 20.81	99.61	1.369	± 0.198
02C2221	1847.10	± 12.17	100.00	6.417	± 2.632
02C2242	1866.20	± 21.47	99.56	1.102	± 0.077
02C2249	1896.59	± 8.34	99.88	0.000	± 0.000
02C2245	1943.08	± 10.11	99.89	15.598	± 7.971
02C2225	1984.39	± 12.16	99.53	15.488	± 5.774
02C2231	1995.12	± 9.64	99.92	5.901E-11	± 0.000
02C2243	1999.19	± 36.08	99.54	2.098	± 0.605
02C2227	2033.87	± 84.45	92.38	0.122	± 0.012
02C2222	2044.98	± 10.66	99.83	9.826	± 3.447
02C2215	2045.23	± 8.13	99.84	16.380	± 9.994
02C2223	2181.79	± 13.07	99.89	5.851	± 0.985
02C2228	2270.12	± 11.68	99.91	8.795E-11	± 0.000
02C2216	2279.01	± 11.41	99.92	32.356	± 50.877
02C2237	2297.69	± 6.78	100.00	33.774	± 36.269
02C2241	2844.78	± 58.84	98.89	1.456	± 0.439

Table D.13: $^{40}Ar/^{39}Ar$ ages of glacially-derived feldspars in till sample CTY02

Sample: CTY02			Site 1 latitude: N 41°04'27"		
Till group: R2 Till			longitude: W 95°57'50"		
Lab No.	Age (Ma)	±2σ (Ma)	^{40}Ar (%)	K/Ca	±2σ
02C2492	582.70	± 5.31	98.11	20.828	± 44.836
02C2509	669.19	± 5.08	99.70	16.202	± 8.462
02C2513	682.88	± 6.73	99.97	36.787	± 70.557
02C2483	682.99	± 6.93	99.35	5.325E-16	± 0.000
02C2494	899.39	± 7.65	99.59	21.669	± 47.863
02C2485	924.61	± 9.05	99.70	49.131	± 280.242
02C2489	984.59	± 19.55	99.90	195.912	± 6927.721
02C2510	984.66	± 9.26	99.40	14.029	± 9.729
02C2488	993.02	± 11.40	99.62	12.453	± 15.659
02C2499	1005.51	± 15.82	99.66	1.190E-08	± 0.000
02C2481	1021.85	± 11.22	99.72	1.093E-16	± 0.000
02C2486	1031.26	± 12.16	99.22	1.072E-13	± 0.000
02C2500	1031.54	± 10.60	99.75	1.190E-08	± 0.000
02C2501	1050.09	± 10.37	99.87	25.831	± 118.310
02C2480	1057.80	± 11.56	99.65	18.438	± 41.702
02C2511	1070.91	± 10.00	99.63	12.388	± 4.510
02C2490	1071.74	± 10.08	99.41	18.221	± 44.405
02C2508	1093.89	± 8.03	99.60	9.742	± 5.817
02C2512	1107.05	± 8.91	99.90	4.260	± 1.528
02C2515	1117.03	± 11.54	99.61	4.304	± 2.115
02C2493	1119.17	± 12.90	99.81	24.624	± 45.594
02C2514	1135.07	± 11.97	99.57	8.569	± 4.502
02C2484	1135.73	± 14.06	99.74	5.325E-16	± 0.000
02C2496	1181.74	± 13.57	99.76	18.045	± 33.129
02C2503	1224.06	± 11.95	100.00	1.206E-06	± 0.000
02C2502	1227.51	± 16.63	100.00	1.206E-06	± 0.000
02C2482	1228.84	± 8.96	99.18	16.605	± 32.295
02C2478	1254.18	± 13.84	99.91	19.275	± 36.593
02C2495	1260.06	± 10.21	98.37	690.670	± 73651.061
02C2505	1268.84	± 17.56	100.00	6.587E-06	± 0.000
02C2504	1289.25	± 8.90	99.84	11.213	± 13.486
02C2497	1306.69	± 9.29	99.65	40.317	± 123.061
02C2506	1351.64	± 10.28	99.68	6.587E-06	± 0.000
02C2479	1505.50	± 16.43	99.80	73.633	± 888.754
02C2491	2137.27	± 16.07	99.77	14.206	± 17.428

Table D.14: $^{40}Ar/^{39}Ar$ ages of glacially-derived feldspars in till sample ELC02

Sample: ELC02			Site 17 latitude: N 40°15'56"		
Till group: R2 Till			longitude: W 96°09'37"		
Lab No.	Age (Ma)	± 2σ (Ma)	^{40}Ar (%)	K/Ca	± 2σ
02C1913	648.95	± 5.68	99.08	13.126	± 7.696
02C1931	834.98	± 7.87	99.60	5.952E-09	± 0.000
02C1903	912.69	± 7.42	99.86	36.837	± 106.441
02C1905	925.67	± 8.24	99.47	11.983	± 11.734
02C1910	925.77	± 5.32	99.69	43.024	± 36.299
02C1897	945.03	± 20.94	99.54	0.000	± 0.000
02C1939	951.30	± 13.87	100.00	44.506	± 204.422
02C1929	1004.94	± 12.70	99.68	46.882	± 166.229
02C1917	1039.81	± 8.41	99.58	61.322	± 71.105
02C1920	1048.32	± 11.27	99.53	10.588	± 8.581
02C1906	1051.82	± 5.71	99.65	19.796	± 15.835
02C1925	1054.51	± 10.47	99.62	9.231E-12	± 0.000
02C1901	1060.15	± 6.65	99.56	10.779	± 3.966
02C1940	1065.95	± 14.59	99.96	23.550	± 45.057
02C1937	1067.76	± 11.48	100.00	23.719	± 18.964
02C1928	1079.61	± 10.52	99.54	9.231E-12	± 0.000
02C1938	1079.72	± 8.15	100.00	697.088	± 23984.247
02C1912	1089.76	± 13.23	99.86	32.438	± 17.433
02C1935	1096.31	± 10.06	99.81	163.911	± 717.596
02C1900	1100.03	± 7.39	99.87	44.607	± 51.399
02C1914	1104.60	± 13.83	99.71	1.063E-22	± 0.000
02C1927	1121.87	± 11.08	99.96	9.231E-12	± 0.000
02C1921	1156.99	± 13.18	99.64	9.932E-15	± 0.000
02C1918	1196.83	± 9.72	98.71	6.723E-17	± 0.000
02C1924	1204.76	± 9.58	99.93	9.231E-12	± 0.000
02C1898	1212.44	± 14.45	99.41	140.381	± 890.557
02C1904	1221.76	± 5.84	99.95	13.583	± 6.719
02C1919	1222.02	± 10.83	99.48	77.028	± 337.905
02C1926	1225.74	± 9.58	99.86	9.231E-12	± 0.000
02C1933	1245.01	± 12.50	99.94	161.631	± 1445.776
02C1908	1277.19	± 15.72	99.80	5.728	± 3.228
02C1911	1327.36	± 12.61	99.34	11.793	± 3.821
02C1934	1601.12	± 22.21	99.69	1.396E-06	± 0.000
02C1932	1677.15	± 11.62	99.79	35.821	± 46.769
02C1922	1691.97	± 16.99	99.50	336.435	± 4067.441
02C1907	1698.96	± 10.09	99.87	4.359E-25	± 0.000
02C1899	1907.07	± 22.02	99.93	19.184	± 14.650